Applied Energy 288 (2021) 116555

Contents lists available at ScienceDirect

Applied Energy

journal homepage: www.elsevier.com/locate/apenergy

# A comprehensive review on sub-zero temperature cold thermal energy storage materials, technologies, and applications: State of the art and recent developments

Lizhong Yang [a,b], Uver Villalobos [a], Bakytzhan Akhmetov [a], Antoni Gil [a], Jun Onn Khor [a], Anabel Palacios [c], Yongliang Li [c], Yulong Ding [c], Luisa F. Cabeza [b], Wooi Leong Tan [d], Alessandro Romagnoli [e,*]

[a] Surbana Jurong – Nanyang Technological University Corporate Lab, 61 Nanyang Drive, 637355, Singapore
[b] GREiA Research Group, Universitat de Lleida, Pere de Cabrera s/n, 25001 Lleida, Spain
[c] Birmingham Centre for Energy Storage (BCES), School of Chemical Engineering, University of Birmingham, Birmingham, Birmingham B15 2TT, United Kingdom
[d] Energy & Industrial Division, Surbana Jurong, 168 Jalan Bukit Merah, 150168, Singapore
[e] School of Mechanical and Aerospace Engineering, Nanyang Technological University, 50 Nanyang Avenue, 639798, Singapore

## HIGHLIGHTS

- Summarizes a wide temperature range of Cold Thermal Energy Storage materials.
- Phase change material thermal properties deteriorate significantly with temperature.
- Simulation methods and experimental results analyzed with details.
- Future studies need to focus on heat transfer enhancement and mechanical design.
- Analyzes applications with technology readiness and more should be explored.

## GRAPHICAL ABSTRACT

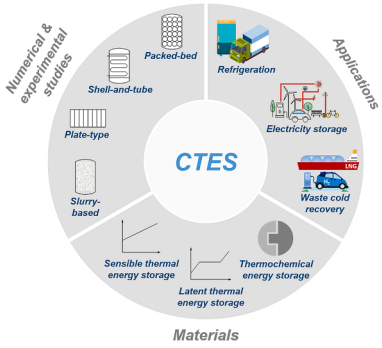


## ARTICLE INFO

*Keywords:*
Cold thermal energy storage
Sub-zero
Phase change materials (PCMs)
Numerical
Storage system
Encapsulation method

## ABSTRACT

The energy industry needs to take action against climate change by improving efficiency and increasing the share of renewable sources in the energy mix. On top of that, refrigeration, air-conditioning, and heat pump equipment account for 25–30% of the global electricity consumption and will increase dramatically in the next decades. However, some waste cold energy sources have not been fully used. These challenges triggered an interest in developing the concept of cold thermal energy storage, which can be used to recover the waste cold energy, enhance the performance of refrigeration systems, and improve renewable energy integration. This paper comprehensively reviews the research activities about cold thermal energy storage technologies at sub-zero temperatures (from around −270 °C to below 0 °C). A wide range of existing and potential storage materials are tabulated with their properties. Numerical and experimental work conducted for different storage types is systematically summarized. Current and potential applications of cold thermal energy storage are analyzed with

* Corresponding author. Tel.: +65 6790 5941; fax: +65 6791 9690.
*E-mail address:* a.romagnoli@ntu.edu.sg (A. Romagnoli).

https://doi.org/10.1016/j.apenergy.2021.116555
Received 28 October 2020; Received in revised form 12 January 2021; Accepted 24 January 2021
Available online 23 February 2021

their suitable materials and compatible storage types. Selection criteria of materials and storage types are also presented. This review aims to provide a quick reference for researchers and industry experts in designing cold thermal energy systems. Moreover, by identifying the research gaps where further efforts are needed, the review also outlines the progress and potential development directions of cold thermal energy storage technologies.

**Nomenclature**

*Acronyms*

| | |
|---|---|
| BOG | Boil-off Gas |
| CMC | Oxyethylmethylcellulose |
| COP | Coefficient Of Performance |
| CTES | Cold Thermal Energy Storage |
| HDPE | High-Density Polyethylene |
| HTF | Heat Transfer Fluid |
| LAES | Liquid Air Energy Storage |
| LNG | Liquefied Natural Gas |
| PTES | Pumped Thermal Energy Storage |
| PCM | Phase Change Material |
| PCT | Phase Change Temperature |
| PCS | Phase Change Slurry |
| PET | Polyethylene terephthalate |
| PP | Polypropylene |
| PS | Polystyrene |
| SFES | Superconducting Flywheel Energy Storage |
| TCM | Thermal Chemical Storage Material |
| TES | Thermal Energy Storage |
| TRL | Technology Readiness Level |

*Symbols*

| | |
|---|---|
| $c_p$ | Specific heat capacity [kJ/(kg·K)] |
| $G$ | Gas |
| $k$ | Thermal conductivity [W/(m·K)] |
| $m$ | Mass [kg] |
| $Q$ | Energy [kJ] |
| $S$ | Solid |
| $T$ | Temperature [°C] |
| $x$ | Fraction [–] |

*Subscripts*

| | |
|---|---|
| final | Final |
| initial | Initial |
| l | Latent |
| s | Sensible |

*Greek symbols*

| | |
|---|---|
| $\Delta H$ | Specific heat [kJ/kg] |
| $\rho$ | Material density [kg/m$^3$] |

## 1. Introduction

During the next few decades, the worldwide energy industry and cold supply chain are projected to face a massive challenge considering the climate change and global population increase. The world population is projected to reach 9.7 billion by 2050 [1]. On the opposite side, more than 820 million people worldwide suffer from starvation, partially associated with the loss of food products due to a lack of cold chain [2]. Such changes will substantially increase the energy demand in the refrigeration market. By 2015, refrigeration, air-conditioning, and heat pump equipment already accounts for 25–30% of the global electricity consumption and is expected to surge 33-fold by 2100 [3]. Meanwhile, various sources of cold energy have not been fully utilized. For example, the global liquefied natural gas (LNG) demand will double by 2040, reaching more than 700 MTPA [4]. However, during the regasification process of LNG, a massive amount of cold energy (approximately 830 kJ/kg at −162 °C) is generally wasted into seawater or ambient air [5]. Furthermore, the worldwide growth of intermittent renewable energy sources also poses the need for efficient and cost-effective electricity storage technologies. Therefore, the increasing demand for refrigeration energy consumption globally, the availability of waste cold sources, and the need for using thermal energy storage for grid integration of renewable energy sources triggered the research to develop cold thermal energy storage (CTES) systems, materials, and smart distribution of cold.

CTES have already been developed for decades, especially to preserve and transport food and medical goods at a wide range of temperatures. Many authors have presented reviews about technologies and materials to be applied in this field.

Li et al. [6] conducted a review study in which various cold storage technologies and applications were classified. Besides, emerging cold storage technologies and different types of phase change materials (PCMs) in the range of 7–14 °C were introduced. Research works carried out on thermal energy storage at low temperatures were also reviewed. The results showed that most of the works were focused on studies of storage materials, especially on analyses and characterization of PCMs. Only some of them were concentrated in cold storage applications. Despite their efforts to overview different methods of energy storage for air conditioning applications, they affirmed the research presented in their paper was still in its initial stage and required further development.

Li et al. [7] reviewed the PCMs and sorption materials for sub-zero thermal energy storage applications from −114 °C to 0 °C. The authors categorized the PCMs into eutectic water-salt solutions and non-eutectic water-salt solutions, discussed the selection criteria of PCMs, analyzed their advantages, disadvantages, and solutions to phase separation, subcooling, corrosion, flammability issues. Various types of microencapsulation and nanoparticle additives to enhance the heat transfer of the PCMs are also introduced. For sorption materials, the authors focused on the working pairs and concluded that absorption storage had been commercially deployed while adsorption storage was still progressing towards commercialization. However, CTES system design and applications were only briefly mentioned.

Another relevant review on CTES materials was presented by Oró et al. [8], where up to 88 PCMs, with melting temperatures varied from −86 °C to 20 °C, were listed. Analyses of the long-term stability of the materials, such as corrosion, phase segregation, stability under extended thermal cycling, and subcooling, were discussed. Moreover, different methods of PCM encapsulation and applications of PCMs in various cooling systems were reviewed in this paper. However, in this review, most of the applications introduced were around 0 °C.

Hence, even if many references of materials and methods for storing cold energy can be found at low temperatures, we detected the need for a comprehensive updated paper that synthesizes the information available on materials, technologies, and applications progress in the field for sub-zero, especially extremely low temperatures.

The present paper aims to fill up the gap in the existing literature of a comprehensive review on sub-zero cold energy storage and bring to light

a structured document of CTES technologies. Compared to previous review works, the novelties of this paper are: covers a broader temperature range from around −270 °C to below 0 °C for CTES materials and from −210 °C to below 0 °C for CTES applications; provides a series of comprehensive lists of the thermophysical properties of current and potential sensible, latent, and thermochemical CTES materials, alongside with their pros and cons and suitable applications; systematically reviews the numerical methods and experimental results about CTES containment and heat transfer for all types of CTES technologies used for sub-zero temperatures; analyzes the usage of CTES in a wider range of conventional and novel applications, remarks the Technology Readiness Levels (TRL), and identifies more potential applications for CTES technologies (Fig. 1). This article can be readily used by researchers and industry experts who need a quick and handy reference in the designing work of CTES systems. Moreover, based on this review, existing research gaps in CTES materials, numerical studies, experimental studies, and applications may also be noticed to guide the readers to develop new research lines to address the gaps: including searching for more CTES materials with higher heat capacity and better performance for cryogenic temperatures, focusing on heat transfer enhancement and mechanical design of storage containment, improving the design and exploring the use of CTES in more potential applications.

The structure of this paper is illustrated in Fig. 2.

The first part of the paper presents a collection of potential materials to be used for CTES with storage temperature below 0 °C, including their corresponding fundamental thermophysical properties. The lists should help the readers select the correct materials which fit their application and assess potential designs of CTES systems. Moreover, this part also aims to discuss how to improve the materials' thermal conductivity or heat storage capacity by using different methods like the addition of highly thermal-conductive additives, porous matrix, nucleating and thickener agents, and encapsulation.

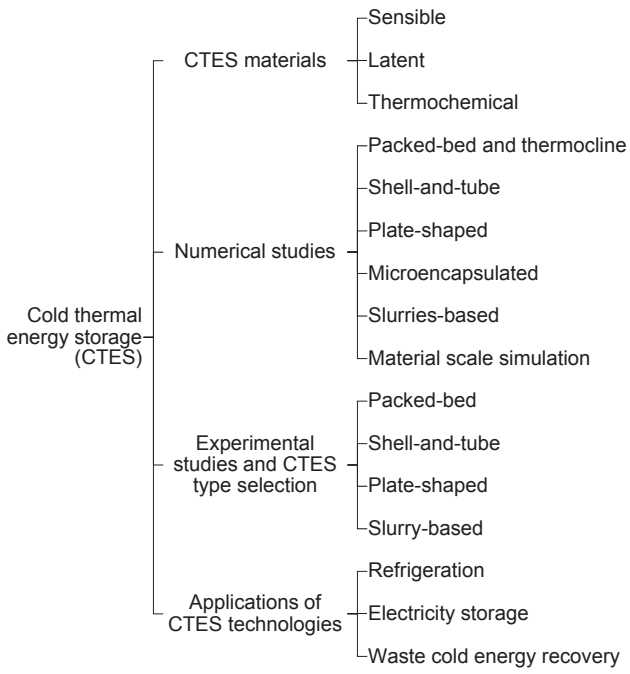


**Fig. 2.** Research work conducted for CTES technologies.

The second part of the paper presents the review of up-to-date numerical studies on the charging/discharging processes and numerical models developed to evaluate the storage performance of different types of materials for CTES applications. They are discussed in a categorized manner so that readers could gain an overall understanding of the

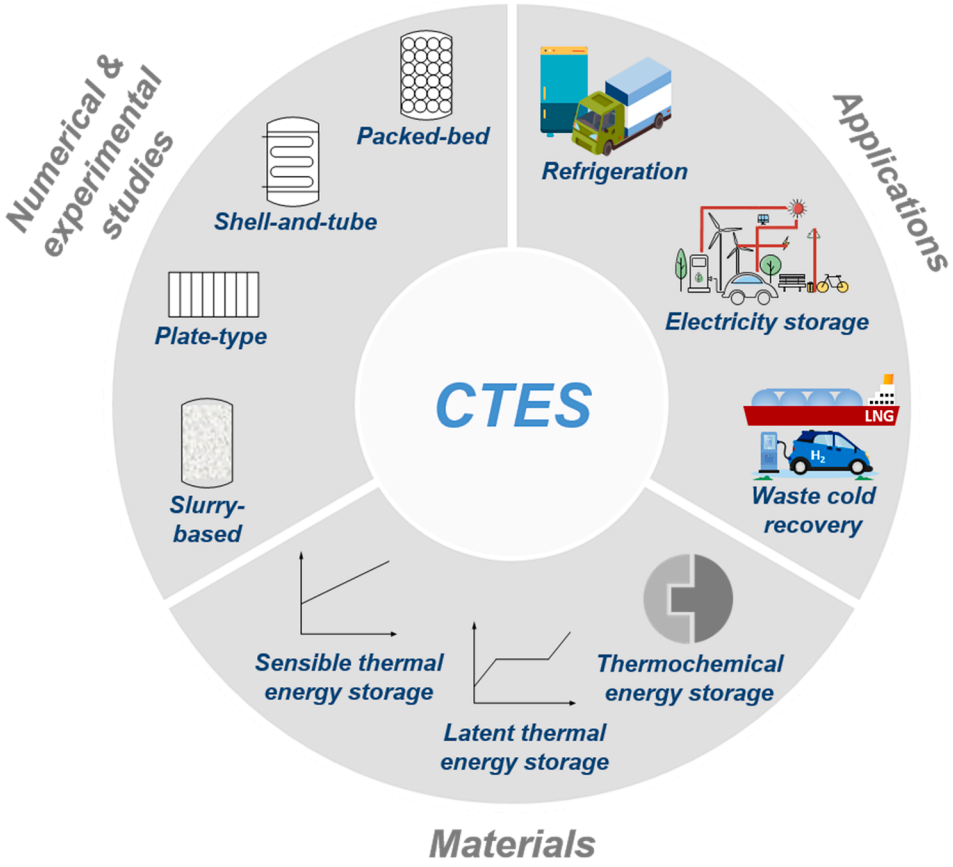


**Fig. 1.** Structure of this work.

numerical methods specialized to particular cold storage types. It turns out sensible and latent heat based cold energy storage methods have been widely studied using numerical methods. Therefore, they are considered as subcategories for each storage design. Numerical modeling of new trending methods of cold energy storage, such as slurry and microencapsulated PCMs, are discussed independently. Validation of numerical methods using experimental studies is considered along with several numerical studies if the referred work includes such information.

A complete review of experimental studies of CTES containment and heat transfer for sub-zero temperature applications is also presented in this review. The experimental part covers packed-bed, shell-and-tube, plate-shaped, and slurry-based. The design of these types of thermal energy storage (TES) systems is mostly similar to the ones used for higher temperature ranges. However, some specific requirements need to be taken into account at sub-zero temperatures, like volume change control and mechanical properties of the containment.

Finally, the last part of this paper reviews and classifies the existing and proposed cases of CTES systems integrated into active and passive refrigeration, electricity storage, and waste cold recovery. The roles of CTES in these applications are summarized, such as efficiency increase, energy consumption reduction, temperature control improvement, and renewable energy integration. CTES technologies used for refrigeration are commercially available or have been widely investigated. Various research opportunities for using CTES electricity storage and waste cold energy recovery are also discussed.

## 2. Cold thermal energy storage materials

The selection of the storage material is an essential step at the initial phases of a CTES system design, which determines the storage capacity and eventually affects the system's final design. It is widely accepted that the desired requirements for CTES materials are [9–11]:

- An appropriate operating temperature range depending on the application
- High energy density
- High thermal conductivity
- High density
- Low degree of subcooling (or supercooling)
- Corrosion resistance
- Chemical and physical stability
- Not poisonous, toxic, flammable, or explosive
- Small vapor pressure and volume change
- Low cost and available in large quantities

There is no ideal CTES material that meets all of the requirements, and each material has its own strength and weakness [7,12]. Therefore, selecting the material is usually a trade-off process to find the most suitable material to meet the application's specific requirements.

CTES materials for different applications can be classified into sensible thermal energy storage materials, latent thermal energy storage materials, and thermochemical energy storage materials. Each category can be further classified into several types. Following the classification shown in Fig. 3, this section describes the physical and thermal properties of different CTES materials over a broad temperature range and discusses the research directions for future material development.

### 2.1. Sensible thermal energy storage materials

Sensible thermal energy storage materials store thermal energy (heat or cold) based on a temperature change. The amount of energy a sensible material can store depends on the specific heat capacity and the mass of the material, according to Equation (1):

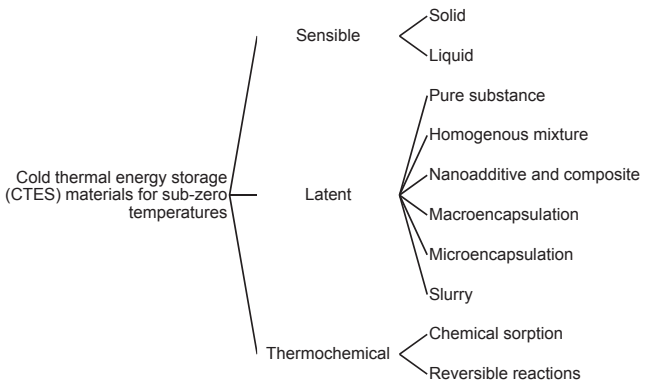


**Fig. 3.** Classification of CTES materials for sub-zero temperatures.

$$Q_s = \int_{T_{initial}}^{T_{final}} (m \cdot c_p)\, dT \quad (1)$$

where $Q_s$ [kJ] is the sensible thermal energy stored, $m$ [kg] and $c_p$ [kJ/kg·K] are the total mass and specific heat capacity of the storage material, and $T$ [K] the temperature.

Using sensible thermal energy storage for CTES is simpler and less expensive than latent thermal energy storage systems [13–15]. Most of the materials suitable for CTES are solid. Rocks, plastics, metals, quartz, concrete, rock pebbles, among others, have been studied as storage materials from room temperature to around −170 °C [16–18]. Sensible thermal energy storage materials mentioned above are commonly used in packed-bed systems. Due to the high density and low specific heat capacity of these materials, the size and weight of the system are the aspects to consider during the feasibility analysis of such projects. Numerical and experimental studies on a Liquid Air Energy Storage (LAES) system demonstrated that the high-grade cold energy storage can be effectively realized using packed-beds with rocks as the fillers [19,20]. The commercially available polymer materials, such as polypropylene (PP) and high-density polyethylene (HDPE), have also been studied as sensible solid CTES materials [21]. Their specific heat capacities are competitive to make them attractive materials for packed-bed systems. More solid materials, especially locally available materials and recycled materials are worth exploring in the future as long as they are stable at sub-zero temperatures and have good thermophysical properties.

Table 1 presents a list of tested and potential solid sensible thermal energy storage materials for sub-zero temperatures. The application of a material is added if it is mentioned in the literature about a specific application and claimed that this material is suitable for that application.

Liquid sensible thermal energy storage materials can act as both the thermal energy storage material and the HTF at the same time in a CTES system, which is different from the solid sensible materials. However, the applications' working temperatures must be between the freezing and boiling points of such materials. One criterion for selecting liquid sensible materials proposed by Laughlin [44] for pumped thermal energy storage (PTES) is that they need to remain liquid at sub-zero temperatures and have a vapor pressure below 1 atm. Liquid sensible materials that meet these criteria are mainly hydrocarbons and their derivatives. For example, hexane was proposed by Laughlin for a PTES system. Since these materials can be toxic and flammable, their health and safety issues are worth considering. Laughlin proposed that methods like halogenation can make the hydrocarbons flame-resistant [44]. An ethylene glycol/water solution can also be used as sensible storage materials. It is odorless, has a freezing temperature below 0 °C, and a low vapor pressure [45]. Shorter-chain alcohols, such as methanol, ethanol, propanol, propylene glycol, and their water solutions can also

**Table 1**
Existing and potential sensible solid thermal energy storage materials for sub-zero temperatures.

| Material | Density (kg/m$^3$) | Specific heat capacity (J/g·K) | Thermal conductivity (W/(m·K)) | Application(s) mentioned in the literature | Reference |
|---|---|---|---|---|---|
| Water (Ice) | 926–916 (−100 °C to 0 °C) | 1.39–2.05 (−100 °C to 0 °C) | 3.48–2.22 (−100 °C to 0 °C) | | [22,23] |
| Granite | 2600–2688 (NA) | 0.72–0.95 (NA) | 1.9–3.5 (NA) | | [20,24] |
| Rocks | 1810–7500 (NA) | 0.74–2.15 (NA) | 0.82–7.2 (NA) | Liquid air energy storage, pumped thermal energy storage | [19,24–26] |
| Concrete | 500–2400 (NA) | 0.83–1.16 (NA) | 0.6–1.3 (0 °C) | Pumped thermal energy storage | [26–28] |
| Polypropylene | 900–910 (NA) | 0.64–1.51 (−173 °C to 0 °C) | 0.18–0.22 (−173 °C to 25 °C) | | [23,29–32] |
| High Density Polyethylene | 930–965 (NA) | 1.9–2.25 (NA) | 0.42–0.51 (25 °C) | | [23,33,34] |
| Quartz | 2600–2650 (NA) | 0.41–0.70 (−123 °C to 0 °C) | 0.78–1.30 (−153 °C to 0 °C) | Liquid air energy storage | [19,24,35–37] |
| Sodium chloride | 2170 (25 °C) | 0.6–0.85 (−173 °C to −23 °C) | 22.73–7.52 (−173 °C to −23 °C) | | [38–40] |
| Aluminum oxide | 3400–4000 (NA) | 0.10–0.72 (−183 °C to 0 °C) | 27.01–15.51 (−173 °C to 0 °C) | | [41–43] |

be candidates as liquid sensible thermal energy storage materials. However, most liquid sensible materials become viscous at cryogenic temperatures [44], and thus the operating conditions should be carefully selected.

### 2.2. Latent thermal energy storage materials

Latent thermal energy storage materials store and release thermal energy during the material's phase transitions and are commonly known as phase change materials (PCMs). The temperature at which the phase change happens is called the phase change temperature (PCT).

The latent heat stored by a PCM, $Q_l$ [kJ], can be calculated using Equation (2):

$$Q_l = x_l \cdot m \cdot \Delta H_l \tag{2}$$

where $x_l$ is the fraction of the storage material that changed the phase and $\Delta H_l$ [kJ/kg] is the specific latent heat of the material. The total amount of energy stored will be the contribution of both sensible heat (before and after the phase change) and latent heat.

PCMs have been under continuous development for decades. They can store a remarkably more considerable amount of energy than sensible thermal energy storage materials [7,8]. However, the system complexity for latent thermal energy storage materials is also higher than that of sensible thermal energy storage materials [15].

The latent thermal energy storage processes consider four different types of phase changes: solid–solid, solid–liquid, liquid–gas, and solid–gas. Solid-liquid transitions are the most studied and utilized form of PCM. This transformation has a higher latent heat than solid–solid. The thermal expansion of the material during the phase change can reach 10% of the original material volume or less [46]. The solid–solid transition changes between the polymorphic phases of the material release a lower latent heat compared to solid–liquid transition [46]. Solid-gas and liquid–gas transitions store and release the highest amount of thermal energy accompanied by a significant volume change during the phase change, which requires storage vessels or open-air systems. In the latter case, only air, nitrogen, and carbon dioxide are practical since they can be safely released into the atmosphere.

In this paper, existing and potential PCM products worth mentioning due to their high latent heat and availability are classified into six types: pure substance PCMs, homogenous mixture PCMs, nanoadditive and composite PCMs, macroencapsulated PCMs, microencapsulated PCMs, and slurry PCMs.

#### 2.2.1. Pure substance PCM

Pure substance PCM suitable for sub-zero temperature applications includes organic and inorganic compounds and elements. A collection of existing and potential pure substance PCMs are listed in Table 2.

Organic PCMs are mostly composed of hydrogen and carbon structures such as alkanes (paraffins), alkanones, esters, fatty acids, alcohols, glycols, and polymers [15,46,87]. Alkane is the most widely studied type of organic PCM. Alkane's melting point and latent heat increase with the length of the carbon chain [7,39]. They are generally less expensive, reliable, predictable, non-corrosive and available for a wide temperature range. For sub-zero temperature applications, existing and potential organic PCMs are available from around −200 °C to 0 °C. In general, most organic PCMs have low or no subcooling, melt congruently, are non-corrosive and chemically stable, but the volume change during phase change can be significant [8]. Organic PCMs can also be flammable and sometimes oxidizing [46], indicating the need to develop fire suppression techniques.

The inorganic pure substance PCM group mainly consists of elements, salts, salt hydrates, and metals. For sub-zero temperatures, the most basic options of PCMs are elements such as nitrogen, hydrogen, helium, oxygen, neon. Their transition temperatures are below −173 °C, which is suitable for extremely low temperature applications. Solid $CO_2$ (dry ice) and liquid nitrogen are commonly used CTES materials for cold chain applications [88,89]. Solid nitrogen has been tested on a superconducting flywheel setup to store both the cold energy and mechanical kinetic energy [90], showing that the concept is theoretically viable. On the other hand, ammonia, whose melting temperature is −78.2 °C, has the largest heat of fusion among all pure substances collected by this work. However, it is toxic and corrosive [91].

#### 2.2.2. Homogenous mixture PCM

A homogenous mixture PCM is a combination of two or more substances that are not chemically combined, yet the composition is uniform. The percentage of each component of the mixture can be varied to obtain different phase transition temperatures [15,46].

The most commonly used homogenous mixture PCM is eutectic material. A eutectic material is a mixture of two or more substances with a particular composition, whose melting temperature is the lowest of all such mixtures formed by the same substances [92]. This kind of material melts and freezes congruently without phase separation and has high thermal conductivity and density [15,46]. Eutectic materials can be inorganic or organic. Inorganic eutectic PCMs are generally low cost, have high latent heat and thermal conductivities; however, they can be chemically unstable and corrosive [8]. Aqueous salt mixture, or eutectic water-salt solution, is the most widely analyzed and applied PCM type for sub-zero temperature range [8]. A collection of existing and potential eutectic water-salt solutions can be found in Table 4.

Organic homogenous PCMs are also widely studied. Rasta et al. [93,94] worked on a bio-PCM based on a mixture of vegetable oil and

**Table 2**
Existing and potential pure substance PCMs for sub-zero temperatures.

| Material | Density (kg/m$^3$) | Transition Temperature (°C) | Specific heat Capacity (J/(g·K)) | Thermal Conductivity (W/(m·K)) | Latent heat (J/g) | Phase | Application(s) mentioned in literature | Reference |
|---|---|---|---|---|---|---|---|---|
| Helium (He) | 148.3–125.0 (l) (−270.65 °C to −268.93 °C) | −272.2 | 2.05–9.78 (l) (−270.65 °C to −268.93 °C) | 0.0167–0.0196 (l) (−270.65 °C to −268.93 °C) | | Solid-liquid | | [22,23,47] |
| | 16.89–0.18 (g) (−268.93 °C to 0 °C) | −268.93 | 9.78–5.19 (g) (−268.93 °C to 0 °C) | 0.0106–0.137 (g) (−268.93 °C to −23.15 °C) | 23.30 | Liquid-gas | | |
| Hydrogen ($H_2$) | 77.1–70.8 (l) (−259.32 °C to −252.88 °C) | −259.32 | 6.38–9.66 (l) (−259.32 °C to −252.88 °C) | 0.073–0.099 (l) (−259.32 °C to −252.88 °C) 0.017–0.167 (g) | 58.00 | Solid-liquid | | [22,23,48] |
| | 1.34–0.094 (g) (−252.88 °C to −13.15 °C) | −252.88 | 12.15–14.12 (g) (−252.88 °C to −13.15 °C) | (−252.88 °C to −13.15 °C) | 461.00 | Liquid-gas | | |
| Neon (Ne) | 1251.6–1207.7 (l) (−248.54 °C to −246.09 °C) | −248.54 | 2.12–1.86 (l) (−248.54 °C to −246.09 °C) | | 16.44 | Solid-liquid | | [22,49] |
| | 9.46–0.90 (g) (−246.09 °C to −3.15 °C) | −246.09 | 0.83–1.03 (g) (−246 °C to 0 °C) | 0.023–0.045 (g) (−173 °C to 0 °C) | 85.75 | Liquid-gas | | |
| Nitrogen ($N_2$) | 860–806 (l) (−209.26 °C to −195.80 °C) | −209.85 | 1.97–2.06 (l) (−209.26 °C to −195.80 °C) | 0.163–0.136 (l) (−209.26 °C to −195.80 °C) | 25.80 | Solid-liquid | Superconducting flywheel energy storage | [15,16,22,23,40] |
| | 4.61–1.25 (g) (−195.80 °C to −0.93 °C) | −195.80 | 1.12–1.04 (g) (−195.80 °C to −0.93 °C) | 0.0075–0.024(g) (−195.8 °C to −0.93 °C) | 199.18 | Liquid-gas | Medical and food product transportation | |
| Carbon Monoxide (CO) | 847.4–791.4 (l) (−205.00 °C to −191.52 °C) | −205.00 | 2.12–2.21 (l) (−205.00 °C to −191.52 °C) | 0.18–0.15 (l) (−205.00 °C to −191.52 °C) | | Solid-Liquid | | [22] |
| | 4.36–1.27 (g) (−191.52 °C to −3.15 °C) | −191.52 | 1.14–1.04 (g) (−192 °C to 0 °C) | 0.0082–0.025 (g) (−192 °C to 0 °C) | 214.86 | Liquid-gas | | |
| Propane ($C_3H_8$) | 732–581 (l) (−186.67 °C to −42.12 °C) | −186.67 | 1.87–2.25 (l) (−186.67 °C to −42.12 °C) | 0.21–0.13 (l) (−186.67 °C to −42.12 °C) | 79.60 | Solid-Liquid | | [22,50] |
| 1-Butene ($C_4H_8$) | 734.1–601.3 (l) (−137.25 °C to −0.49 °C) | −185.35 | 1.97–2.31 (l) (−137.25 °C to −0.49 °C) | 0.22–0.12 (l) (−137.25 °C to −0.49 °C) | 68.58 | Solid-Liquid | | [22,51–54] |
| Propene ($C_3H_6$) | 754.9–609.1 (l) (−173.15 °C to −47.69 °C) | −185.15 | 0.85–1.29 (s) (−223 °C to −193 °C) 1.81–2.18 (l) (−173.15 °C to −47.69 °C) | 0.18–0.15 (l) (−173.15 °C to −47.69 °C) | 71.29 | Solid-Liquid | | [22,51–53] |
| Oxygen ($O_2$) | 1302–1141 (l) (−217.79 °C to −182.96 °C) | −218.35 | 1.67–1.70 (l) (−217.79 °C to −182.96 °C) | 0.20–0.15 (l) (−217.79 °C to −182.96 °C) | 13.70 | Solid-Liquid | | [22,23,48] |
| | 4.47–1.43 (g) (−182.96 °C to 0 °C) | −182.96 | 0.971–0.917 (g) (−182.96 °C to 0 °C) | 0.008–0.025 (g) (−182.96 °C to 0 °C) | 213.06 | Liquid-gas | | |
| Methane ($CH_4$) | 450–422 (l) (−181.46 °C to −161.48 °C) | −182.5 | 3.37–3.48 (l) (−181.46 °C to −161.48 °C) | 0.21–0.18 (l) (−181.46 °C to −161.48 °C) | 58.43 | Solid-Liquid | | [22,50] |
| | 1.82–0.72 (g) (−161.48 °C to 0 °C) | −161.48 | 2.22–2.18 (g) (−161.48 °C to 0 °C) | 0.012 to 0.03 (g) (−161.48 °C to 0 °C) | 510.83 | Liquid-gas | | |
| Isopentane ($C_5H_{12}$) | 787.8–639.9 (l) (−160 °C to 0 °C) | −160.15 | 1.87–2.15 (l) (−160 °C to 0 °C) | 0.187–0.117 (l) (−160 °C to 0 °C) | 71.10 | Solid-Liquid | Pumped thermal energy storage (used as a sensible material) | [18,22,50,53,55] |
| 2-Methylpentane ($C_6H_{14}$) | 807–671 (l) (−153 °C to 0 °C) | −153.15 | 1.77–2.12 (l) (−153 °C to 0 °C) | 0.144–0.114 (l) (−113 °C to 0 °C) | 72.76 | Solid-Liquid | Space exploration | [22,53,56] |
| Isoprene ($C_5H_8$) | 854–843 (s) (−170 °C to −158 °C) 829–700 (l) (−143 °C to 0 °C) | −142.15 | 0.95–1.08 (s) (−170 °C to −158 °C) 1.80–2.10 (l) (−143 °C to 0 °C) | 0.18–0.13 (l) (−123 °C to 0 °C) | 72.22 | Solid-Liquid | | [22,53,57,58] |
| Dimethyl ether ($C_2H_6O$) | 735 (l) (−25 °C) | −141.50 | 2.22 (l) (−33 °C) | 0.24–0.18 (l) (−123 °C to -25 °C) | 107.23 | Solid-Liquid | | [22,53,54] |
| Butane ($C_4H_{10}$) | 735–602 (l) (−138 °C to −1 °C) | −137.15 | 1.97–2.31 (l) (−138 °C to −1 °C) | 0.18–0.12 (l) (−138 °C to −1 °C) | 80.2 | Solid-Liquid | | [22] |
| Pentane ($C_5H_{12}$) | | −129.75 | | 0.173–0.121 (l) (−123 °C to 0 °C) | 116.43 | | | [22,59,60] |

(*continued on next page*)

**Table 2** (*continued*)

| Material | Density (kg/m$^3$) | Transition Temperature (°C) | Specific heat Capacity (J/(g·K)) | Thermal Conductivity (W/(m·K)) | Latent heat (J/g) | Phase | Application(s) mentioned in literature | Reference |
|---|---|---|---|---|---|---|---|---|
| | 756–645 (l) (−123 °C to 0 °C) | | 1.97–2.21 (l) (−123 °C to 0 °C) | | | Solid-Liquid | Boil-off Gas (BOG) re-liquefaction of an LNG terminal | |
| Nitrogen Trifluoride ($NF_3$) | 1776–1538 (l) (−183 °C to −129 °C)<br>6.24–3.19 (g) (−129 °C to 0 °C) | −128.95 | 1.00–1.02 (l) (−183 °C to −129 °C)<br>0.56–0.72 (g) (−129 °C to 0 °C) | | 162.71 | Liquid-gas | | [22] |
| Cyclopropane ($C_3H_6$) | 733–678 (l) (−79 °C to −34 °C) | −127.15 | 1.93 (l) (−33 °C) | 0.136 (l) (−37 °C) | 129.28 | Solid-Liquid | | [22,61] |
| Ethanol ($C_2H_6O$) | 826–807 (l) (−25 °C to 0 °C) | −114.35 | 1.02–1.38 (s) (−173 °C to −123 °C)<br>2.02–2.27 (l) (−25 °C to 0 °C) | 0.167 (l) (25 °C) | 108.53 | Solid-Liquid | | [22,62] |
| Methanol ($CH_4O$) | 904–810 (l) (−97 °C to −0 °C) | −97.15 | 1.46–1.62 (s) (−113 °C to −98 °C)<br>2.20–2.40 (l) (−97 °C to 0 °C) | 0.210–0.206 (l) (−50 °C to −10 °C) | 99.25 | Solid-Liquid | Space exploration | [22,23,63,64] |
| n-Hexane ($C_6H_{14}$) | 760–677 (l) (−93 °C to 0 °C) | −95.15 | 1.88–2.15 (l) (−93 °C to 0 °C) | 0.156–0.135 (l) (−93 °C to 0 °C) | 151.78 | Solid-Liquid | Pumped thermal energy storage (used as a sensible material) | [22,44] |
| Cyclopentane ($C_5H_{10}$) | 751 (l) (25 °C) | −93.95 | 1.30–1.27 (s) (−133 °C to −103 °C)<br>1.42–1.69 (l) (−93 °C to 0 °C) | 0.143 (l) (−20 °C) | 8.56 | Solid-Liquid | | [22,65,66] |
| Methylamine ($CH_5N$) | 700 (l) (−10 °C) | −93.15 | 1.60–2.23 (s) (−143 °C to −96 °C)<br>3.19–3.26 (l) (−87 °C to −21 °C) | 0.219 (l) (−7 °C) | 197.38 | Solid-Liquid | | [22,43,67] |
| n-Heptane ($C_7H_{16}$) | 774–700 (l) (−88 °C to 0 °C) | −90.55 | 1.96–2.15 (l) (−88 °C to 0 °C) | 0.156–0.138 (l) (−88 °C to 0 °C) | 140.12 | Solid-Liquid | | [22,68] |
| Ethane ($C_2H_6$) | 641–544 (l) (−173 °C to −88 °C)<br>2.05–1.36 (g) (−88 °C to 0 °C) | −88.15 | 2.33–2.43 (l) (−173 °C to −88 °C)<br>1.34–1.66 (g) (−88 °C to 0 °C) | 0.25–0.17 (l) (−173 °C to −88 °C)<br>0.009–0.018 (g) (−88 °C to 0 °C) | 489.47 | Liquid-gas | | [22,50] |
| Methyl ethyl ketone ($C_4H_8O$) | 826 (l) (0 °C) | −86.65 | 0.98–1.42 (s) (−173 °C to −93 °C)<br>2.07–2.16 (l) (−83 °C to 0 °C) | 0.17–0.15 (l) (−73 °C to 0 °C) | 117.05 | Solid-liquid | | [22,43,53,69,70] |
| Acetylene ($C_2H_2$) | 764.3–760.2 (s) (−142 to −132 °C) | −84.15 | 1.37 (g) (−73 °C) | 0.020 (g) (0 °C) | 144.39 | Solid-gas | | [22,54,71] |
| Carbon Dioxide ($CO_2$) | 1562 (s) (−79 °C)<br>2.47–1.98 (g) (−53 °C to 0 °C) | −78.46 | 0.78–0.83 (g) (−53 °C to 0 °C) | 0.011–0.015 (g) (−53 °C to 0 °C) | 574 | Solid-gas | Medical and food product transportation | [22,23,72] |
| Ammonia ($NH_3$) | 728–682 (l) (−73 °C to −33 °C) | −78.2 | 4.23–4.45 (l) (−73 °C to −33 °C) | 0.80–0.67 (l) (−73 °C to −33 °C) | 332.2 | Solid-liquid | | [22,54] |
| n-Octane ($C_8H_{18}$) | 761–718 (l) (−53 °C to 0 °C) | −56.85 | 2.02–2.14 (l) (−53 °C to 0 °C) | 0.15–0.13 (l) (−53 °C to 0 °C) | 181.57 | Solid-liquid | | [22,73] |
| 2-Hexanone ($C_6H_{12}O$) | 830 (l) (0 °C) | −55.45 | 2.02–2.08 (l) (−53 °C to 0 °C) | 0.16–0.15 (l) (−53 °C to 0 °C) | 148.7 | Solid-liquid | | [7,22,32,53,74] |
| 3-Hexanone ($C_6H_{12}O$) | 833 (l) (0 °C) | −55.65 | 2.05–2.12 (l) (−53 °C to 0 °C) | 0.17–0.16 (l) (−53 °C to 0 °C) | 134.5 | Solid-liquid | | [7,22,32,53,74] |
| n-Nonane ($C_9H_{20}$) | 773–734 (l) (−50 °C to 0 °C) | −53.65 | 1.99–2.12 (l) (−50 °C to 0 °C) | 0.15–0.13 (l) (−53 °C to 0 °C) | 117.0 | Solid-liquid | | [7,22] |
| 3-Heptanone ($C_7H_{14}O$) | 822 (l) (15 °C) | −37.1 | | 0.15–0.14 (l) (−33 °C to 0 °C) | 153.5 | Solid-liquid | | [7,32,53] |
| | | −35.0 | | 0.15–0.14 (l) (−33 °C to 0 °C) | 172.6 | | | [7,22,32,53] |

(*continued on next page*)

**Table 2** (*continued*)

| Material | Density (kg/m$^3$) | Transition Temperature (°C) | Specific heat Capacity (J/(g·K)) | Thermal Conductivity (W/(m·K)) | Latent heat (J/g) | Phase | Application(s) mentioned in literature | Reference |
|---|---|---|---|---|---|---|---|---|
| 2-Heptanone ($C_7H_{14}O$) | 851–834 (l) (−20 °C to 0 °C) | | | | | Solid-liquid | | |
| Ammonia ($NH_3$) | 0.89–0.77 (g) (−33 °C to 0 °C) | −33.33 | 2.30–2.18 (g) (−33 °C to 0 °C) | 0.021–0.023 (g) (−33 °C to 0 °C) | 1372 | Liquid-gas | | [22,23] |
| 4-Heptanone ($C_7H_{14}O$) | 851–834 (l) (−20 °C to 0 °C) | −32.45 | | 0.15–0.14 (l) (−23 °C to 0 °C) | 141.5 | Solid-liquid | | [7,22,32,53] |
| n-Decane ($C_{10}H_{22}$) | 766–746 (l) (−25 °C to 0 °C) | −29.85 | 2.03–2.10 (l) (−25 °C to 0 °C) | 0.143–0.136 (l) (−25 °C to 0 °C) | 194 | Solid-liquid | | [7,22] |
| n-Undecane ($C_{11}H_{24}$) | 775–751 (l) (−25 °C to 0 °C) | −25.75 | 2.11–2.14 (l) (−23 °C to 0 °C) | 0.153–0.147 (l) (−23 °C to 0 °C) | 143.9 | Solid-liquid | Household refrigerator | [7,22,32,53,75,76] |
| 2-Octanone ($C_8H_{16}O$) | 854–837 (l) (−20 °C to 0 °C) | −21.55 | 2.13 (l) (25 °C) | 0.15–0.14 (l) (−18 °C to 0 °C) | 190.4 | Solid-liquid | | [7,22,32,53] |
| Diethylene glycol ($C_4H_{10}O_3$) | 1120 (l) (15 °C) | −10.4 | 2.21 (l) (0 °C) | 0.200–0.202 (l) (−8 °C to 0 °C) | 247 | Solid-liquid | Refrigeration system | [8,22,43,53,77–79] |
| n-Dodecane ($C_{12}H_{26}$) | 771–764 (l) (−9 °C to 0 °C) | −9.65 | 2.11–2.14 (l) (−9 °C to 0 °C) | 0.144–0.142 (l) (−9 °C to 0 °C) | 216.05 | Solid-liquid | | [22,43] |
| Tert-amyl alcohol ($C_5H_{12}O$) | 833–826 (l) (−5 °C to 0 °C) | −8.95 | 2.57 (l) (2 °C) | 0.149–0.147 (l) (−8 °C to 0 °C) | 50.6 | Solid-liquid | | [22,32,53,77,80] |
| Triethylene glycol ($C_6H_{14}O_4$) | 1127 (l) (15 °C) | −7 | 2.08 (l) (0 °C) | 0.193 (l) (0 °C) | 247 | Solid-liquid | | [8,22,43,53,81] |
| Heptanoic acid ($C_7H_{14}O_2$) | 918.1 (l) (20 °C) | −7 | 1.52–1.65 (s) (−43 °C to −23 °C) 1.95 (l) (−3 °C) | 0.17 (l) (−3 °C) | 118.6 | Solid-liquid | | [22,43,53,82,83] |
| Butyric acid ($C_4H_8O_2$) | 959 (l) (20 °C) | −5.4 | 1.46–1.82 (s) (−73 °C to −5 °C) 1.91 (l) (−3 °C) | 0.154 (l) (−3 °C) | 131.55 | Solid-liquid | | [22,43,53,83,84] |
| n-Tridecane ($C_{13}H_{28}$) | 775–770 (l) (−8 °C to 0 °C) | −5.15 | 1.31–1.75 (s) (−73 °C to −23 °C) 2.15 (l) (−3 °C) | 0.143 (l) (−5.3 °C) | 156.76 | Solid-liquid | | [7,22,32,75,85] |
| Caproic acid ($C_6H_{12}O_2$) | 929 (l) (20 °C) | −4 | 1.94 (l) (25 °C) | 0.15 (l) (0 °C) | 146.18 | Solid-liquid | | [22,43,53,79,83,86] |
| 5-Nonanone ($C_9H_{18}O$) | 830 (l) (10 °C) | −3.84 | 2.08 (l) (−3 °C) | 0.14 (l) (−3 °C) | 175.3 | Solid-liquid | | [7,22,32,53,74] |
| Butane ($C_4H_{10}$) | 2.70 (g) (0 °C) | −0.34 | 1.64 (g) (0 °C) | 0.0145 (g) (0 °C) | 385.71 | Liquid-gas | | [22] |

**Table 3**
Performance of nanoadditive and composite PCMs.

| Method | Additive | Remarks | Reference |
|---|---|---|---|
| Nanoparticles | Graphene Nanoplatelets (GnP) | Water with 0.5 vol% of GnP increased the thermal conductivity by ~24% in the liquid state and ~53% in the solid state. Freezing and melting times decreased with increased concentration of GnP. Used acid treatment to achieve stability after more than 10 cycles. | [98] |
| | | When added 1.2 wt% in water, increased the thermal conductivity by 12% in the liquid state and 56% in the solid state. The presence of GnP helped the nucleation process, reducing the solidification time by 25%. | [108] |
| | Graphene Oxide (GO) | The inclusion of 50 mg in 100 ml of deionized water reduces subcooling by 69% and reduces nucleation time by 91%. By using ultrasonic oscillation, the subcooling effect can be suppressed. Good stability was achieved with no visible sedimentation found after 6 months without vibration. | [109] |
| | | In combination with a carboxylic group, GO with 1 wt% could reduce the subcooling of ethylene glycol solution by 63%. | [110] |
| | $TiO_2$ | For $BaCl_2$ aqueous solution with a 0.5 wt%, the thermal conductivity is increased by 13%, and the subcooling is reduced by 85%. The PCT did not change significantly, and the latent heat decreased by 9.6%. Thermal stability proved after 50 cycles. | [111] |
| | | With 0.4 wt% in ethylene glycol water solution, the thermal conductivity increases by 7%, subcooling is reduced by 76%, and reduced the latent heat by 12%. Good dispersion stability achieved. | [112] |
| | MultiwalledCarbon Nanotubes (MWCNT) | Increased the thermal conductivity by 10.72% and reduced the subcooling by 86.9% when combined with nucleating agents. The melting temperature was not affected significantly. Decreased the latent heat by approximately 10%. Good thermal stability assured by adding thickeners (xanthan gum). | [99] |
| Thickening agents | Xanthan gum (XG) | The addition of 0.5 wt% of XG in a nanofluid PCM (based on a 23 wt% $MgCl_2$ eutectic solution) helped prevent phase separation and agglomeration after 400 thermal cycles. The presence of XG did not affect the subcooling. | [99] |
| | Sodium alginate | Used as an additive to a salt hydrate PCM. Decreased the enthalpy of fusion while significantly increased the phase stability, suppressed the subcooling and phase separation together with the nucleating agents (sodium tetraborate, sodium fluoride, and nanoactivated carbon). Thermally stable after 50 cycles. | [113] |
| Material Matrix | Graphite | A composite PCM made of compressed expansed natural graphite matrix with up to 95% of paraffin exhibited the same thermal conductivity as the sole porous graphite matrix (from 4 to 70 $W\,m^{-1}\,K^{-1}$ instead of the 0.24 $W\,m^{-1}\,K^{-1}$ of the pure paraffin). The presence of the matrix decreased the overall solidification time and maintained a stable thermal storage power. | [114] |
| | | A graphite matrix with water (90% volume fraction) as PCM showed a reduction of 67% in cooling time compared to water without additives. The presence of the matrix reduced the volumetric latent heat by 10%. When using the graphite matrix, the heat flux is about 4 and 3 times larger on heating and cooling than using pure water. | [115] |
| | Copper | Composite PCM made of copper foam and water reduced the solidification time by 88% and 77%, with foam porosities of 93% and 97%, respectively. | [116] |
| | | Composite PCM made of copper foam and water as PCM showed that the solidification time could be reduced by approximately 3 times with foam porosity of 90%. As the foam porosity increased, the effective conductivity was reduced. | [117] |
| | Porous silica | The composite made of porous silica and dodecane with several concentrations avoided the leakage of the PCM. By increasing the concentration of porous silica, the latent heat decreased up to 25% with 25 wt% of concentration. Also, by decreasing the density of porous silica, the thermal conductivity decreased (up to 45% decrease). The composite showed good performance and stability after more than 500 thermal cycles. | [118] |

water. The results showed a decrease in the freezing point of water while maintaining similar thermal properties as water itself. Also, there is a reduction in the subcooling effect due to the presence of oil. The aqueous alcohol solution is another option as PCM storage materials from 0 °C to −60 °C. Glycol and ethanol were studied at several concentrations to determine its freezing point and latent heat of fusion [95]. An increase in the concentration of alcohol decreases the freezing temperature of the solution. However, it also decreases the latent heat of fusion. Gunasekara et al. [96] studied mixtures of paraffins (dodecane and tridecane) as PCMs for refrigeration applications. These mixtures melted between −17 °C and −12 °C with latent heat from 165 kJ/kg to 185 kJ/kg and showed no subcooling. However, fewer organic homogenous PCMs are commercially available compared to inorganic homogenous PCMs.

### 2.2.3. Nanoadditive and composite PCM

There has been a development of innovative nanoadditive and composite PCMs for CTES at sub-zero temperatures. This type of PCM is formed by including complementary materials into the formula, such as adding nanoparticles, thickeners, or embedding the PCM in a matrix of porous material [77,97]. Combining these materials with the PCM can reduce subcooling, decrease nucleation time, increase thermal conductivity, and prevent leakage. Many commercial PCM products take advantage of including additives. However, in general, the nanoadditives and matrixes can reduce the latent heat, increase the cost of the PCM products, and deteriorate the stability. Therefore, the effect of including nanoadditives and matrixes should be evaluated carefully to ensure an overall enhancement in the performance of PCMs.

Nanoparticles in PCM increase thermal conductivity, improve nucleation, and reduce the subcooling effect. Many nanoparticles have been investigated for sub-zero temperature PCMs. The performance of graphene nanoplatelets (GnP), graphene oxide (GO), $TiO_2$, and multiwalled carbon nanotubes (MWCNT) are listed in Table 3. Some of them can act as nucleating agents to induce nucleation sites and reduce the subcooling; some can also enhance the heat transfer or decrease the PCT. Therefore, all of the listed materials realized a significant increase in thermal conductivity and a decrease in subcooling. However, they may also decrease the latent heat, agglomerate over time, and affect the uniformity of the material [77]. Acid treatment [98] or adding thickening agents [99] were reported to enhance the stability for some PCMs significantly, yet not all studies tested the long-term performance of adding nanoparticles in PCMs. Besides the materials listed in Table 3, more have been used for above-zero PCMs, for example, copper oxide (CuO) [100], aluminum oxide ($Al_2O_3$) [101], barium carbonate ($BaCO_3$) [102], silicon dioxide ($SiO_2$) [103,104], graphite powder [105], nano silver-titania (Ag-$TiO_2$) [106], magnesium sulfate ($MgSO_4$), strontium chloride ($SrCl_2$) [7], and sodium hexafluoroaluminate ($Na_3AlF_6$) [107]. Their potential of being used for sub-zero PCMs are worth exploring.

Adding thickening agents to PCMs improves their performance during thermal cycles by preventing nucleating agent precipitation and reducing phase separation. Sometimes, thickening agents are used together with nucleating agents jointly. However, thickening agents could compromise the thermal properties of the storage materials as well [25]. The use of sodium alginate and xantham gum (XG) are presented in Table 3; both helped enhance stability significantly. More thickening agents, especially various types of cellulose, can also be investigated in future studies for sub-zero temperature PCMs.

Matrix composite materials mainly improve the heat conductivity of the PCMs at a low cost. This method also helps with phase separation and leakage problems during phase change [107]. Metal matrixes can improve thermal conductivity and hold the PCM during the melting

process, reducing phase separation [116]. Carbon-based matrixes are also suitable due to their high porosity, low density, superior thermal conductivity, and high surface area [87]. In general, as long as the inserted matrix material is highly conductive, a fin effect can be expected to significantly enhance the heat transfer with minimum compromising of the energy density [115]. The composite PCM's overall effective thermal conductivity can even be as high as that of the matrix material, which is much higher than the thermal conductivity of the PCM without the matrix [114]. The performance of graphite, copper, and porous silica matrix is shown in Table 3. More matrixes, such as aluminum foam, graphene, carbon nanotubes, porous nano-titanium dioxide, porous expanded perlite, diatomite and montmorillonite, are also worth exploring for sub-zero temperature composite PCMs.

A list of existing and potential homogenous mixtures, nanoadditive and composite PCMs, is provided in Table 4 with their thermophysical properties and applications mentioned in the literature. Table 5 shows a list of commercial PCMs available for sub-zero applications.

As a summary and comparison of the pure substance, homogenous mixture, nanoadditive and composite PCMs, the heat of fusion of 101 different non-commercial solid-liquid PCMs (taken from Table 2 and Table 4) and 5049 commercial PCMs (taken from Table 5 and categorized into organic and inorganic materials according to the claims of the suppliers) are plotted against their melting temperatures in Fig. 4. In general, the heat of fusion decreases significantly as the melting temperature decreases for both non-commercial and commercial PCMs. For non-commercial PCMs, eutectic water-salt solutions have large heat of fusion, but their melting temperatures are also high. The melting temperatures of organic materials range from almost 0 °C to nearly −200 °C, yet their heat of fusion is usually lower than the inorganic material on the same temperature levels. Inorganic pure substances have the lowest melting temperatures but stay in the liquid phase for limited temperature ranges between the melting points and the boiling points.

On the other hand, compared to various non-commercial PCM candidates available at all temperature ranges, the lowest melting temperature reported for commercial PCM products is −114 °C, and the thermal conductivities of commercial PCM products decrease significantly if the melting temperature is around −100 °C. Moreover, similar to non-commercial PCMs, the inorganic commercial PCMs generally have a higher heat of fusion and thermal conductivities. Although many organic materials have the potential to be used as PCMs, more inorganic PCMs have been developed commercially, many of which are eutectic water-salt solutions with additives.

Furthermore, the energy density of the existing PCMs below −150 °C is not obviously higher than sensible materials anymore. New PCMs with higher heat of fusion and thermal conductivity in low-temperature ranges can be the directions for future research in CTES material development.

#### 2.2.4. Macroencapsulated PCM

Macroencapsulation refers to confining PCMs in containments from several milliliters to several liters. It can be used standalone as a thermocline CTES unit in an active or passive refrigeration system or as the filler of a packed-bed CTES system. Macroencapsulation is, by far, the most widely used PCM encapsulation technique [136]. It incorporates large amount of PCM in a low-cost way [136], protects the PCM from contamination and volume change from the outside [137], helps enhance the heat transfer by providing a larger heat transfer surface and reduced thermal resistance due to limited thickness [138].

Various research groups and companies have developed macroencapsulation containment concepts for sub-zero temperature. A macroencapsulation containment always includes an air cushion to compensate for the material volume change, especially for rigid capsules, which also enhances the mechanical stability of the storage system [139,140]. The containment shapes can be spherical, rectangular, cylindrical, pouches, flat-plate, and other specially made shapes to fit specific uses [8,140–142]. Examples of some typical macroencapsulation containment are illustrated in Fig. 5.

Materials for the macroencapsulation containment can be both metallic or plastic [140]. Since the containment is in direct contact with the PCMs, and sometimes with the HTFs as well, the containment materials should be carefully selected to avoid potential corrosion problems for each application. Oró et al. [143] tested the corrosion effect of four metals (copper, aluminum, stainless steel, carbon steel) and four polymers (polypropylene (PP), high-density polyethylene (HDPE), polyethylene terephthalate (PET) and polystyrene (PS)) against three commercial PCM materials and six PCM materials developed at the University of Lleida (PCT between −22 °C and −16 °C). Some materials used oxyethylmethylcellulose (CMC), $AlF_3$, NaCl, and $NH_4Cl$ as the additives. After one, four, and twelve weeks of testing, stainless steel 316 showed a low corrosion rate and was the only metallic material recommended for long use by the authors. Copper and carbon steel showed high corrosion rates as well as the presence of precipitates and pH changes; therefore, they cannot be used as the containment material. Aluminum has already been used in several macroencapsultion applications [144–146]. However, in this study, pitting and bubbles appeared on the surfaces of the aluminum samples, indicating that holes may form if the containment is made by aluminum for these PCMs. On the other hand, all four polymers – PP, PS, PET, and HDPE – turned out to be suitable materials for macroencapsulation containment. Other advantages of polymers include lost cost, low density, and easy shaping. The results are summarized in Table 6.

#### 2.2.5. Microencapsulated PCM

Microencapsulation, on the other hand, refers to containing the PCM in capsules at a micro-scale (a few millimeters or less) that hold the material inside and avoids changing the composition of the material due to contact with the environment [140]. The capsule shells are usually made from polymers such as polyamides, polyurethanes, polyureas, and polyesters [147,148]. Microencapsulation creates a large surface area, improves the heat transfer and mechanical stability, diminishes agglomeration, minimizes phase separation, and improves cycling stability [7,25,140,149].

However, there is limited literature regarding the long-term thermal performance of microencapsulated PCM. This method needs improvements to avoid the destruction of the capsules during thermal cycles [150]. Microencapsulation techniques have also been shown to increase the subcooling effect in PCMs, which is a major drawback for its application as CTES materials [151]. Methods to solve the problem include adding nucleating agents as well as changing the composition and structure of the shell. Future work can also be done to develop standardized procedures to test the leakage and stability performance of microcapsules, which is crucial for further commercial development and acceptance [152].

Regarding the microencapsulation manufacturing processes, both physical and chemical methods are still too complicated, which should be improved to reduce the production costs [149]. If using the physical methods, there can be a considerable decrease in the PCM's energy storage capacity [25].

A qualitative comparison of macroencapsulation and microencapsulation of PCMs is presented in Table 7 with their advantages and disadvantages.

#### 2.2.6. Slurry PCM

The slurry is a unique type of PCM, which is a stable suspension of PCM particles in a carrier fluid. The energy stored is the combination of the PCM's latent heat and the sensible heat of the carrier fluid. The slurry performs like a liquid at all times; therefore, it can be pumped, stored in tanks, discharged directly, and passed through a heat exchanger to work as the storage material and HTF simultaneously [153,154]. Among various types of phase-change slurries (PCS), ice slurry, dry ice slurry, and microencapsulated PCS can be or has the potential to be used for sub-zero temperature applications [149,155].

**Table 4**
Existing and potential homogenous mixture/nanoadditive and composite PCMs for sub-zero temperatures.

| Composition | Type | Melting Temperature (°C) | Heat of fusion (kJ/kg) | Thermal conductivity (W/(m·K)) | Density (kg/m$^3$) | Application(s) mentioned in the literature | Refs. |
|---|---|---|---|---|---|---|---|
| 24.8 wt% HCl | Eutectic water-salt solution | −86 | 73.77 (kJ/mol) | | | | [8] |
| 24 wt% LiCl | Eutectic water-salt solution | −67 | 36.26 (kJ/mol) | | | | [8] |
| 51 wt% $ZnCl_2$ | Eutectic water-salt solution | −62 | 116.84 | | | | [7] |
| 33.1 wt% $FeCl_3$ | Eutectic water-salt solution | −55 | 155.52 | | | | [7] |
| 29.8 wt% $CaCl_2$ | Eutectic water-salt solution | −55 | 164.93 | | | | [7] |
| 30.5 wt% $CaCl_2$ | Eutectic water-salt solution | −49.5 | 76.81 (kJ/mol) | | | | [8] |
| Sodium lactate/$H_2O$ (85.15:14.85 wt%) | Multicomponent organic mixture | −49 | 28.3 | | | | [7] |
| Sodium acetate/$H_2O$ (23.96:76.04 wt%) | Multicomponent organic mixture | −43 | 29.7 | | | | [7] |
| 36 wt% $CuCl_2$ | Eutectic water-salt solution | −40 | 166.17 | | | | [7] |
| Ethylene glycol/$H_2O$ (50:50 wt %) | Multicomponent organic mixture | −37.1 | 41.59 | | | | [110] |
| 39.6 wt% $K_2CO_3$ | Eutectic water-salt solution | −36.5 | 165.36 | | | | [7] |
| 17.1 wt% $MgCl_2$ | Eutectic water-salt solution | −33.6 | 221.88 | | | | [7] |
| 21.01 wt% $MgCl_2$ | Eutectic water-salt solution | −33.5 | 36.30 (kJ/mol) | | | | [8] |
| 30.5 wt% $Al(NO_3)_3$ | Eutectic water-salt solution | −30.6 | 131–207.63 | | 1283 (l)<br>1251 (s) | | [7,8] |
| 34.6 wt% $Mg(NO_3)_2$ | Eutectic water-salt solution | −29 | 186.93 | | | | [7] |
| 39.4 wt% $Zn(NO_3)_2$ | Eutectic water-salt solution | −29 | 169.88 | | | | [7] |
| 32.3 wt% $NH_4F$ | Eutectic water-salt solution | −28.1 | 187.83–199.1 | | | | [7,107] |
| 40.3 wt% NaBr | Eutectic water-salt solution | −28 | 175.69 | | | | [7,119] |
| NaCl-$NaNO_3$-$H_2O$ | Eutectic water-salt solution | −27 | 50–150 | | | | [120] |
| Corn-oil ester/Tap water (35:65 vol%) | Multicomponent organic mixture | −27 | 68.7 | | | | [94] |
| Ethylene glycol/Sodium formate/$H_2O$ (1:1:8 wt%) | Multicomponent organic mixture | −25 | 173.1 | | | | [7] |
| 27.9 wt% $Li_2SO_4$ | Eutectic water-salt solution | −23 | 26.10 (kJ/mol) | | | | [8] |
| NaCl-KCl-$H_2O$ | Eutectic water-salt solution | −23 | 260 | | | | [120] |
| Glycerol/Sodium formate/$H_2O$ (1:1:8 wt%) | Multicomponent organic mixture | −23 | 174.5 | | | | [7] |
| Corn-oil ester/Tap water (30:70 vol%) | Multicomponent organic mixture | −23 | 78.6 | | | | [94] |
| 21.5 wt% KF | Eutectic water-salt solution | −21.6 | 225.2–227.13 | | | | [7] |
| 22.4 wt% NaCl | Eutectic water-salt solution | −21.2 | 222–235 | 0.57 | 1165 (l)<br>1180 (s) | | [7,8,107,119] |
| NaCl-$Na_2SO_4$-$H_2O$ | Eutectic water-salt solution | −21 | 200 | | | | [120] |
| 34% Ethylene glycol/$H_2O$ (vol. %) | Multicomponent organic mixture | −20.3 | 164 | 0.482 | 1481 (l) | | [112] |
| Polyethylene glycol 200/ Polyethylene glycol 300 (4:96 wt%) | Multicomponent organic mixture | −20 | | | | Household freezer | [121] |
| Corn-oil ester/Tap water (25:75 vol%) | Multicomponent organic mixture | −19.5 | 85 | | | | [94] |
| 25 wt% $MgCl_2$ | Eutectic water-salt solution | −19.4 | 223.1 | | | | [7] |
| Ethylene glycol/Sodium acetate/$H_2O$ (1:1:8 wt%) | Multicomponent organic mixture | −19 | 118.5 | | | | [7] |
| 18% NaCl/5% super absorbent polymer (SAP)/0.03% diatomite/$H_2O$ | Eutectic water-salt solution | −19 | 120.6 | 0.48 | | Freezer | [122,123] |
| 39.7 wt% $(NH_4)_2SO_4$ | Eutectic water-salt solution | −18.5 | 187.75–269 | | | | [7,107] |

(*continued on next page*)

**Table 4** (*continued*)

| Composition | Type | Melting Temperature (°C) | Heat of fusion (kJ/kg) | Thermal conductivity (W/(m·K)) | Density (kg/m$^3$) | Application(s) mentioned in the literature | Refs. |
|---|---|---|---|---|---|---|---|
| Sodium formate/$H_2O$ (1:4 wt%) | Multicomponent organic mixture | −18 | 250.2 | | | | [7] |
| 36.9 wt% $NaNO_3$ | Eutectic water-salt solution | −17.7 | 187.79 | | | | [7] |
| 41.2 wt% $NH_4NO_3$ | Eutectic water-salt solution | −17.4 | 186.29 | | | | [7] |
| 35 wt% $Ca(NO_3)_2$ | Eutectic water-salt solution | −16 | 199.35 | | | | [7] |
| 19.5 wt% $NH_4Cl$ | Eutectic water-salt solution | −16 | 248.44–289 | | | Freezer | [7,107] |
| Polyethylene glycol 200/ Polyethylene glycol 300 (20:80 wt%) | Multicomponent organic mixture | −15 | | | | Household freezer | [121] |
| Ethylene glycol/Sodium propionate/$H_2O$ (1:1:8 wt%) | Multicomponent organic mixture | −15 | 127.8 | | | | [7] |
| Corn-oil ester/Tap water (20:80 vol%) | Multicomponent organic mixture | −15 | 107.3 | | | | [94] |
| Glycerol/Sodium acetate/$H_2O$ (1:1:8 wt%) | Multicomponent organic mixture | −14 | 156 | | | | [7] |
| Glycerol/Sodium propionate/ $H_2O$ (1:1:8 wt%) | Multicomponent organic mixture | −14 | 123.2 | | | | [7] |
| 36.8 wt% $K_2HPO_4$ | Eutectic water-salt solution | −13.5 | 189–197.79 | | | | [7,107] |
| Ethylene glycol/Sodium lactate/$H_2O$ (1:1:8 wt%) | Multicomponent organic mixture | −12 | 157.4 | | | | [7] |
| 30 wt% $Na_2S_2O_3$ | Eutectic water-salt solution | −11 | 219.86 | | | | [7] |
| 19.5 wt% KCl | Eutectic water-salt solution | −10.7 | 253.18 | | | | [7] |
| 32.2 wt% $MnSO_4$ | Eutectic water-salt solution | −10.5 | 213.07 | | | | [7] |
| Corn-oil ester/Tap water (15:85 vol%) | Multicomponent organic mixture | −10.5 | 125.0 | | | | [94] |
| 22% Ethylene glycol/$H_2O$ (vol.%) | Multicomponent organic mixture | −10.3 | 252 | 0.523 (l) | 1313 (l) | | [112] |
| Dodecane encapsulated in zein | Multicomponent organic mixture | −10 | 34.5–30.7 | | | Food packaging | [124] |
| Glycerol/Sodium lactate/$H_2O$ (1:1:8 wt%) | Multicomponent organic mixture | −10 | 159.3 | | | | [7] |
| Polyethylene glycol 200/ Polyethylene glycol 300 (30:70 wt%) | Multicomponent organic mixture | −10 | | | | Household freezer | [121] |
| 20 wt% KCl | Eutectic water-salt solution | −10 | 284 | | | Household refrigerator | [125] |
| 32.4 wt% $NaH_2PO_4$ | Eutectic water-salt solution | −9.9 | 214.25 | | | | [7] |
| 40:60 Tridecane:Dodecane (wt.%) | Paraffin mixture | −9.7 | 159 | | | | [7] |
| n-Dodecane ($C_{12}H_{26}$) | Alkane (Paraffin) (Microencapsulated) | −9.5 | 216.2 | 2.21 (l) | 748–764.84 (l) | | [7,8,22,77] |
| 50:50 Tridecane:Dodecane (wt.%) | Paraffin mixture | −9.1 | 145 | | | | [7] |
| $TiO_2$/$BaCl_2$/$H_2O$ ($TiO_2$ 0.283 vol%) | Nanofluid PCM | −8.6 | 258.3 | | | | [7] |
| $TiO_2$/$BaCl_2$/$H_2O$ ($TiO_2$ 1.13 vol%) | Nanofluid PCM | −8.5 | 254.2 | | | | [7] |
| $TiO_2$/$BaCl_2$/$H_2O$ ($TiO_2$ 0.167 vol%) | Nanofluid PCM | −8.5 | 279.5 | | | | [7] |
| $TiO_2$/$BaCl_2$/$H_2O$ ($TiO_2$ 0.565 vol%) | Nanofluid PCM | −8.2 | 257.4 | | | | [7] |
| 60:40 Tridecane: Dodecane (wt.%) | Paraffin mixture | −8 | 147 | | | | [7] |
| 22.5 wt% $BaCl_2$ | Eutectic water-salt solution | −7.8 | 246.44 | | | | [7] |
| Corn-oil ester/Tap water (10:90 vol%) | Multicomponent organic mixture | −7.5 | 171.7 | | | | [94] |
| 27.2 wt% $ZnSO_4$ | Eutectic water-salt solution | −6.5 | 208–235.75 | | | | [7,107] |
| Corn-oil ester/Tap water (7.5:92.5 vol%) | Multicomponent organic mixture | −6.0 | 222.7 | | | | [94] |
| 24.5 wt% $Sr(NO_3)_2$ | Eutectic water-salt solution | −5.75 | 243.15 | | | | [7] |
| 16.95 wt% $KHCO_3$ | Eutectic water-salt solution | −5.4 | 268.54 | | | | [7] |

(*continued on next page*)

**Table 4** (*continued*)

| Composition | Type | Melting Temperature (°C) | Heat of fusion (kJ/kg) | Thermal conductivity (W/(m·K)) | Density (kg/m$^3$) | Application(s) mentioned in the literature | Refs. |
|---|---|---|---|---|---|---|---|
| 80:20 Tridecane:Dodecane (wt.%) | Paraffin mixture | −5.4 | 126 | | | | [7] |
| 10 wt% NaCl | Eutectic water-salt solution | −5 | 289 | | | Household refrigerator | [125] |
| 12% Ethylene glycol/$H_2O$ (vol.%) | Multicomponent organic mixture | −4.9 | 281 | 0.558 (l) | 1172 (l) | | [112] |
| 20.6 wt% $NiSO_4$ | Eutectic water-salt solution | −4.15 | 258.61 | | | | [7] |
| Tetradecane/octadecane | Paraffin mixture | −4.02 | 227.52 | | | | [8] |
| 19 wt% $MgSO_4$ | Eutectic water-salt solution | −3.9 | 264.42 | | | | [7] |
| 12.7 wt% $Na_2SO_4$ | Eutectic water-salt solution | −3.55 | 284.95 | | | | [7] |
| 3.9 wt% NaF | Eutectic water-salt solution | −3.5 | 309.2–314.09 | | | | [7,107] |
| Corn-oil ester/Tap water (5:95 vol%) | Multicomponent organic mixture | −3.5 | 227.8 | | | | [94] |
| Propylene glycol/$H_2O$ (10:90 vol%) | Multicomponent organic mixture | −3 | | | | Chilled food refrigerated cabinet | [126] |
| 19 wt% NaOH | Eutectic water-salt solution | −2.8 | 265.98 | | | | [7] |
| 9.7 wt% $KNO_3$ | Eutectic water-salt solution | −2.8 | 296.02 | | | | [7,119] |
| 5.9 wt% $Na_2CO_3$ | Eutectic water-salt solution | −2.1 | 281–310.23 | | | | [7,107] |
| 13.04 wt% $FeSO_4$ | Eutectic water-salt solution | −1.8 | 286.81 | | | | [7] |
| 11.9 wt% $CuSO_4$ | Eutectic water-salt solution | −1.6 | 290.91 | | | | [7] |
| 6.49 wt% $K_2SO_4$ | Eutectic water-salt solution | −1.55 | 268.8 | | | | [107] |
| 80:20 Tridecane:Tetradecane (wt.%) | Paraffin mixture | −1.5 | 110 | | | | [7] |
| 60:40 Tridecane:Tetradecane (wt.%) | Paraffin mixture | −0.5 | 138 | | | | [7] |

Ice slurry is the most common kind of slurry for cooling applications and the food industry [149,156]. It is formed by liquid water as the carrier liquid and ice particles as the dispersed phase. During the melting process, the dispersed phase disappears and has to be reintroduced by an ice slurry generator. Freezing point depressants can reduce the freezing point of the ice slurry from 0 to −30 °C and lower [157,158]. Theoretically, any organic or inorganic material that can form a water solution (as listed in Table 4) can be used as a freezing depressant to generate an ice slurry [159]. The most commonly used freezing point depressants are sodium chloride, ethanol, ethylene glycol, and propylene glycol [158], while methanol, glycerol, ammonia, potassium carbonate, calcium chloride, magnesium chloride, potassium acetate, and potassium formiate were also studied [159,160]. However, an ice slurry's energy density is more related to the ice fraction than the type of freezing point depressants [157]. The enthalpies of various ice slurries have been calculated and plotted in enthalpy-phase diagrams by Melinder et al. [161].

Similar to ice slurry, dry ice slurry contains liquid carbon dioxide and dry ice particles. The theoretical temperature range is between −56 and −80 °C, which is suitable for low-temperature refrigeration [155,162].

A microencapsulated slurry is a stable solid–liquid suspension consists of a carrier liquid and microencapsulated PCMs. It contains the PCM in small droplets by microencapsulation made from polymers [149]. The microencapsulation helps avoid the PCM dispersion in the carrier liquid, avoid the agglomeration of PCM particles, protect the PCM from the environment, and improve mechanical stability. However, they usually have high cost, relatively low thermal conductivity, and their performances tend to deteriorate after long-term operation [149,163].

In general, slurry systems with additives can offer promising opportunities for CTES applications, especially for refrigeration and air conditioning [8,163]. Future research still needs to understand the basic physical properties of the slurries for system design; new additives should also be tested for sub-zero temperature applications [155].

### 2.3. Thermochemical energy storage materials

Thermochemical materials (TCMs) store and release thermal energy through chemical reactions. The energy stored through a solid–gas reaction can be described using Equation (3):

$$S' + \mathrm{HEAT} \leftrightarrow S + G \tag{3}$$

where $S'$ and $S$ are solid, and $G$ is a gas.

These materials' heat storage capacity can be between 5 and 15 times higher than sensible materials, but the system complexity is the highest among all thermal storage technologies [156].

Chemical sorption storage is the most widely investigated type of thermochemical storage for CTES. There are two kinds of sorption storage: absorption (on liquid materials) and adsorption (on solid materials) [164]. Both absorption and adsorption involve two kinds of materials – a sorbent and a refrigerant known as a working pair – to transfer cold energy through an absorption or adsorption process performed in a sorption cycle. The working principle of sorption storage is discussed in detail by Hauer [164] and Li et al. [7].

Several working pairs have been investigated for absorption storage at sub-zero temperatures, and the most commonly used working pair is water and ammonia ($H_2O/NH_3$) since $NH_3$ can evaporate below 0 °C

**Table 5**
Commercial Latent thermal energy storage materials.

| Material | Producer | Density (kg/m$^3$) | Transition temperature (°C) | Specific heat capacity (J/(kg·K)) | Thermal conductivity (W/(m·K)) | Latent heat (kJ/kg) | Reference |
|---|---|---|---|---|---|---|---|
| E-114 | PlusIce | 782 | −114.0 | 2390 | 0.170 | 107 | [127] |
| E-90 | PlusIce | 786 | −90.0 | 2560 | 0.140 | 90 | [127] |
| E-78 | PlusIce | 880 | −78.0 | 1960 | 0.140 | 115 | [127] |
| E-75 | PlusIce | 902 | −75.0 | 2430 | 0.170 | 102 | [127] |
| E-65 | PlusIce | 1180 | −65.0 | 3280 | 0.560 | 240 | [127] |
| E-62 | PlusIce | 1300 | −62.0 | 4010 | 0.580 | 180 | [127] |
| E-60 | PlusIce | 1280 | −60.0 | 2900 | 0.440 | 172 | [127] |
| SP −50 | Rubitherm | 1300 | −50.0 | 2000 | 0.600 | 200 | [128] |
| E-50 | PlusIce | 1325 | −50.0 | 3280 | 0.560 | 175 | [127] |
| – | TEAP | – | −50.0 | – | – | 325 | [129] |
| E-46 | PlusIce | 1205 | −46.0 | 3050 | 0.540 | 240 | [127] |
| va-Q-accu −37G | Va-Q-Tec | 1500 | −37.0 | 3150 | – | 213 | [130] |
| E-37 | PlusIce | 1500 | −37.0 | 3150 | 0.540 | 225 | [127] |
| Puretemp −37 | Puretemp | 880 | −37.0 | 1990 | 0.150 | 145 | [131] |
| E-34 | PlusIce | 1205 | −34.0 | 3050 | 0.540 | 200 | [127] |
| SN 33 | Cristopia | 1240 | −33.0 | – | – | 245 | [132] |
| HS 30 N | Pluss | 1425 | −33.0 | 2700 | – | 224 | [134] |
| va-Q-accu −32G | Va-Q-Tec | 1300 | −32.0 | 2950 | – | 243 | [130] |
| E-32 | PlusIce | 1290 | −32.0 | 2950 | 0.560 | 225 | [127] |
| TH 31 | TEAP | – | −30.5 | – | – | 131 | [129] |
| PCM −30 | Microtek | 730 | −30.0 | – | – | 150 | [133] |
| E-29 | PlusIce | 1420 | −29.0 | 3690 | 0.640 | 250 | [127] |
| SP −30 | Rubitherm | 1200 | −28.5 | 2000 | 0.600 | 250 | [128] |
| SP −28 | Rubitherm | 1300 | −28.5 | 2000 | 0.600 | 260 | [128] |
| SN 29 | Cristopia | – | −29.0 | – | – | 233 | [132] |
| SN 26 | Cristopia | – | −26.0 | – | – | 268 | [132] |
| E-26 | PlusIce | 1250 | −26.0 | 3670 | 0.580 | 265 | [127] |
| HS 26 N | Pluss | 1200 | −25.0 | 3600 | – | 272 | [134] |
| – | TEAP | – | −23.0 | – | – | 330 | [129] |
| SP −24 | Rubitherm | 1300 | −22.5 | 2000 | 0.600 | 250 | [128] |
| Climsel C-21 | Climator | 1100 | −22.5 | – | 0.330 | 285 | [135] |
| E-22 | PlusIce | 1180 | −22.0 | 3340 | 0.570 | 305 | [127] |
| HS 23 N | Pluss | 1140 | −22.0 | 3400 | 0.702 | 262 | [134] |
| TH 21 | TEAP | – | −21.0 | – | – | 222 | [129] |
| SN 21 | Cristopia | 1120 | −21.0 | – | – | 240 | [132] |
| va-Q-accu −21G | Va-Q-Tec | 1150 | −21.0 | 3300 | – | 234 | [130] |
| E-21 | PlusIce | 1240 | −21.0 | 3130 | 0.510 | 285 | [127] |
| Puretemp −21 | Puretemp | 1060 | −21.0 | 3430 | 0.550 | 239 | [131] |
| Climsel C-18 | Climator | 1150 | −20.5 | – | 0.560 | 288 | [135] |
| SP −21 | Rubitherm | 1200 | −20.0 | 2000 | 0.600 | 285 | [128] |
| E-19 | PlusIce | 1125 | −19.0 | 3290 | 0.580 | 300 | [127] |
| HS 18 N | Pluss | 1095 | −18.0 | 3480 | 0.440 | 242 | [134] |
| SP −17 | Rubitherm | – | −17.5 | 2000 | 0.600 | 300 | [128] |
| SN 18 | Cristopia | 1210 | −17.5 | – | – | 268 | [132] |
| – | TEAP | | −16.0 | | | 330 | [129] |
| HS 15 N | Pluss | 1070 | −15.0 | 3400 | 0.530 | 308 | [134] |
| TH 16 | TEAP | – | −15.5 | – | – | 289 | [129] |
| E-15 | PlusIce | 1060 | −15.0 | 3870 | 0.530 | 320 | [127] |
| Puretemp −15 | Puretemp | 1030 | −15.0 | 2060 | 0.550 | 301 | [131] |
| E-14 | PlusIce | 1220 | −14.8 | 3510 | 0.530 | 243 | [127] |
| AN 15 | Cristopia | – | −15.44 | – | – | 311 | [132] |
| E-12 | PlusIce | 1110 | −12.3 | 3470 | 0.560 | 250 | [127] |
| E-11 | PlusIce | 1090 | −12.0 | 3550 | 0.570 | 310 | [127] |
| SP −11 UK | Rubitherm | 1200 | −11.5 | 2000 | 0.600 | 330 | [128] |
| SP −11 | Rubitherm | 1200 | −11.5 | 2000 | 0.600 | 290 | [128] |
| AN 12 | Cristopia | – | −11.72 | – | – | 306 | [132] |
| AN 10 | Cristopia | – | −10.41 | – | – | 310 | [132] |
| PCM −10 | Microtek | 750 | −10.0 | – | – | 180 | [133] |
| E-10 | PlusIce | 1140 | −10.0 | 3330 | 0.560 | 286 | [127] |
| HS 10 N | Pluss | 1125 | −10.0 | 3400 | 0.602 | 290 | [134] |
| TH 10 | TEAP | – | −10.0 | – | – | 283 | [129] |
| MPCM (−10) | Microtek | – | −9.5 | – | – | 150–160 | [133] |
| RT − 9 HC | Rubitherm | 760 | −9.0 | 2000 | 0.200 | 250 | [128] |
| SP −7_2 | Rubitherm | 1200 | −6.0 | 2000 | 0.600 | 290 | [128] |
| E-6 | PlusIce | 1110 | −6.0 | 3830 | 0.560 | 300 | [127] |
| HS 7 N | Pluss | 1120 | −7.0 | 3500 | 0.550 | 296 | [134] |
| AN 06 | Cristopia | – | −5.5 | – | – | 284 | [132] |
| RT − 4 | Rubitherm | 760 | −4.0 | 2000 | 0.200 | 180 | [128] |
| E-3 | PlusIce | 1060 | −4.0 | 3840 | 0.600 | 330 | [127] |
| E-4 | PlusIce | 1060 | −3.9 | 3780 | 0.580 | 282 | [127] |

(*continued on next page*)

**Table 5** (*continued*)

| Material | Producer | Density (kg/m$^3$) | Transition temperature (°C) | Specific heat capacity (J/(kg·K)) | Thermal conductivity (W/(m·K)) | Latent heat (kJ/kg) | Reference |
|---|---|---|---|---|---|---|---|
| TH 4 | TEAP | – | −4.0 | – | – | 386 | [129] |
| HS 3 N | Pluss | 1060 | −2.5 | 3980 | 0.350 | 346 | [134] |
| AN 03 | Cristopia | – | −2.6 | – | – | 328 | [132] |
| E-2 | PlusIce | 1070 | −2.0 | 3800 | 0.580 | 325 | [127] |
| Puretemp −2 | Puretemp | 1020 | −2.0 | 4020 | 0.600 | 277 | [131] |

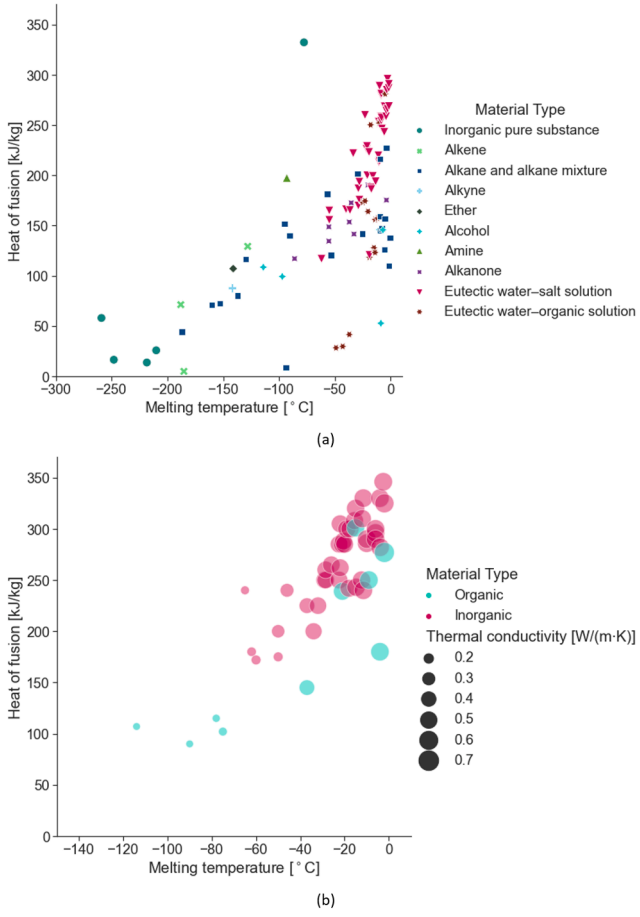


**Fig. 4.** (a) The heat of fusion of 95 non-commercial PCM compositions mentioned in the literature (taken from Table 3 and Table 5). (b) The heat of fusion and thermal conductivity of 50 commercial PCM products claimed by the suppliers (taken from Table 6). In general, the heat of fusion decreases with the melting temperature. Inorganic PCMs have larger heat of fusion, but organic PCMs cover a wider temperature range. Most commercial PCM products are inorganic, while no commercial product is available for temperatures lower than −114 °C.

[7,165]. The disadvantages of $H_2O/NH_3$ are: ammonia is toxic, and the system requires high operating pressures. Other working pairs proposed are $LiNO_3/NH_3$, $NaSCN/NH_3$, $SrCl_2/NH_3$, $MgCl_2/NH_3$, $CaCl_2/NH_3$, $MnCl_2/NH_3$, $FeCl_2/NH_3$, and $NiCl_2/NH_3$ as listed in Table 8 [7,165]. Among them, $SrCl_2/NH_3$ delivers the highest storage capacity. For the adsorption process, $CaCl_2/NH_3$ has a high adsorption capacity, but it has problems such as expansion, corrosion, and deterioration [7]. Improvements in sorption storage can be made by enhancing the heat and mass transfer of the reactors, looking for more working pairs, and using composite materials [166].

Since chemical sorption storage involves a sorption cycle, which is an energy conversion process different from the other CTES materials, and thermochemical storage based on reversible reactions is rarely mentioned in the literature for sub-zero temperatures, the rest of this paper will mainly focus on CTES technologies using sensible and latent thermal energy storage materials.

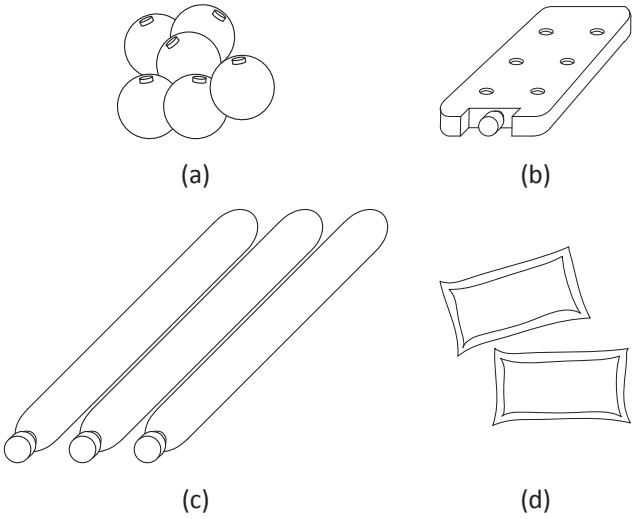


**Fig. 5.** Schematics of PCM macroencapsulation shapes: (a) spherical; (b) rectangular; (c) cylindrical; (d) pouches.

### 2.4. Summary and outlook of CTES material studies

The selection of a suitable thermal energy storage material is the foremost step in CTES design. The materials that can be used for cold storage applications are mainly sensible thermal energy storage materials and PCMs. However, many of the listed materials present corrosion, safety, and phase separation issues (in the case of PCMs) to be overcome before considering them as proper CTES material candidates. For example, fire retardants can be added to suppress the flammability of organic materials used for low-temperature applications [167,168].

A series of comprehensive lists of existing and potential materials are presented in this section and summarized in Table 9. The development stage of each type of material is summarized according to the Technology Readiness Level (TRL) defined by the National Aeronautics and Space Administration (NASA) of the United States of America [169]. TRL of 1 represents the most fundamental research, and TRL of 9 denotes actual systems deployed in real applications. Suitable applications are summarized from existing literature and suggested according to the characteristics of the materials.

Sensible materials are low cost, reliable, and have been used in various commercial applications. For sensible solid materials, future research can pay attention to the use of locally available materials and recycled materials. On the other hand, sensible liquid materials need to overcome corrosion and safety issues before being used for CTES.

The amount of the PCMs investigated is significant compared to sensible thermal energy storage materials. Among the lists of PCMs, chemical elements, compounds, and homogenous mixtures are the majority. There are also new materials under development, such as microencapsulated PCMs and PCMs with improved thermal properties based on additives. Off-the-shelf availability of the complete lists of

**Table 6**
Stability of metallic containment materials by Oró et al. [143].

| | Copper | Aluminum | Stainless steel | Carbon steel |
|---|---|---|---|---|
| PCM-A: C-18 | Not recommended | Not recommended | Recommended | Not recommended |
| PCM-B: E-21 | Not recommended | Not recommended | Recommended | Caution recommended |
| PCM-C: PCM-B + 1% CMC | Not recommended | Not recommended | Recommended | Caution recommended |
| PCM-D: 19% $NH_4Cl + H_2O$ | Not recommended | Not recommended | Recommended | Not recommended |
| PCM-E: PCM-D + 1% CMC | Not recommended | Caution recommended | Recommended | Not recommended |
| PCM-F: PCM-D + 3% $AlF_3$ | Not recommended | Not recommended | Recommended | Not recommended |
| PCM-G: PCM-F + 1% CMC | Not recommended | Not recommended | Not recommended | Not recommended |
| PCM-H: PCM-D + 3% NaCl | Not recommended | Not recommended | Recommended | Not recommended |
| PCM-I: PCM-H + 1% CMC | Caution recommended | Recommended | Recommended | Caution recommended |

**Table 7**
Advantages and disadvantages of macroencapsulation and microencapsulation.

| Advantages | Disadvantages | Suitable CTES type(s) |
|---|---|---|
| *Macroencapsulation* | | |
| Lower cost<br>Large surface area and limited thickness to enhance heat transfer<br>Avoidance of contamination of PCM and change of properties<br>Various shapes available with flexible or rigid materials<br>Rigid macroencapsulation enhances the mechanical stability of the storage system | There could be corrosion between the PCM and the container | Packed-bed and thermocline |
| *Microencapsulation* | | |
| Large surface area to enhance heat transfer<br>Improve cycling stability<br>Avoid the agglomeration of PCM particles<br>Avoid contamination of PCM and change of properties | Higher cost<br>Increase the subcooling<br>Possible destruction of the capsules | Shell-and-tube<br>Slurry-based |

materials with their corresponding thermo-physical properties in low-temperature ranges allows readers to start evaluating the overall storage capacity of CTES and further select the appropriate CTES design. A significant portion of PCMs have already been applied mostly to the refrigeration sector, yet the rest are experimentally and numerically tested with various cold storage designs. There is a selection of commercial and non-commercial PCMs, with good and moderate thermo-physical properties, currently clustered in a temperature range of −50 °C to 0 °C. Due to the lack of options among current PCMs available for cryogenic applications, one clear future research direction in cold storage materials using PCMs should move towards cryogenic temperature ranges to explore new materials with high thermal storage capacity. Besides, one should prioritize the energy density and the cost when developing PCMs for cryogenic cold storage applications to replace earth-abundant rock-like sensible thermal energy storage materials, which are currently used for cryogenic cold storage applications. More methods to resolve subcooling and phase separation effects should also be investigated, including a deeper understanding of the mechanisms of heat transfer, transport characteristics, and stability of microencapsulation and nanoparticle additives [7]. It is also important to search for more additives that allow for easy adjustment of the melting temperatures and evaluate the long-term performance of nanoadditive and composite materials [8].

For thermochemical energy storage, the sorption cycle is the only type that has been widely studied. Ammonia/water is the most commonly used working pair. Due to the toxicity and high-pressure requirement on the systems based on ammonia, other alternative pairs of sorbents and refrigerants should be investigated. Future research can also optimize the sorption system, reduce the system cost [7], and search for more sorption and reversible reaction materials.

## 3. Numerical studies of CTES containment and heat transfer

Using numerical modeling tools before prototype construction for a detailed analysis is an essential part of any TES system design. Usually, parameters like storage capacity, operating conditions (mainly temperatures and pressures) of the storage are estimated firstly. Subsequently, the storage materials and storage types are selected. The subcooling effect should also be considered in the case where PCM is used as the storage material. Finally, mechanical properties of materials such as elasticity, plasticity, and transition to glassy state at sub-zero temperatures also need special attention in the numerical models to better understand the full CTES system.

Regarding the existing literature, almost all of the numerical studies found are limited to simple rectangular, cylindrical, or spherical forms of cold storage containers, while computational domains were mainly 1-D, 2-D, and 2-D axisymmetric, meaning that the geometries of storage devices were purposefully simplified to reduce computational costs and complexity of the model.

This part of the review presents the up-to-date available research papers related to the numerical modeling of CTES, which are classified according to their storage design, together with information about the numerical method and dimension of the simulation domain, software used, temperature range, and storage material.

An exception is made on numerical studies related to materials, where heat transfer analysis is carried out to understand the fundamentals of thermal energy storage process in a small amount of cold storage material effectively encapsulated.

### 3.1. Packed-bed and thermocline CTES

A packed-bed system consists of a single tank of storage material, also called filler material, which takes profit of the thermocline effect. The filler materials can be solid, like rocks, quartzite, ceramic pebbles [175], or PCMs contained in macroencapsulated containments. To charge and discharge the energy to and from the system, a liquid or gas is used as HTF to transfer the energy from the heat/cold source to the filler material.

Together with experimental studies, numerical analyses – mostly in 1-D computational domains – have been conducted to estimate the cold storage performance of packed-bed technology.

**Table 8**
Energy storage capacity for working pairs [7,165].

| Working Pairs | Evaporator temperature (°C) | Energy stored (kJ/kg) |
|---|---|---|
| $H_2O/NH_3$ | −20 | 122.4 |
| $LiNO_3/NH_3$ | −20 | 129.6 |
| $CaCl_2/NH_3$ | −20 | 295.2 |
| $SrCl_2/NH_3$ | −20 | 432.0 |
| $MgCl_2/NH_3$ | −20 | 360.0* |
| $FeCl_2/NH_3$ | −20 | 316.8* |
| $NiCl_2/NH_3$ | −20 | 313.2* |
| $MnCl_2/NH_3$ | −20 | 324.0* |

* Approximate values from Fig. 3 of [165].

**Table 9**
Summary of CTES materials.

| Material type | Temperature range mentioned in the literature (°C) | Compatible CTES types | Current development stage and Technology Readiness Level (TRL) | Pros | Cons/technical challenges | Suitable applications |
|---|---|---|---|---|---|---|
| Sensible materials (solids) | −170 to 0 | Packed-bed and thermocline | Commercially available for some applications TRL: 8–9 [19,20] | Low cost and high reliability, materials widely available, wide temperature range, suitable for large scale storage, environmentally friendly | Lower energy and exergy density, larger pressure drop | Large-scale electricity storage*, large-scale refrigeration, large-scale waste cold recovery |
| Sensible materials (liquids) | −153 to 0 | Packed-bed and thermocline | Some candidate materials selected but have not been widely applied TRL: 2–5 [18,44,170] | Can act as the HTF and the thermal energy storage material at the same time | Working temperature range limited by freezing and boiling point, low energy and exergy density, can be flammable, corrosive and toxic, become viscous at cryogenic temperatures | Large-scale electricity storage*, large-scale refrigeration, large-scale waste cold recovery |
| Pure substances PCMs | −210 to 0 | Packed-bed and thermocline, shell-and-tube, plate-shaped | Some materials are already deployed commercially TRL: 5–9 [59,60] | High energy and exergy density, wide temperature range | Can be flammable, corrosive, and toxic, need to be stored in pressurized or open containers for solid–gas/liquid–gas phase transition, need to handle subcooling and volume change | Small- and large-scale active and passive refrigeration*, large-scale waste cold recovery*, small- and large-scale electricity storage* |
| Homogeneous mixture PCMs | −86 to 0 | Packed-bed and thermocline, shell-and-tube, plate-shaped | Many eutectic solutions are commercially available, more under development TRL: 5–9 [121,144,145,171,172] | High energy and exergy density, tunable freezing point | Need to handle subcooling, volume change, and phase separation due to incongruent melting | Small-scale active and passive refrigeration*, small-scale waste cold recovery*, small-and large-scale refrigeration |
| Nanoadditive and composite PCMs | −114 to 0 | Packed-bed and thermocline, shell-and-tube, plate-shaped | Additives for salt mixture and paraffin available, more under development TRL: 3–9 [123,173,174] | Improves the thermal conductivity, avoids phase separation, reduces of subcooling effect, increases the growth rate | Reduces latent heat, increases cost, particles tend to agglomerate over time | Small- and large-scale active and passive refrigeration*, small- and large-scale waste cold recovery* |
| Microencapsulation and other slurry PCMs | −140 to 0 | Packed-bed and thermocline, shell-and-tube, plate-shaped, slurry-based | Ice slurry for refrigeration commercially available, dry ice slurry in a conceptual phase, more microencapsulation under development TRL: 3–6 [149,155–157] | Better heat capacity and heat transfer coefficient, avoids agglomeration, slurries can be used as the storage and HTF at the same time, able to be pumped and have the combined energy density of the PCM latent heat and sensible heat of the carrier fluid | Microcapsulation related: high cost, microcapsulation can be destroyed at mid/long term, increase subcooling Slurry related: stratification issue, heavy mechanical power required to generate small and smooth ice crystals and to maintain the ice slurry in the homogeneous state, lack of full understanding of the basic physical properties | Small- and large-scale active refrigeration*, small- and large-scale waste cold recovery |
| Thermochemical materials | −30 to 0 | Absorption and adsorption cycles | Ammonia absorption commercially available, other types in the early stages TRL: 1–9 [7,165] | Higher energy and exergy density | High system complexity, can be toxic and corrosive, may require high pressure to operate, low heat and mass transfers in adsorbent beds | Small- and large-scale active refrigeration* |

* Mentioned in the literature.

1-D numerical studies of packed-bed technology are often carried out using two phase models including Schumann's model, one and two-dimensional continuous solid phase models, and concentric dispersion model, where HTF and storage materials have separate energy equations to model their temperature profiles, while in one and two-dimensional single phase models, the temperature profiles of both HTF and storage materials are assumed to be the same and evaluated using a single energy equation. The latter model is applicable and able to provide reasonably accurate numerical results provided that the storage materials are highly thermal conductive that it can resemble the HTF temperature. Otherwise, two phase models are reliable, yet it requires stiffer control on the grid size and time step of the solver or numerical scheme compared to single-phase models.

Several studies have been devoted to assessing the storage performance of sensible packed-bed technology for cold storage purposes. Hüttermann et al. [17] numerically studied and compared packed-bed

storages based on nine different sensible storage materials: 4 metals – lead, aluminum 6061, zinc, stainless steel 304; 1 ceramic – aluminum oxide; 2 minerals – quartz, sodium chloride; and 2 plastics – polypropylene (PP) and polyethylene (PE). The influence of the temperature-dependent heat capacity of these nine materials at the cryogenic temperature range (i.e., charging at −150 °C and discharging at 20 °C) on the efficiencies of the storages with different materials under constant boundary conditions were compared. The materials are assumed to be spherical in shape, with the diameter and bed porosity assumed to be 10 mm and 0.4, respectively, while the mass flow rate at the inlet was set at 10 kg/s. Based on these parameters, the calculated Biot number was below 0.1, meaning that homogeneous temperature distribution within a particle could be a reasonable approximation. 1-D continuous solid phase model was adopted to consider the heat transfer between HTF and storage materials within the packed-bed along the flow direction. The equations were numerically solved, applying an explicit Lax-Wendroff scheme with second-order accuracy in time and space. According to the numerical results and calculation of the energy storage efficiency, materials such as PP, PE, sodium chloride, and quartz were promising candidates in terms of storage capacity, feasibility, and cost.

Sciacovelli et al. [19] numerically studied packed-bed cold storage as a component of a LAES system (shown in Fig. 6). The results were compared with the experimental data obtained from charging studies of the modular packed-bed comprising 4 U-shaped cells filled with quartzite pebbles. 1-D continuous solid phase model was adopted to estimate the performance of the packed-bed numerically. It was assumed that the heat transfer is significant along the flow direction only; therefore, the radial component of the model was neglected. Thus, the energy equations for HTF and storage materials were solved using Comsol Multiphysics software. The diameter and height of the storage were 12 m and 13.65 m, respectively. Furthermore, the average diameter of pebbles and the porosity of the bed were assumed to be 5 mm and 0.38 accordingly. The numerical results showed a good correspondence with the experimental temperature measurements at locations of 0.27, 1.7, and 3.13 m along the packed-bed axis during the charging studies. The actual packed-bed storage consisted of six identical partitioned cells, with equally distributed mass flow rate along with the cells. Numerical studies considered only one of the cells, where heat exchange between cells was also neglected.

Davenne et al. [18] compared the performance of a packed-bed and a liquid thermocline (as shown in Fig. 7) as cold storages for an off-shore wind driven pumped thermal energy storage system using a 1-D numerical modeling approach. The packed-bed was assumed to consist of concrete spheres with nitrogen gas as the HTF, while isopentane was considered as the storage/HTF medium in the liquid thermocline. Balancing the energy between convective HTF and storage materials and evaluating the rate of energy change within the elements of the liquid thermocline, 1-D single-phase convection–diffusion equations were developed for both storage types, where the equations included the speed of the thermal front and the effective diffusivity coefficient in the storage. Based on the numerical studies, it was found that the stratified liquid thermocline had significantly lower thermal diffusivity than the effective diffusivity of the packed-bed, giving it correspondingly lower heat transfer losses during the charging and discharging. Furthermore, the optimum radius of the packed-bed spheres and the aspect ratio of the storage tank was calculated based on the simulation results and calculations of exergy losses. The simulation results of the thermocline based thermal storage filled with liquid isopentane showed that the exergy loss could be reduced with increasing aspect ratio. The exergy loss for the thermocline was also calculated over the same example duty cycle with the packed-bed, and it was found to be significantly lower than the packed-bed with the exergy loss of 3.7 kW.

When encapsulated PCM is considered as the storage medium in packed-bed, enthalpy method is most commonly applied to capture both latent heat of fusion and sensible heat capacity in PCM capsules when solving for temperature profiles using the energy equations. The simplicity of the method allows using the same energy equation for both HTF and PCM storage, while introducing a “mushy zone” at the PCM phase transition range to disregard sharp discontinuities, which otherwise can create numerical instabilities. Besides, the necessity for tracking the phase transition front using computationally expensive adaptive mesh methods is diminished; therefore, a simplified fixed grid approach is applicable together with the enthalpy method to address the phase transition simulation in PCM storage containers with a reduced computational cost.

Thus, a few numerical studies have been conducted on the application of packed-bed technology filled with PCM capsules for cold energy storage below 0 °C. One of them belongs to Bejanaro et al. [176], where the authors proposed to improve the energy efficiency of the vapor-compression system integrating a PCM based packed-bed cold storage (Fig. 8a). Since the operation of the vapor-compression system is based on the circulation of two different fluids: refrigerant and secondary fluid, the standard packed-bed storage device was modified. Thus, the cold storage included PCM spheres bathed into an intermediate fluid and two bundles of pipes installed separately on the sides of the storage to circulate the refrigerant and secondary fluid. The ad hoc designed vegetable oil with the PCT of −30 °C was used as the PCM, and it was enclosed into spherical polymer capsules made of high-density polyethylene. An aqueous solution of 60% v/v ethylene glycol was used as the intermediate fluid, which transferred the thermal energy between the refrigerant and PCM capsules during the charging mode or between PCM capsules and the secondary fluid during the discharging mode. The pipe bundle in the storage system was assumed to be made of carbon steel. The preliminary results were obtained using only numerical studies since the proposed storage design had not been built. Thus, the numerical studies regarding the charging and discharging of the storage were carried out between the refrigerant (R404a) temperature −41 °C and secondary fluid (60% v/v propylene glycol) temperature −20 °C. The proposed discrete model, which considered the enthalpy method to model the heat transfer in the PCM, allowed to numerically simulate the full charging and discharging modes as well as series of partial charging and discharging modes.

Khor et al. [177] numerically studied the cascaded packed-bed storage containing three different encapsulated PCMs with cascaded phase change temperature values (PCT) along with the storage tank (Fig. 8(b)). Thus, the high-grade PCM had the lowest PCT with the value of −49 °C, while medium-grade and low-grade PCMs had PCTs equaled to −19.5 and 6.5 °C, respectively. The 1-D numerical approach based on the two-phase model was adopted to study the cascaded packed-bed numerically. The temperature change is assumed to be along the axial direction of the packed-bed only. The concentric dispersion model, together with the enthalpy method, was used to numerically study the heat transfer and resulting phase-change processes in the PCM capsules in a one-dimensional manner along the capsule radius. The results of the numerical studies could provide several performance maps of the

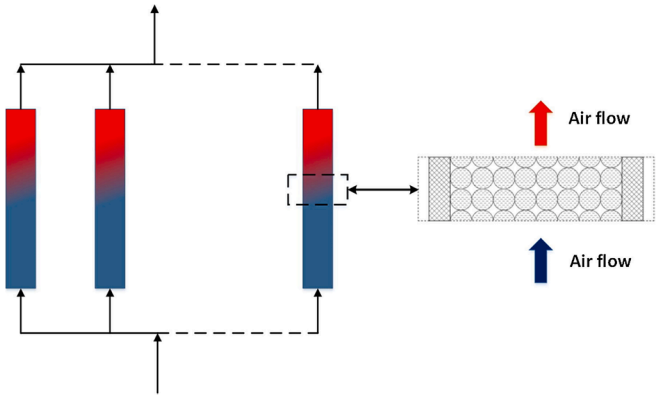


**Fig. 6.** Schematic of modular packed-bed high grade cold storage [19].

cascaded packed-bed storage, where different storage capacities within each temperature region depending on the amounts of the PCMs and various diameters of the encapsulated PCM particles showed a significant effect. Numerical simulation of packed-bed technology in higher dimensions (i.e., 2-D and 3-D) has been carried out so far only for above-zero thermal energy storage applications. However, the same approach is easily acceptable for the simulation of packed-bed technology designed for cold/cryogenic storage. Some of the advanced CFD studies on packed-beds can be found in the references [178,179].

Furthermore, Khor et al. [180] numerically studied the effect of granular material addition into voids of packed-bed storage filled with macroencapsulated PCM. Three different macroencapsulated PCM and four granular materials were considered, respectively. 1-D two-phase model was adopted, where heat transfer in macroencapsulated PCM was evaluated using the concentric dispersion model. Once validated with an experimental study, the 1-D model was used for the parametric analysis carried on a scaled-up cold storage tank. The parametric analysis included different macroencapsulated PCMs, types of granular materials, encapsulation sizes, and flow rates. The results showed that alumina particles resulted in the highest overall increment in the amount of the stored thermal energy due to their large density and heat capacity. Microencapsulated n-decane particles provided the highest overall enhancement on the cyclic efficiency of the packed-bed storage.

Macroencapsulation of PCMs in rectangular plate-shaped containers can be used standalone as a thermocline CTES unit in an active or passive refrigeration system. Zarajabad and Ahmadi [181] (Fig. 9) numerically studied the plate type PCM-based cold storage with various thicknesses (0.5, 1, 2, 3, 4, 5, and 6 cm), but with the constant surface area (28 × 43.5 $cm^2$) mounted in the freezer with the dimensions of 28 × 31.5 × 43.5 $cm^3$ to evaluate the effect of the stored cold in the PCM plate on the cooling efficiency of the freezer when the compressor of the refrigeration cycle was off. The eutectic solution of NaCl-$H_2O$ with the PCT of −21 °C was chosen as the PCM. The numerical simulation was based on the enthalpy method, and it was carried out in a 2-D rectangular domain with appropriate initial and boundary conditions. The results of the numerical study estimated that 3 cm thick PCM plate was the most appropriate one for this particular application.

Xu et al. [184] numerically studied the temperature development inside the refrigerated truck (3.8 × 1.75 × 1.75 $m^3$) due to the placement of the cold PCM plates to the walls. The eutectic salt-based cold storage PCM was said to have its melting point of around – 21.2 °C, which was cooled down to −30 °C, and the latter was considered in the numerical studies as the initial condition for the PCM plates in the refrigerator. On the other hand, three different temperature values were taken as the initial conditions of the refrigerator space: 20 °C, 25 °C, and 30 °C. Due to these temperature differences in the PCM plates and the refrigerating space, buoyancy forces driven flow takes place in the refrigerating space, and it was numerically studied using ANSYS software, where phase change processes in the PCM plates were modeled using the enthalpy method. The results showed that the complete discharging of the cold from the eight PCM plates by the natural convection

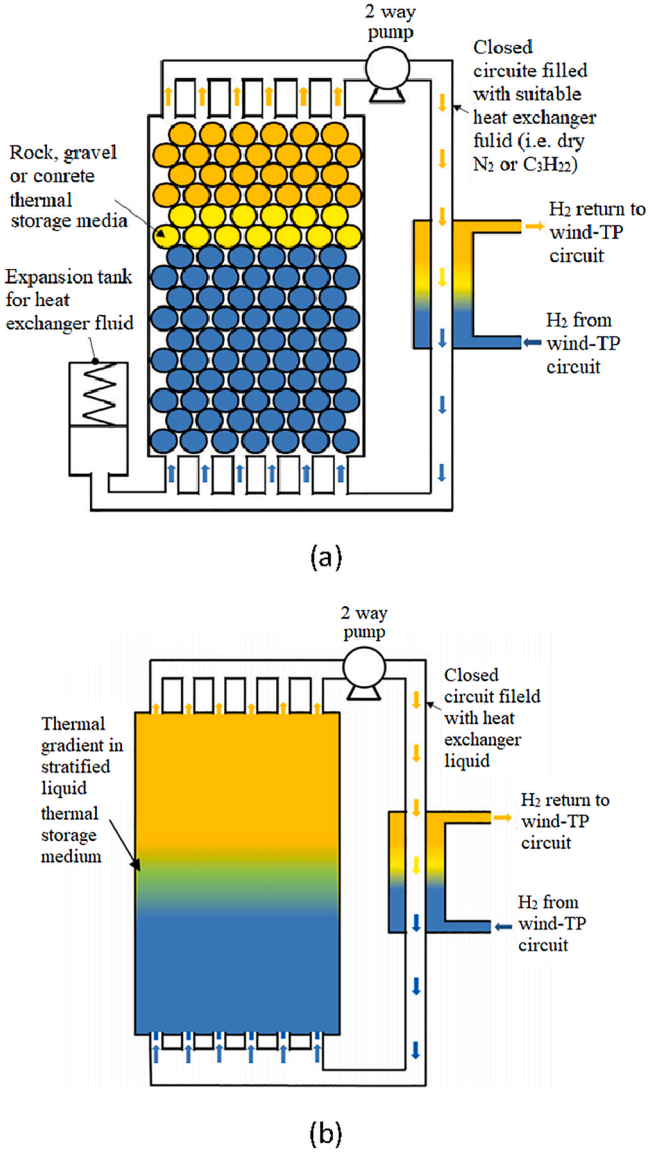


**Fig. 7.** CTES system for a pumped thermal energy storage system: (a) Packed-bed and (b) Liquid thermocline [18].

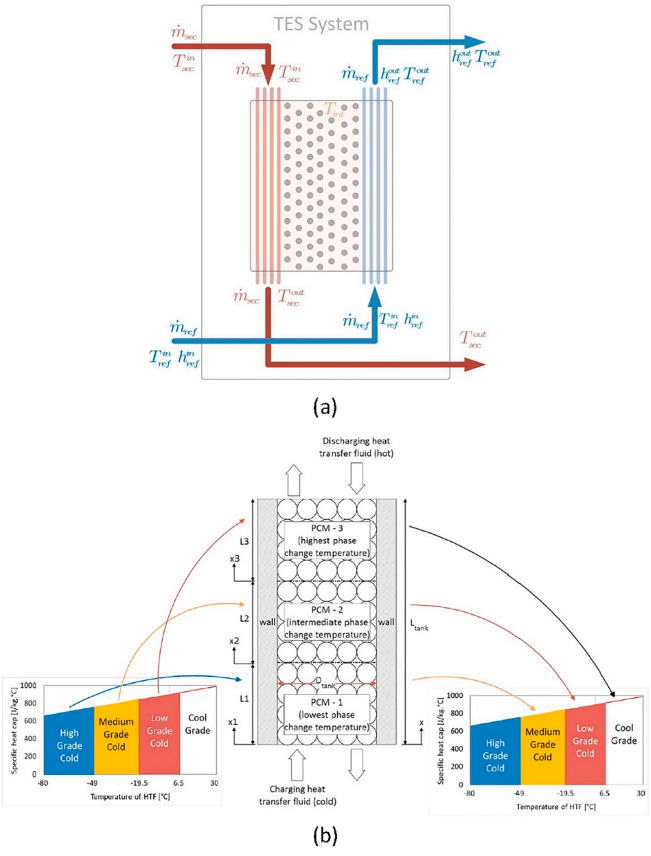


**Fig. 8.** Packed-bed type latent heat cold storage systems: (a) PCM spheres submerged into the intermediate fluid; [176] and (b) column of spheres with cascaded PCTs [177].

lasted up to nearly 82 h, leading to the stabilized temperature of the refrigerating space around 0 °C.

### 3.2. Shell-and-tube CTES

The operation principle of this type of TES system is similar to a shell-and-tube heat exchanger, where the thermal energy storage material locates on the shell side and the HTF on the tube side. During the charging phase, cold energy will be transferred to the thermal energy storage material; and during discharging, thermal energy storage material is heated by the HTFs inside the pipes. For systems using PCMs, the melted liquid will flow around the solid parts to enhance the heat transfer due to natural convection. The number of tubes in the heat exchanger, as well as their diameter and length, is going to determine the heat exchange coefficient for a given HTF flow rate, which is one of the more relevant parameters to optimize in models and simulations.

Several numerical studies have been conducted on shell-and-tube systems, where the PCM is water – mostly without any additives to lower the phase change temperature sub-zero. In the following references, attention should be paid to the extremely low values of the charging temperature, even though the PCM is water with a PCT of 0 °C.

Torras et al. [185] numerically studied the shell-and-tube CTES designed for a low thrust cryogenic propulsion system with a commercial software called TermoFluids. The numerical model was based on the coupling of the three subroutines: 1-D single-phase/two-phase flow model inside the heat transfer tube; 2-D axisymmetric heat conduction model in the solid parts; and 3-D solid–liquid two-phase flow model for the PCM storage, taking into account the turbulence convection modeling from the liquid side. Water is considered as the PCM, and the operating temperature range of the storage was taken to be from −195.0 °C up to 7.74 °C.

In another study, Tan et al. [186] simulated the operation of a rectangular container filled with water as the PCM and equipped with a copper tube for cryogenic gas (nitrogen) flow as the HTF in FLUENT. 2-D numerical studies were adopted, which included the enthalpy-porosity method for phase change modeling, and the results of the simulation could provide the temperature development (from −120 to 7 °C) from the side view of the tank.

Sang et al. [182] studied phase change processes of the full-scale vertical ice-on-coil type CTES using a numerical approach (Fig. 10). To reduce the pressure drop, tubes were partitioned into 8 passes, where each pass consisted of 92 series of tubes having an external diameter of 12.75 mm. Since these copper tubes were arranged into a staggering array and assuming that there was no thermal interaction between these tubes, the numerical problem was simplified to heat transfer simulation of 92 hexagonal 3-D tubes, numerically connected by using the outlet temperature of one tube to the inlet condition to the neighboring tube. The heat transfer and ice formation/melting around the coils were estimated using the enthalpy method, incorporated into the commercial software STAR-CCM.

### 3.3. Plate-shaped CTES

This type of CTES system uses plate-shaped storage materials. Thermal energy storage materials and the HTFs are separated by large plates parallels aligned in the storage unit. The plates are used to store energy in the form of latent heat, and are placed in a container tank, usually with a rectangular cross-section, separated with a fixed distance. The HTF circulates through the free room between the plates, allowing for the heat exchange between the storage materials and the HTF. The dimensions of the plates (thickness, height, and length) and the distance between the plates determine the final dimensions of the storage tank, which should be optimized according to the application requirements and the material thermo-physical properties.

Liu et al. [183] numerically and experimentally studied PCM slabs with dimensions of 0.26 m × 1.70 m × 0.025 m bundled together with the uniform gap of 0.6 cm into the container as the cold storage for the refrigerated enclosure (Fig. 11). The developed mathematical model was 1-D, where only the half-thickness of the PCM slab and the HTF passage (the gap between slabs) were numerically studied along the flow direction since slabs were bundled parallel to each other. Consequently, the heat transfer in the PCM slab along the axial direction, as well as the temperature variation of the HTF in the normal direction to the flow were ignored. Thus, considering the energy balance for the HTF along the flow direction between PCM slabs, and taking into account the convective heat transfer between HTF and PCM through the slab walls, the charge or discharge duration of the storage were numerically studied, and the accuracy of the model was validated through experimental studies.

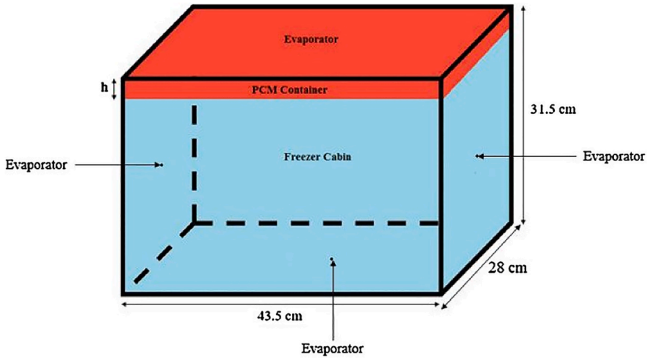


**Fig. 9.** Macroencapsulation used as a thermocline CTES installed on top of a freezer [181].

This model was later used for the optimization of the storage effectiveness of such CTES systems by Amin et al. [187]. The results showed that the storage density coefficient decreases with increasing gap thickness between the plates and mass flow rates. An optimized plate thickness can be found for a gap thickness and mass flowrate.

### 3.4. Microencapsulated PCM

Yu et al. [188] numerically described the thermo-mechanical behavior of microencapsulated phase change material slurries using spherical microcapsules filled with a commercial HTF, Dowtherm J as the core material with the PCT of −81 °C for dynamic and static cryogenic cold storage applications (Fig. 12). The numerical model is composed of energy conservation equations, pressure-dependent solid–liquid equilibria, Lamé's equations, and buckling theory. While microcapsules were charged with cryogenic cold, the PCM solidification resulted in the volume shrinkage and pressure decrease in the capsules. Due to the pressure difference between outside and inside media of the capsules, the deformation of the shell, made of melamine–formaldehyde (MF), was considered to take place. The shell thickness of microcapsules was optimized for mechanical stability using the thermo-mechanical model, as it was observed that the shell thickness had a negligible effect on the solidification of the PCM. Resistance to the buckling of the shell due to the pressure difference was increased by adding $Al_2O_3$ nanoparticles and electroless Cu plating on the shell surface. Thus, the thicknesses to avoid buckling of materials MF, MF-Cu, and MF-Cu-Al during the solidification of the PCM were optimized, and the ratio of the core radius to the shell thicknesses was suggested to be less than 72, 92, and 160, respectively.

### 3.5. Slurries-based CTES

In a slurry-based CTES system, ice-slurries or microencapsulated slurries are used as both the thermal energy storage material and the HTF. The numerical analysis carried out on CTES based on slurries are mostly divided into two types: (i) the development of slurries within

slurry generating units or heat exchangers; and (ii) the flow of slurries within pipes or channels under forced convection – pumping process to deliver generated slurry mass for certain applications. The flow and thermal behavior of slurries within pipes/channels are complex phenomena due to the simultaneous flow of ice particles and carrier fluid, especially under conditions of non-isothermal heat transfer with ambient.

The numerical studies that have been conducted regarding the latter so far have been mostly dedicated to understanding how flow regime (laminar or turbulent), rheological behavior, inlet slurry concentration, velocity, particle diameter, and particle volume fraction within the flow could affect the pressure drop along pipe/channels, mass transfer rate and eventually the quality of the slurry to be delivered for required applications. Since the transport of slurry is out of the scope of the current studies, only numerical studies of slurry generation (i.e., charging/discharging) and storage are reviewed. The reader may refer to [189] to get acquainted with the review studies on the transportation/flow of ice slurries.

A number of studies have been conducted to numerically study the generation of slurry mass. The hypereutectic binary aqueous ammonium chloride ($H_2O + NH_4Cl$) solution was proposed as the slurry for cold energy storage by Kumar et al. [190], and the process of the slurry generation was numerically modeled. The sidewalls of the cylindrical cavity – the slurry generating unit, which was assumed to have an initial temperature of 25 °C, was maintained below the eutectic temperature of the solution (−15.4 °C) for slurry development. The top and bottom surfaces of the unit were assumed to be insulated; therefore, the adiabatic boundary condition was assigned for these boundaries in the numerical studies. Different configurations and conditions such as cold boundary temperature, the initial concentration of the depressant, and the geometry (H:D ratio) of the cavity were set up as initial conditions in the numerical model to analyze the cold storage and effectiveness of the system (Fig. 13). The numerical studies were based on the fixed-grid continuum media formulation with the multiphase model, where three

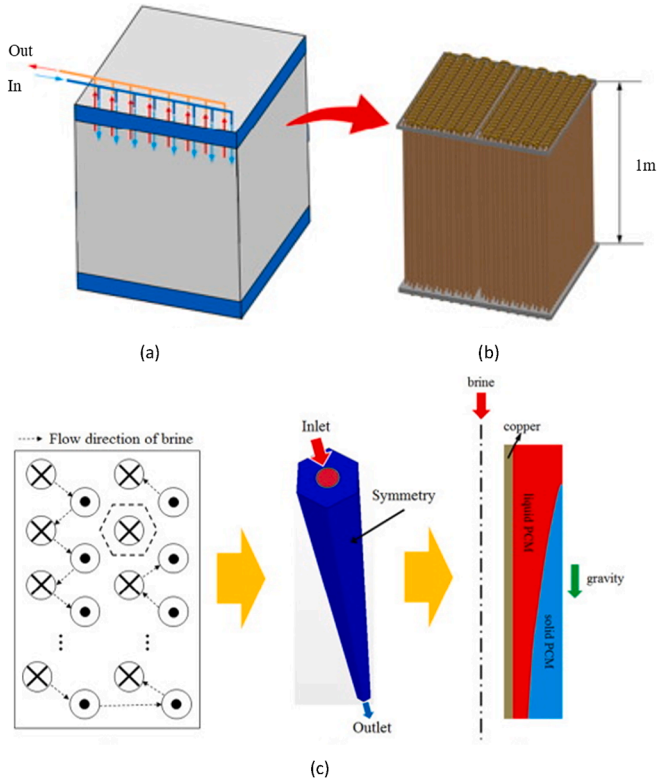


**Fig. 10.** Ice-on-coil type CTES: (a) overall design; (b) tube array; (c) simplifications for numerical modeling [182].

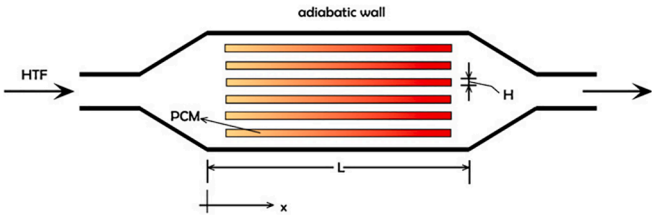


**Fig. 11.** Plate-shaped CTES equipped in the cold storage tank [183].

zones – a fixed solid region, a coherent mushy zone (immobile mushy region) and a non-coherent mushy zone (mobile mushy region) – were distinguished by the value of the so-called "critical ice fraction" or "packing fraction". In the vertical component of the momentum equation, three important terms were considered: Darcy effect in the porous packed region in the coherent zone with the permeability coefficient determined by Carman-Kozeny model; the sedimentation of the solid ice (i.e., gravity-related term); and the density change due to the concentration and temperature gradients (i.e., buoyancy related term), where the latter coupled the momentum equations with the energy and concentration equations. The 2-D axisymmetric computational domain was used to carry out the simulations, and the results provided time-dependent evolution of ice fraction, temperature, and concentration fields in the slurry generator, including the solid–liquid drift velocity field under the aforementioned configurations and initial conditions. The optimum slurry generating conditions were achieved at the values of 0.75H/D aspect ratio, 0.1527 Stefan number, and 24% depressant concentration.

The same numerical approach was further used to study the inclination effect of the generator to the improvement of the slurry formation in the unit [191]. According to the experimental as well as numerical analysis, the inclination of the slurry generation unit could improve ice particle detachment from the solidifying mushy zone, consequently increased the ice slurry production (Fig. 14). It was concluded that the optimum generation of the ice slurry could be achieved under 60 inclination angle, 0.150 Stefan number, and 24% depressant concentration.

### 3.6. Material scale simulation

To complement the achieved results of the numerical studies of CTES, a summarized review focused on materials modeling at continuum levels under-zero temperature is presented in this part.

Ismail et al. [192] reported numerical studies carried out on the solidification of certain PCMs encapsulated in spherical and cylindrical shells made of glass and plastic materials with the diameters of 0.035, 0.076, 0.106, and 0.131 m subject to different constant surface temperatures −5, −10, −12, −15, −18, −20 and −25 °C (Fig. 15). The evaluated PCMs were pure water and mixtures of water with 3.75%, 7.5%, 15%, 25%, 30%, 40% and 50% glycol content. The heat

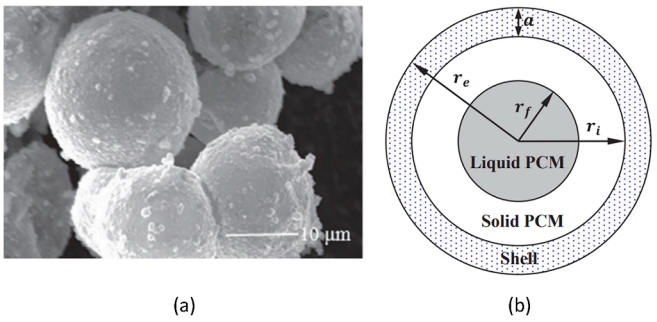


**Fig. 12.** a) Cryo-SEM image of MF-Cu-Al microcapsules; b) Representation of 1-D numerical domain [188].

conduction equation in spherical coordinates, which considered the temperature change over the time and radial direction of the sphere, was used to simulate the phase change. Considering the heat balance between solid and liquid regions, as well as the thermal resistance across the layers in the radial direction, the front of the solidification was tracked numerically. The validity of the numerical approach was confirmed with the experimental results. It was found that for up to 0.076 m diameter of the PCM encapsulation, the increase of the phase transition completion was relatively small, yet it significantly increased due to the larger diameters, which lead to the dominance of the natural convection on the heat transfer efficiency in the liquid region.

Song et al. [193] developed the shape-stabilized PCM based on dodecane mixed with expanded graphite as the skeleton with the PCT of −9.57 °C and latent heat of 151.7 kJ/kg. The developed material was experimentally studied to characterize its thermal properties. Subsequently, these thermal properties were introduced into the numerical model, which simulated the charging and discharging of the shape-stabilized PCM filled in the hollow cylinder-shaped encapsulation. ANSYS was used to simulate the heat transfer, where the enthalpy-porosity model was applied to capture the phase change process in the encapsulation. The simulation results, which were experimentally validated, showed a significant reduction of the charging/discharging time of the cylindrical encapsulation when the PCM contained the expanded graphite.

### 3.7. Summary and outlook of CTES numerical studies

As illustrated in Table 10, the number of research works that included numerical simulations on CTES at sub-zero temperature ranges is still few. However, the majority was published within the last years, indicating the increasing interest in CTES systems.

Among the storage types, most of the numerical analysis focused on developing sensible materials or PCMs (as slurry-based, slurry mixtures, and microencapsulated) based CTES with the following design configurations.

The packed-bed and thermocline type CTES system is the most numerically studied design configuration, and the purpose of the numerical study regarding the final application can be seen from the inter-related graph. From the review, it is explicit that 1-D numerical models are primarily applied to simulate this type of storage design. Liquid thermocline type CTES system has been studied only once together with a packed-bed type CTES as a comparative analogy. Other studies used macroencapsulation type of CTES for refrigeration applications.

For shell-and-tube type CTES, water was considered as one of the main storage materials, and the charging temperature values achieved the cryogenic region. Several shell-and-tube units filled with PCMs in the cylindrical, plate, and box-shaped containers have been tested or commercially deployed.

The development of plate-shaped CTES is at an early stage. Few numerical and optimization studies were conducted for plate-shaped CTES at sub-zero temperatures. More designs and applications can be explored.

Overall, the research stage of numerical studies for CTES systems has not reached the maturation level yet. Thus, there are potential pathways to research in the numerical analysis of CTES, especially in terms of developing advanced numerical methods or using available multi-physics software to develop new designs of CTES systems. There is a need to improve the heat transfer in all of the cases to increase the overall efficiency of the energy systems in which the CTES units are used. It is also worth noticing that system-level simulation may involve a large number of assumptions and reduce the accuracy of the results [194]. The thermo-mechanical simulation should also be carried out for better thermal design. Particular attention should be paid to the slurry, which is becoming a promising material for CTES systems.

## 4. Experimental studies of CTES containment and heat transfer

Despite intensive studies carried out in the containment and heat transfer design of CTES systems using water/ice as the storage material, only a few experimental or commercial systems have been built or experimented with for the sub-zero temperature applications. Some of these systems are developed on a lab-scale for new technology development or validation of numerical simulations; some have already served in the industry for years.

According to how CTES materials are contained and how heat is transferred, thermal energy systems can be categorized into many types. Although most of these designs have the potential to be used for sub-zero temperature applications, existing CTES systems mainly contain four types: packed-bed, shell-and-tube, plate-shaped, slurry-based.

Designs of these types are mostly similar to the TES systems used for higher temperature ranges but have taken into account some unique requirements for sub-zero applications, including moisture control, the volume change of the thermal energy storage material and the containment structure, and component material selection.

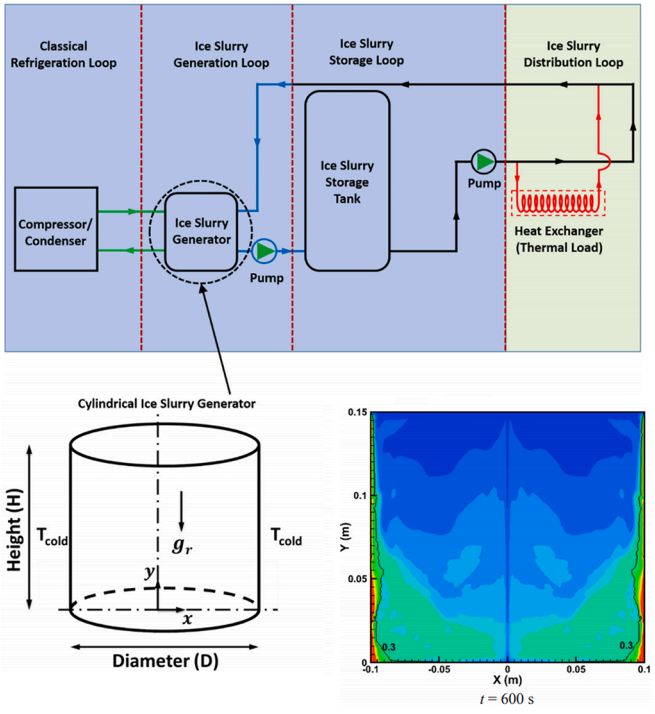


**Fig. 13.** Ice slurry generator and simulation result at 600 s [190].

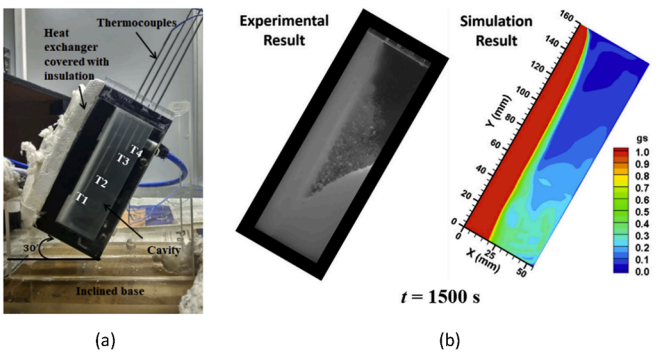


**Fig. 14.** Slurry generation container: a) inclined for better mixing; b) simulation and experimental results after 1500 s of charging [191].

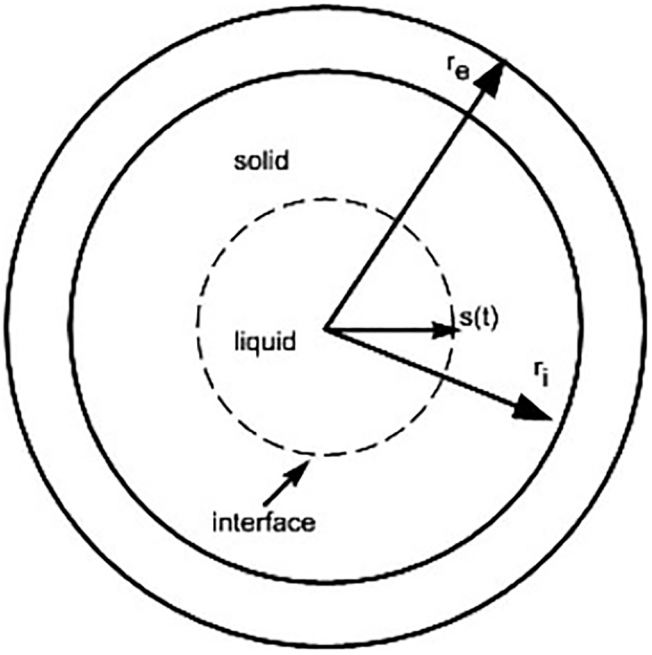


**Fig. 15.** Layout of the solidification problem of PCM confined in a spherical shell. $r_e$ and $r_i$ are the external and internal radius, and s(t) is the position of the interface between the solid and liquid region [192].

### 4.1. Packed-bed CTES

The packed-bed concept is one of the most commonly used thermal energy storage technologies. It is also widely used for sub-zero temperature applications. This technology's advantage is its simplicity in design and manufacturing, low cost, and reliability over thermal charging and discharging cycles [195–197]. The larger heat exchange area of a packed-bed system can make its charging and discharging rates 1.8–3.2 times of a shell-and-tube system [198]. However, the drawbacks of packed-bed systems are also apparent; for example, larger pressure loss on the HTF side, high void fraction/less compact resulting in lower energy density.

If the packed-bed system directly uses sensible materials as the fillers, the system can be simple, low-cost, and reliable over extended thermal charging and discharging cycles [13,197]. Since the HTF and the fillers are in direct contact, corresponding corrosion and compatibility studies are needed to avoid the mid- or long-term chemical reaction causing degradation of the materials of the fillers, the tank shell, and the fluids [199]. Morgan et al. [196]described a modular packed-bed concept of CTES system used in a LAES pilot plant (Fig. 16). The cold storage unit consists of eight identical cells, each filled with low-cost quartzite based river gravels. The packed-beds are installed in a shipping container and insulated by perlite. Due to the significantly different flow rates during the operation of the LAES system, a proper pipe arrangement allowing switching between parallel and series operation is adopted to optimize the cold recovery efficiency and minimize pressure drop. The cellular design showed high thermal efficiency of above 85%, and the quartzite gravel material remained good thermal stability after two years of operation with 100 thermal cycles from ambient to cryogenic temperatures.

The fillers can also be macroencapsulated containers aligned and piled up in the storage facilities. In this case, PCMs can be used to increase the energy density of the storage system. However, there is a trade-off between the size of the macroencapsulation and the overall cost. Smaller encapsulation size leads to a lower void fraction (higher storage capacity), better heat transfer, but higher overall cost. The macroencapsulation should also handle the volume change during the phase transition and the pressure applied to the spheres due to the heavyweight caused by stacking. Therefore, the cost of the macroencapsulation, as well as the overall cost of the system, will increase.

To further increase the storage capacity of the packed-bed CTES system, Khor et al. [180] proposed a packed-bed CTES design that contains two types of fillers: macroencapsulated spheres filled with PCM (Fig. 17a); and granular materials inserted in between the macroencapsulated spheres (Fig. 17b). Each stainless-steel sphere is filled to only 85% to avoid the stress due to the volume change of the PCM. By filling the gaps between the macroencapsulated spheres with quartzite pebbles, the void fraction of the CTES unit decreased from 0.559 to 0.332. Three other granular materials were also analyzed: aluminum particles, alumina particles, and microencapsulated n-decane. Results showed that the storage capacity and the cyclic efficiency of the CTES unit could increase up to 46.2% and 25.0%, respectively. Moreover, the study showed that the size of the macroencapsulated spheres could be increased to reduce the overall cost while inserting granular materials to maintain the storage efficiency.

### 4.2. Shell-and-tube CTES

Shell-and-tube (or ice-on-coil) is another commonly used storage type for CTES applications. Compared to the packed-bed, the shell-and-tube system has a higher packed factor and higher storage capacity. Moreover, this technology can easily handle the expansion of the PCM by not filling the shell side by leaving some void space in the tank and not taking up all of the volumes.

Castell et al. [200] and Tay et al. [201] demonstrated that the shell-and-tube system enables effective heat transfer and high energy density with a large heat exchange area and high compactness. In their designs, HTF flows through one, two, or four coils of tubes in a cylindrical tank (Fig. 18). The packed factors (or compactness factors) of the three designs are 90%, 95%, and 98%, respectively. The tanks are filled with a PCM that freezes at −27 °C. By considering the shell-and-tube system as a heat exchanger that exchanges heat between the fluid and a constant temperature heat sink, the effectiveness of the designs, which is defined as the actual heat exchanged compared to the theoretical maximum heat that can be exchanged, was analyzed and compared. Experiments found out that, with sufficient heat transfer area, the shell-and-tube system can achieve an average effectiveness of 70%. The mass flux was found to be the most dominant factor for the effectiveness, and the melting and freezing processes have the similar effectiveness. For shell-and-tube systems with a factor higher than 90%, the impact of the packed factor to the average effectiveness is also small. Equations were developed for future design and optimization of similar systems.

Some commercial CTES systems also adopt the shell-n-tube configuration. FIC S.p.A. [202] developed a eutectic plate for the passive cooling of cargo trucks. The plate is made up of two steel sheets welded together with a steel pipe coil inside the plate. The plate is then filled with PCM and sealed. During the charging phase, the coil allows fast freezing of the PCM; during the discharging phase, cold energy dissipates through the plates' outer surface.

However, the heat transfer coefficient of a shell-and-tube system is limited due to the smaller heat transfer area. Heat transfer enhancement techniques are usually needed, among which using finned-tubes is recommended to be an easy and most promising technique [203]. Yamashita et al. [59] designed and experimented with a prototype of a fin-tube CTES system to store and release the cold energy of liquefied natural gas (LNG) for re-liquefaction of the boil-off gas (BOG). The vessel is made of stainless steel, and the fin tubes are made of aluminum. A 25 $m^3$ of n-pentane (n-$C_5H_{12}$) with a purity of 98.2%, whose freezing point is 143.55 K, is used as the PCM. Stays are used to stack the fin tubes; therefore, they can move along the axial direction to release the thermal stress. During the charging phase, LNG flows through the tubes to freeze the PCM outside the tubes; during the discharging phase, the PCM melts and converts the LNG/BOG two-phase flow into liquid LNG.

**Table 10**
Characteristics of main numerical models and simulations of packed-bed CTES systems reviewed.

| Storage material and type | Numerical method | Software/ code | Temperature range | Storage material | Reference |
|---|---|---|---|---|---|
| *Packed-bed and thermocline* | | | | | |
| Sensible thermal energy storage type | 1-D simulation: continuous phase model | Ad-hoc code | −150 to 30 °C | Materials: lead, aluminum 6061, zinc, 304 stainless steel | [17] |
| Sensible thermal energy storage type | 1-D simulation: continuous phase model | COMSOL | −150 to 20 °C | Material: Quartzite rock | [19] |
| Sensible thermal energy storage type | 1-D simulation: Schumann's model | Ad-hoc code | − 153 to 26 °C | Material: Concrete spheres and extrudes for packed-bed | [18] |
| Latent heat type | 1-D simulation: Enthalpy method together with a discrete model | Ad-hoc code | −41 to −20 °C | PCM: Vegetable oil. Tpc = -30 °C | [176] |
| Cascaded latent type | 1-D simulation: Enthalpy method with concentric dispersion model | Ad-hoc code | −80 to 30 °C | PCM 1: high-grade PCM Tpc = −49 °C; PCM 2: medium-grade PCM Tpc = −19.5 °C | [177] |
| Latent heat type with granular fillers | 1-D simulation: concentric dispersion model | Ad-hoc code | − 160 to 25 °C | PCM 1: in-house-developed PCM; Tpc1 = −118 °C PCM 2: E-75; Tpc2 = − 75 °C; PCM 3: E-65; Tpc3 = −65 °C; Granular materials: Quartz pebbles, aluminum particles, aluminum particles, and Microencapsulated n-decane with Tpc = -30 °C. | [180] |
| Sensible thermal energy storage type | 1-D simulation: Convection-diffusion equation | Ad-hoc code | − 153 to 26 °C | Material: isopentane | [18] |
| Latent type | 2-D rectangular domain: Enthalpy method | Not specified | −23 to 25 °C | PCM: NaCl-$H_2O$; PCT = −21 °C | [181] |
| Latent type | 2-D simulation: Enthalpy method | ANSYS | −30 to 30 °C | PCT = −21.2 °C | [184] |
| *Shell-and-tube* | | | | | |
| Spherical PCM tank with central heat transfer tube | 3-D CFD with Enthalpy-porosity method | TermoFluids | − 195.0 to 7.74 °C | Ice/water | [185] |
| Horizontal rectangular tank with a copper tube in the middle | A 2-D method with enthalpy-porosity method | FLUENT | − 120 to 7 °C | Ice/water | [186] |
| Shell-and-tube type storage tank | 2-D method with enthalpy method | STAR-CCM | − 5 to 44.5 °C | Ice/water | [182] |
| *Plate-shaped* | | | | | |
| Latent type | 1-D simulation: Enthalpy method | Ad-hoc code | −36 to − 15 °C | PCM: not specified PCT = −26.7 °C | [183] |
| *Microencapsulated PCM* | | | | | |
| Microencapsulated PCM as slurry | 1-D simulation: Enthalpy method, Lamé's equations and buckling theory | Ad-hoc code | − 85 to −80 °C | Material: Dowtherm J. (commercial HTF) PCT = −81 °C | [188] |
| *Slurry-based* | | | | | |
| Ice slurry generator | 2-D axisymmetric simulation: Fixed grid continuum media approach with multiphase flow | Not provided | − 50 to 25 °C | Hypereutectic binary aqueous ammonium chloride (H2O + NH4Cl) solution PCT = −15.4 °C | [190] |
| Tilted container ice slurry generator | 2-D rectangular domain: Fixed grid continuum media approach with multiphase flow | Not provided | − 50 to 25 °C | Hypereutectic binary aqueous ammonium chloride (H2O + NH4Cl) solution PCT = −15.4 °C | [188,191] |
| *Materials simulation* | | | | | |
| Spherical encapsulation | 1-D model with enthalpy method | Ad-hoc code | − 25 to 20 °C | PCM: Various water and glycol mixture; PCT = 0 to −10 °C | [192] |
| Hollow cylinder shaped encapsulation | Enthalpy-porosity model | ANSYS | − 20 to 10 °C | PCM: dodecane/ expanded graphite; PCT = −9.67 °C | [193] |

### 4.3. Plate-shaped CTES

The plate-shaped system is similar to the plate heat exchanger. Compared to shell-and-tube CTES, the plate-shaped CTES system can work with both liquid and gaseous HTFs with a larger heat transfer area with a small pressure loss [187]. Since the TES unit is assembled from a certain number of rectangular plates, flexible operation with different PCMs and thermal loads can be achieved by adjusting the distance between the plates [204] and arranging several plate-shaped CTES units in serial or in parallel [204,205]. The possibility of mass production of the plates can also lead to the economy of scale of manufacturing and decrease the cost. However, similar to a packed-bed system, its void fraction is also larger comparing to the shell-and-tube system. Special attention should also be paid to handle the volume change of the thermal energy storage materials.

Liu et al. [183,187,206] designed a plate-shaped CTES system (Fig. 19) that contains several flat slabs parallelly placed in layers. The HTF (air) passes through the gaps between the plates to charge or discharge the PCMs inside the plates. To handle the volume change during the phase change, the unit is built to be rigid and not deformable.

Selvnes et al. [204,207] developed a pillow-plate based CTES system, which can withstand higher operating pressure of the HTF in $CO_2$ refrigeration systems (Fig. 20). PCM is filled directly into the CTES unit case. Stacks of stainless pillow-plates are immersed into the PCM. Each plate contains two thin metal sheets that are spot-welded and inflated to create the flow channels for the HTF with high operating pressure. The pattern of each plate and the distance between the plates can be changed to make the design flexible for different PCMs. A corresponding testing rig has been built to test the PCMs with PCTs ranging from −45 °C to 0 °C.

### 4.4. Slurry-based CTES

Slurries-based CTES uses phase-change slurry (PCS) as the storage


**Fig. 16.** High grade cold storage used in a 350 kW/2.5 MW h LAES pilot plant at the University of Birmingham, UK [19].

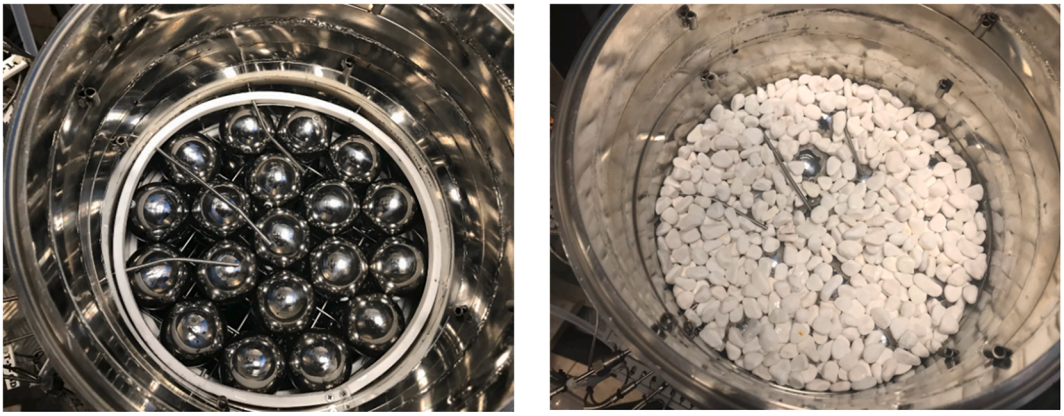


**Fig. 17.** A packed-bed CTES with two types of fillers: (a) macroencapsulated PCM; and b) granular (quartzite pebbles) inserted in the gaps between the sphere tiers [180].

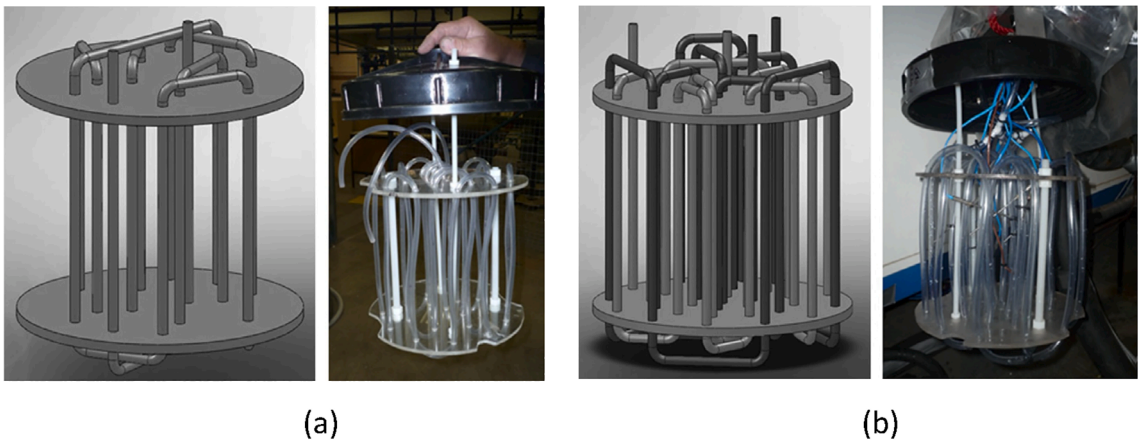


**Fig. 18.** Schematic and photo of (a) one coil tank (high packing factor) and (b) two coils tank (high heat transfer surface) [200].

material. Comparing to packed-bed, shell-and-tube, and plate-shaped CTES systems, a secondary HTF is no longer needed. This leads to several advantages of the slurry-based CTES. First, the slurry can be pumped directly from the storage tank to the heat exchangers to receive or supply the cold energy, which improves efficiency, reduces complexity, and saves the overall system's cost [209]. Second, compared to conventional HTFs that use sensible heat to transfer the energy, slurry also uses latent heat and therefore has a larger heat transfer capacity [140]. Hence, less flow rate is needed to deliver the same amount of cold energy, and the size of the pumping system can be reduced [209]. Third, it has the benefit of transferring the energy at the same volume rate and using the pipe system as part of the storage [140].

Extensive research has mentioned using ice slurry CTES systems for electrical load shifting while working with refrigeration systems. For ice-slurry CTES systems, the slurry should be generated before used as the thermal energy storage material or the HTF. Various ice-slurry generation technologies have been used or proposed [149,155], either using or not using moving parts.

Meewisse [157,210] developed a fluidized ice slurry generator concept that uses fluidized solid particles to prevent the build-up of the solid ice layer on the heat exchanger walls. An experimental setup was built to determine the stable operation range for ice slurries using sodium chloride and ethylene glycol as the freezing point depressant. The author claims that such a system can be low cost and does not require large foot space since the setup should be vertical.

Liu et al. [211] experimented with a scraped-surface method (Fig. 21) for ice slurry production. Two rotating blades were used to scrape the ice deposited on the cold surface. The authors tested with a series of sodium chloride concentrations (from 1% to 6%) and found out that the ice formation temperature is consistent with the theoretical freezing points (from −0.6 to −3.6 °C) without showing obvious subcooling degree. Furthermore, ice formation will be accelerated by adding nanosilica into the slurry.

However, a slurry-based system can suffer from heavy mechanical power to generate small and smooth ice crystals and to maintain the ice slurry in a homogeneous state, as well as pump ice slurries with high ice fraction [149]. New methods for slurry generation and stratification prevention should be continually developed [155]. Recently, Tiwari et al. [191] experimented with a new concept of ice-slurry generation by using an inclined cavity (Fig. 22). The inclined surface provides a shear force, making it easier for the ice particles to detach from the solidifying mushy zone, and therefore increase the slurry production. The authors

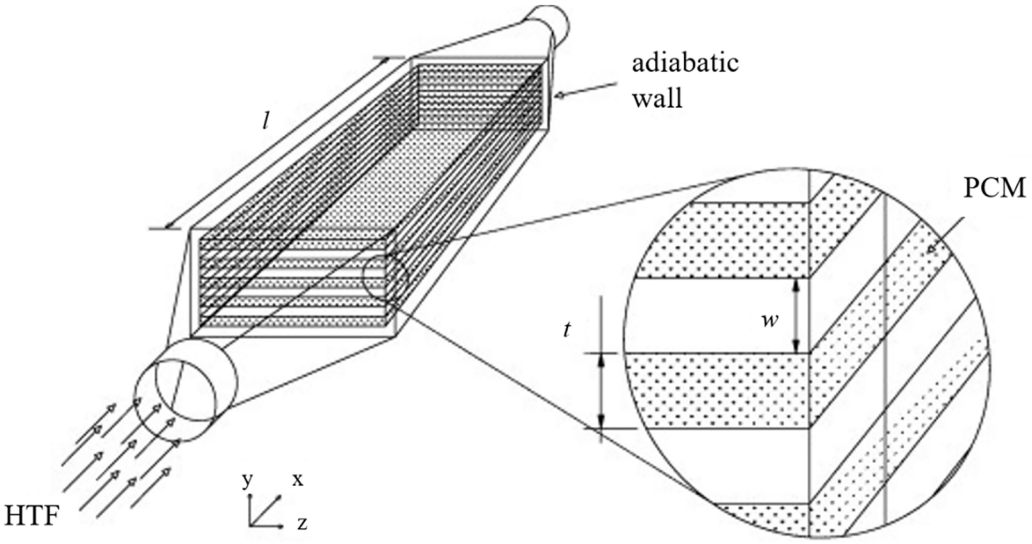


**Fig. 19.** The plate-shaped PCM-Air heat storage unit during the construction phase [187].

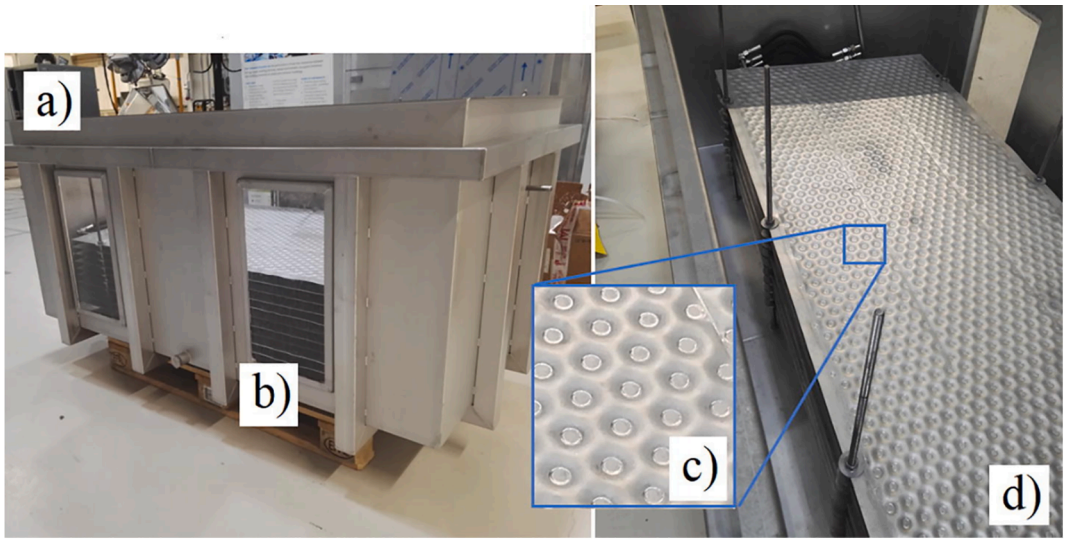


**Fig. 20.** (a) Pillow-plate CTES unit, (b) PCM integration between the pillow plates, (c) and spot-welded sheets (d) stacks of pillow plates [208].

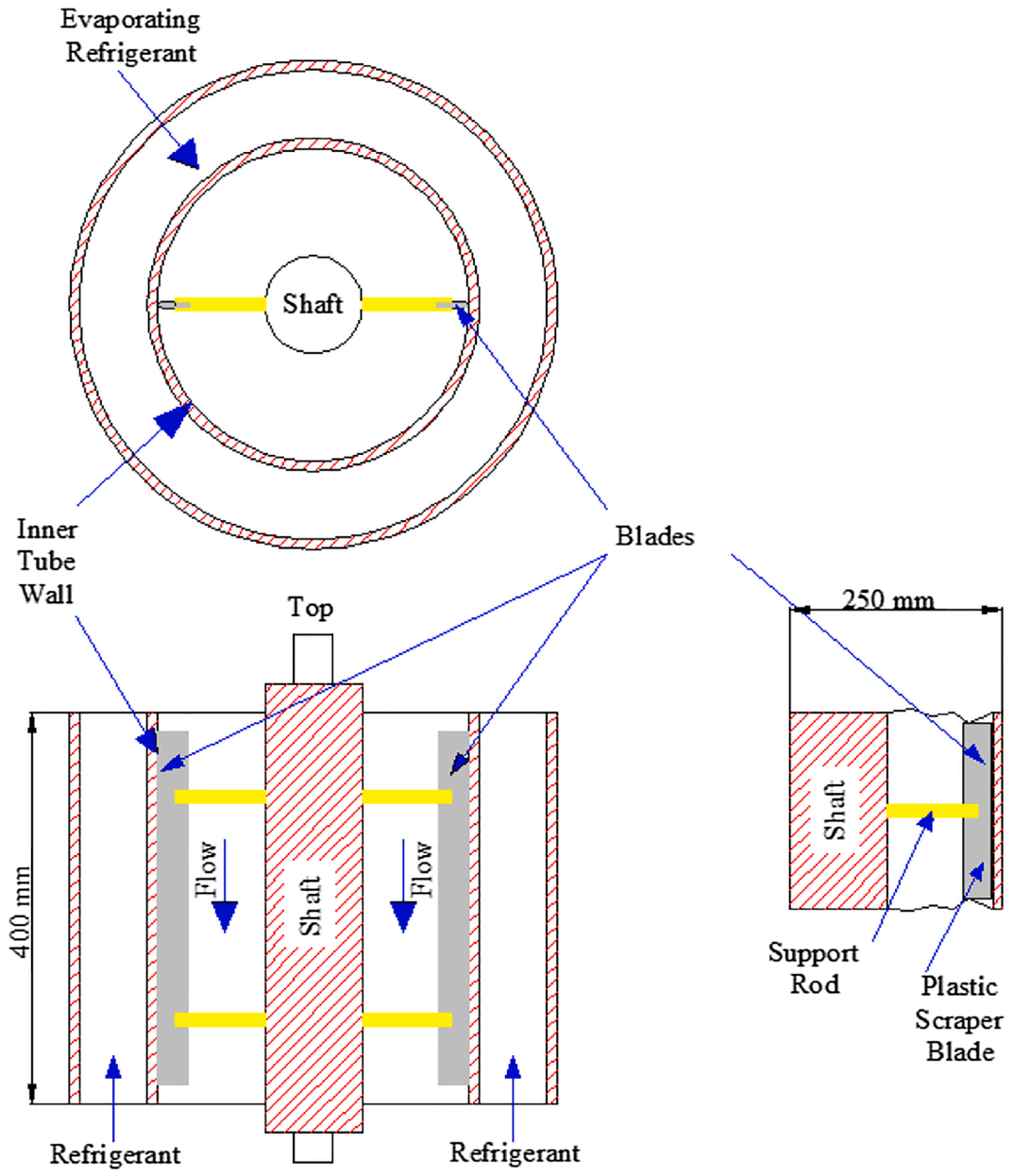


**Fig. 21.** Schematic of a scraped surface ice slurry generator [211].

used $H_2O$-$NH_4Cl$ solution as the slurry material. Temperature and velocity are measured by thermocouples and Particle Image Velocimetry (PIV). Experimental results showed that the cold energy stored and generator efficiency increases along with the inclination angle. For selected inclination angles of 0°, 30°, and 60°, the maximum cold energy and effectiveness were found for 60°. The findings are useful for the design of future ice-slurry generators.

### 4.5. Summary of CTES experimental studies and selection of CTES types

Compared to numerical simulations, even less experimental work has been carried out for sub-zero temperature CTES. Generally, using packed-bed and thermocline, shell-and-tube, plate-shaped, and slurry based storage types for sub-zero temperature ranges are not too different from above-zero temperature ranges. However, special attention should be made for heat transfer enhancement, volume change control, and mechanical design during the designing phase. More experimental studies should be conducted to overcome the low thermal conductivity issue [203], explore more materials for more applications, and enhance system modularity [13].

A comparative summary (Table 11) of CTES type selection, including current TRLs, storage and heat transfer materials, temperature ranges, and pros/cons, is presented based on the research listed in this section. Suitable applications are summarized and recommended in Table 11 based on the pros and cons of each type.

Packed-bed and thermocline CTES is easy to design and simple to manufacture. Its advantages of large heat transfer area, low cost, and high reliability (if using sensible materials) enabled packed-bed and thermocline to be selected by a series of commercial applications. Future research work can therefore focus on overcoming its shortcomings, including large pressure loss, lower energy and exergy density due to larger void volume. Moreover, if using macrocapsulated PCMs as the fillers, besides experimenting with the compatibility of the containment materials, methods to reduce the cost and mechanical design challenges should be explored. Design and experimentation of thermoclines using sensible liquids should also be developed.

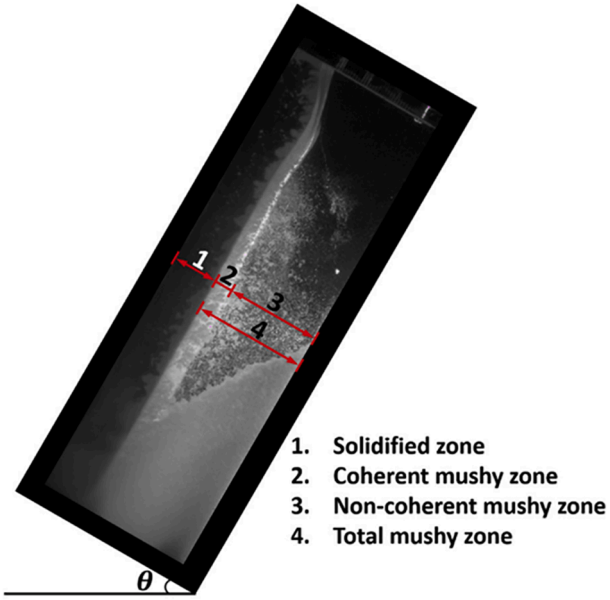


**Fig. 22.** Ice-slurry generation in the inclined cavity for CTES [212].

Shell-and-tube is another commercially available CTES type. Compared to the other storage types, shell-and-tube has the lowest void fraction and, therefore, the highest energy and exergy density. To overcome the limited heat transfer area, enhancement techniques are needed to increase the heat transfer coefficient, for example, using finned-tubes as recommended by various researchers [168].

No plate-shaped CTES has been massively produced. Although the void fraction of plate-shaped CTES facilities is large, it can work with both liquid and gaseous fluids and be flexible to different PCMs and heat loads. Early-stage experimental studies have been carried out for transportation and large-scale refrigeration applications. The most important term for designing plate-shaped CTES is to handle the thermal stress of the plates. More plate-shaped CTES designs and applications can be explored, and their long term operation reliability should be evaluated.

Slurry-based CTES is a promising type for existing and future energy systems with the possibility of acting as both the heat storage material and HTF. Experimental research about slurry-based CTES focuses on the design of the slurry generators, both with and without moving parts. The most important consideration of designing and applying the generators is to reduce power consumption while producing high-quality homogenous slurry products. On the macro-level, proper slurry-based systems should be designed for more applications; on the micro-level, the physical properties of slurries should be better understood.

Furthermore, the thermal storage efficiencies of the four storage types: packed-bed and thermocline [180,217], shell-and-tube [218], plate-shaped [219], and slurry-based [220], can all reach 80% and above without significant differences between each other merely due to the selection of the storage type. The thermal storage efficiency is more related to the design of the storage facility (for example, the shape of the storage tank, the diameter of the tubes, the size of the fillers, and the properties of the storage material and HTF) and the operation conditions (for example, the flow rate, temperature, and pressure of the HTF). Therefore, thermal storage efficiency is not a major concern for the type selection. As long as the CTES unit is well designed and operated, any CTES type is capable to achieve an efficiency of 85% and even more than 90%.

## 5. Applications of CTES technologies

CTES technologies of sub-zero temperature ranges have been used or have the potential to be used in various applications that need generation, utilization, and storage of cold energy below 0 °C. Refrigeration systems operating at sub-zero temperature ranges, both active and passive, are able to adopt CTES to increase efficiency, reduce energy consumption, and shift the power load. CTES for small-scale refrigeration units is commercially available, while its use in large-scale refrigeration systems has not been widely applied. CTES also has a unique use in space exploration. For some emerging electricity storage systems, which might be the key to renewable energy transitions in the future, the CTES is an indispensable part of the system or has the potential to enhance the performance of the overall system. Electricity storage systems that have used CTES include Liquid air energy storage (LAES), Pumped thermal energy storage (PTES), and Superconducting flywheel energy storage (SFES). The use of CTES in LAES is commercially available, while PTES and SFES equipped with CTES are in the prototyping stage. The CTES can also work with other energy systems for waste cold energy recovery to improve the performance of the whole system, including the re-gasification process of LNG terminals and the discharging of high-pressure hydrogen storage tanks.

### 5.1. Active and passive refrigeration

Refrigeration is the most widely studied application of CTES. According to whether the cold energy is generated in situ when it is needed, refrigeration systems of CTES can be divided into types: active and passive. CTES applications in both active and passive refrigeration systems are summarized in this section.

#### 5.1.1. Active refrigeration

Active refrigeration produces cold energy actively, mainly through refrigeration cycles. Extensive studies have been carried out using PCM-based CTES for active refrigeration systems [122,221–224]. For this application, the CTES units are usually placed near or around the evaporator, in the storage compartment (as shown in Fig. 23). The CTES unit can also be located between the refrigeration system and the refrigerated space. A slurry-based CTES system can act as part of a secondary cooling system (as shown in Fig. 24) where it captures and stores the cold energy generated by the primary loop before supplying the cold to the cooling load at another time or location. CTES for active refrigeration systems is summarized in the first part of Table 12. In general, equipping the active refrigeration systems with CTES of sub-zero temperature ranges has the following benefits:

- enhance the performance of the system and decrease energy consumption, especially during peak hours;
- decrease the running time of the compressor;
- achieve more accurate temperature control;
- maintain system temperature at desired ranges for a longer time during a power outage;
- reduce the noise level;
- reduce GHG emission;
- decrease the overall costs of the refrigeration system.

However, the CTES unit reduces the volume of the storage space inside the active refrigeration systems. The temperature of the PCM should also be carefully selected. Higher PCT can lead to an increase in the COP due to reduced compressor work and enhanced evaporator heat transfer, but also an increase in the air temperature inside the compartment [224].

A CTES unit can also be applied to large-scale refrigeration systems for peak load shifting and renewable energy utilization. Ghorbani et al. [78] assessed a hybrid solar-driven water-ammonia absorption refrigeration system using CTES (Fig. 25). Concentrated solar dishes provide the system with 1649 kW of heat from the sun. The system produces 373.7 kW of cold during the day. A portion of the cold energy is directly used in the refrigerator, while the rest is stored at −23.51 °C in the CTES

**Table 11**
Summary of CTES storage types and suitable applications.

| CTES type | Storage material type | Temperature range mentioned in the literature (°C) | Compatible HTFs | Development stage | Pros | Cons / technical challenges | Suitable applications | Current TRL |
|---|---|---|---|---|---|---|---|---|
| Packed bed and thermocline CTES | Sensible material (mostly solid), PCM with macroencapsulation | −170 to 0 | Both gaseous and liquid fluids | Packed-bed with solid sensible filler commercially available, packed-bed with macroencapsulated PCM in lab testing, small-scale thermocline (macroencapsulation) with PCM commercially available, thermocline with sensible liquids in conceptual phase available | Easy to design and simple to manufacture, larger heat transfer area, low cost, and high reliability if using sensible materials | Larger pressure loss, lower energy and exergy density due to larger void volume, higher cost, and mechanical design challenges if using macrocapsulated PCMs | Small-scale active and passive refrigeration, Small-scale waste cold recovery*, large-scale active refrigeration*, large-scale electricity storage*, small-scale active and passive refrigeration* | 3–9 [19,44,56,64,72,78,123,144,145,170–172,174,213–215] |
| Shell-and-tube CTES | Sensible material (mostly liquid), PCM | −210 to 0 | Particularly suitable for liquid fluids | Shell-and-tube with PCM commercially available | Higher energy and exergy density due to the smaller void volume | Less heat transfer area, need for heat transfer enhancement techniques | Small-scale active and passive refrigeration*, large-scale waste cold recovery*, small-scale electricity storage*, small-scale waste cold recovery, large-scale electricity storage | 4–9 [59,60,76,90,121] |
| Plate-shaped CTES | PCM | −45 to 0 | Particularly suitable for gaseous fluids | Various plate-shaped CTES have been tested | Able to work with both gaseous and liquid HTFs, low-pressure drop, flexible design | Lower energy and exergy density due to larger void volume, need to handle the thermal stress on plates due to the volume change of PCM, long term operation has not been evaluated yet | Small- and large-scale active refrigeration*, small- and large-scale waste cold recovery | 3–8 [146,204,216] |
| Slurry | PCM (in phase change slurry form) | −78.5 to 0 | Slurry itself acting as the HTF | Ice slurry for refrigeration commercially available, dry ice slurry in a conceptual phase | The same material can be used as both storage material and HTF, higher heat capacity and heat transfer coefficient, can use the pipe system as part of the storage | Stratification issues, high mechanical power to generate small and smooth ice crystals and to maintain the ice slurry in the homogeneous state, high pressure drop and pumping power of ice slurry with high ice fraction | Small- and large-scale active refrigeration*, small- and large-scale waste cold recovery | 3–9 [155,157] |

* Mentioned in literature.

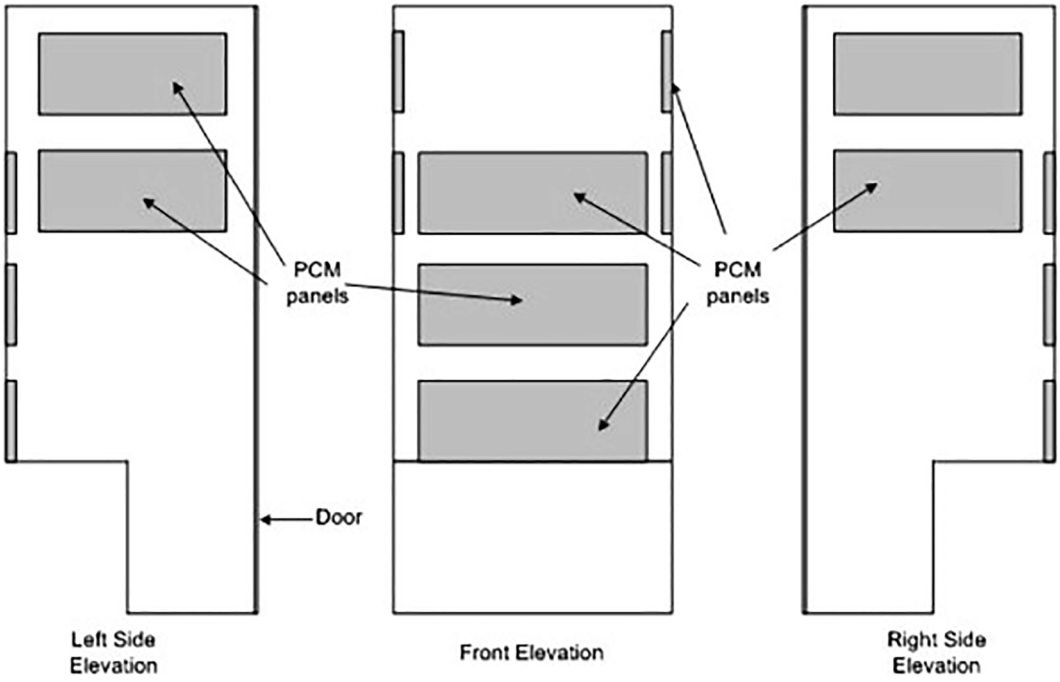


**Fig. 23.** Example of using PCM panels for a freezer [145]

unit. Diethylene glycol is used as the PCM, and ammonia is used as the HTF. The stored cold energy is used during night time. Selvnes et al. [146] analyzed an industrial $NH_3/CO_2$ cascade refrigeration system for a poultry processing plant integrated with six large-scale CTES modules. The CTES system uses a PCM that freezes at −11 °C. Simulation results showed that the CTES system reduces the compressor work by 19% during discharging and a reduction of COP by up to 3%.

Apart from domestic freezers, space exploration is another application where CTES is used for active refrigeration. The NASA designed and experimented with a series of CTES technologies for space applications [56,228]. One of the technologies used PCM for cooling and temperature control of temperature-sensitive sensor components, such as focal planes, optics, mirrors, and telescopes (as illustrated in Fig. 26). The material used is 2-methyl pentane (or isohexane) with 3% acetone, with PCT at −153 °C. Ground and orbit testing results showed that the technology has the capability of significantly reducing the weight of the cooling system of spaceborne infrared sensors. During the operation of the sensors, both electrical and environmental heating significantly increase the cooling loads. The CTES system can be used to average the cooling load on the refrigeration system: the PCM melts and releases cold energy during operation to shave cooling loads, and is recharged during non-operating periods. The CTES also provides tighter temperature control since the operating temperature can be maintained around the PCT. The sizes of refrigerators or radiators can be significantly reduced if working in series with the CTES. Power and weight savings are several times higher than the additional weight due to the CTES. Moreover, by replacing refrigerators that have moving mechanical parts, CTES also helps minimize the vibration of vibration-sensitive sensors. The refrigerators can be turned off during operation and turn on again during the non-operational periods to charge the CTES.

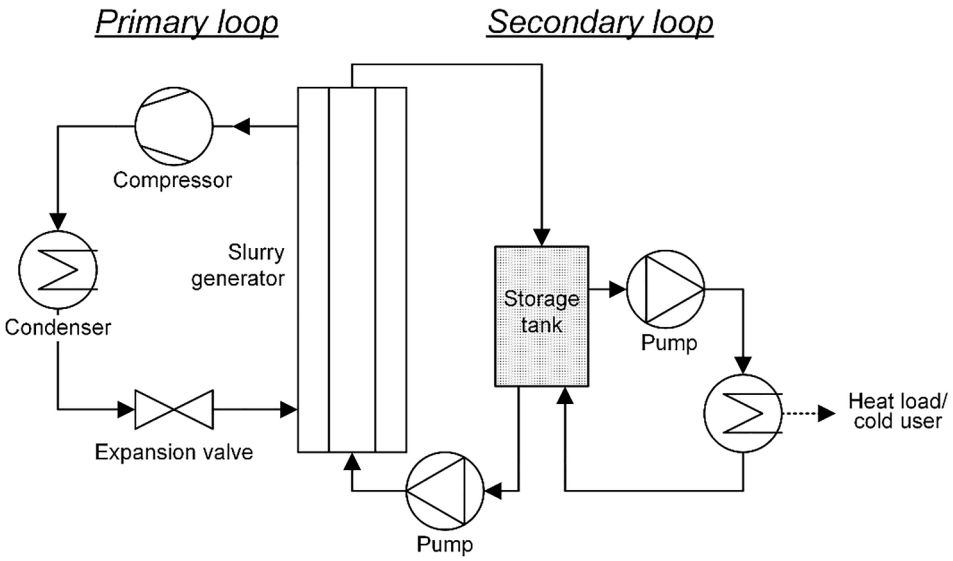


**Fig. 24.** Slurry system as the secondary refrigeration loop.

**Table 12**
Summary of CTES applications.

| Application | CTES type | TRL | Storage material | Material type | Reason for the material selection | Temperature range* (C°) | Latent heat (kJ/kg) | Thermal conductivity (W/(m·K)) | Specific heat (kJ/(kg·K)) | Role of CTES | Reference |
|---|---|---|---|---|---|---|---|---|---|---|---|
| *Refrigeration* | | | | | | | | | | | |
| Household refrigerator | Packed-bed and thermocline | 7 | Water with a eutectic mixture | PCM | Maintain a temperature lower than water | −3 | 310 | – | – | Attached to the evaporator; realized 5–9 h of continuous operation without electrical supply (compared to 1–3 h without PCM) and a 10–30% increase of the COP; maintained the air in the refrigerated cell at proper temperature values. | [171] |
| Air-conditioning | Slurry-based | 3 | Ice slurry with 6.5 wt% of NaCl | PCM | High density, high heat conductivity, relatively low viscosity | −4 to −5 | – | – | around 65** | Used in the secondary cooling system, achieved lower operational cost, smaller heat exchanger size and smaller storage tank size compared to non-phase change CTES systems; | [157] |
| Household refrigerator | Shell-and-tube | 7 | 10 wt% NaCl water solution | PCM | – | −5 | 289 | – | – | Located around the evaporator tubes; realized 20–27% of COP improvement; reduced the average compressor running time per cycle by 2–36%. | [121] |
| | | | 20 wt% KCl water solution | | – | −10 | 284 | – | – | | |
| Domestic freezer | Packed-bed and thermocline | 7 | Potassium chloride aqueous solution (19.5% KCl) | PCM | Less corrosive against aluminum containment | −10 | 253 | 0.6 (l), 2.22 (s) | 3.25 (l), 2.108 (s) | Attached to the internal walls of the freezer; replaced the high torque compressor with a low starting torque compressor powered by PV and held the inside freezer temperature at −8°C for a long time. | [172] |
| Household freezer | Packed-bed and thermocline | 7 | Eutectic solution of Poly-ethylene glycol | PCM | – | −10, −15, −20 | – – – | – – – | – – – | Located on top of the evaporator; decreased the energy consumption by up to 8.37%. | [144] |
| Hybrid solar-driven water-ammonia absorption refrigeration system | Packed-bed and thermocline | 3 | Diethylene glycol | PCM | – | −10 | 247 | – | – | Located in parallel with and connected to the refrigerator; stored the cold energy during the day and use it during the night. | [78] |
| Industrial NH3/CO2 cascade refrigeration system | Plate-shaped | 3 | AdBlue | PCM | – | −11 | 270 | – | – | Integrated with the medium temperature CO2 circuit; considerably reduced the peak electricity use and reduced the required compression power by 19% during discharging. | [146] |
| Domestic freezer | Packed-bed and thermocline | 7 | Eutectic composition of water and ammonium chloride | PCM | – | −15.4 | – | – | – | Attached to the internal walls of the freezer; reduced the rate of temperature increase during power loss; achieved lower temperature fluctuations; led to better food quality. | [145] |
| Low-temperature food storage chambers | Packed-bed and thermocline | 7 | Climsel C-18 | PCM | – | −18 | 306 | 0.5–0.7 | 3.6 | Located On top of the evaporator; minimized the temperature rise of the air and product in the chamber. | [174,225] |
| | | | Cristopia E-21 | PCM | – | −21.3 | 233 | – | – | | |
| Refrigerated warehouse | Packed-bed and thermocline | 9 | – | PCM | – | – | – | – | – | PCM cells placed on top of the goods; allowed the chiller to run less frequently and kept the temperature around −18 °C; saved 40% of refrigeration cost; helped protect food from spoilage during power outages. | [226] |
| Fresh food chamber | Packed-bed and thermocline | 7 | 18% NaCl solution added with 5% | PCM | – | −19 | 120.6 | 0.48 | – | Located on the air duct foam opposite the evaporator and fan (evaporator); reduced the energy consumption by 18.6%. | [123] |

(*continued on next page*)

**Table 12** (*continued*)

| Application | CTES type | TRL | Storage material | Material type | Reason for the material selection | Temperature range* (C°) | Latent heat (kJ/kg) | Thermal conductivity (W/(m·K)) | Specific heat (kJ/(kg·K)) | Role of CTES | Reference |
|---|---|---|---|---|---|---|---|---|---|---|---|
| | | | SAP and 0.03% diatomite | | | | | | | | |
| Household refrigerator | Shell-and-tube | 7 | Undecane shape-stabilized phase change material | PCM | Little shape change | −26 | 100 | 1.35 | – | Located around the evaporator tubes; increased the COP by 16% and 32% (if combined with a condenser CTES as well). | [76] |
| Refrigeration system of a refrigerated truck | Plate-shaped | 5 | Inorganic salt-water solution | PCM | Lower cost compared to commercial PCM product | −26.8 | 154.4 | – | – | Located outside of the refrigerated space, connected to a cooling unit inside the refrigerated space by HTF-circulating pipes; maintained the refrigerated space at −18 °C for 10 h in the hottest summer climatic conditions of Adelaide, Australia; reduced the energy cost up to 86.4% compared with conventional systems; realized much lower local GHG emissions; improved temperature control; reduced noise level. | [216] |
| Passive storage device for vaccine transportation | Packed-bed and thermocline | 9 | Dry ice | PCM | High energy density | −78 | 574 | 0.011–0.14 | – | Placed inside a vacuum storage device and besides the vaccine vials; held the vaccine temperature at −78 °C for around 30 days (dry ice) and 5 days (E-78). | [72] |
| | | | E-78 | PCM | Will be used if dry ice not available | −78 | 115 | 0.14 | 1.96 | | |
| Space exploration | Packed-bed and thermocline | 9 | Methanol | PCM | Appropriate temperature, adequate energy density, simple to implement | −97 | 99.2 | 0.210–0.206 (l) | 2.21–2.40 (l) | Act as a thermal capacitor, absorb the heat loads during the imager operational | [64] |
| | Packed-bed and thermocline | 9 | 2-methyl pentane with 3% acetone | PCM | Use acetone to reduce the subcooling | −153 | 72.76 | 0.144–0.114 (l) | 1.76–2.11 (l) | Realized tighter temperature control of sensor components; reduced the size and weight of cooling systems; averaged the cooling load; minimized the vibration. | [56] |
| *Electricity storage* | | | | | | | | | | | |
| Liquid air energy storage (LAES) | Packed-bed and thermocline | 7–9 | Quartzite-based river shingle | Sensible | High thermal capacity to conductivity ratio and low cost | around −140 to 0 | – | 6.3–9.5 | 0.52–0.72 | Connected to the main heat exchanger; increased the round trip efficiency by 20% and the liquid yield by 30%. | [196,227] |
| Pumped thermal energy storage (PTES) | Packed-bed and thermocline | 3 | Pebbles, gravel, concrete, uniform ceramic matrix | Sensible | Lower losses compared to liquid thermocline | around −150 to −170 | – | – | – | Acted as the cold reservoir to store and release the cold energy. | [170] |
| Pumped thermal energy storage (PTES) | Packed-bed and thermocline | 3 | Isopentane | Sensible | Covers the desired temperature range | −153, 27 | – | 1 × 10–7 m2/s (thermal diffusivity) | 1.84–1.86 | Acted as the cold reservoir; a liquid thermocline can be significantly more effective than a packed bed thermocline. | [18] |
| | Packed-bed and thermocline | 3 | A nitrogen filled packed bed of concrete spheres | | Low cost | | – | | 0.769 | | |
| Pumped thermal energy storage (PTES) | Packed-bed and thermocline | 2 | n-hexane | Sensible | Suitable temperature range, pervasive, biodegradable, and cheap | −93 | – | 0.156–0.135 | 1.88–2.15 | Acted as the cold reservoir to store and release the cold energy. | [44] |
| Superconducting flywheel energy storage (SFES) | Shell-and-tube | 4 | Nitrogen | PCM | Compactness of the overall system | −210 | 25.8 | 0.173–0.146 | 2.02 | Located at the condenser or evaporator; stores cold and mechanical kinetic energy, reduce the energy loss due to cryogenic cooling | [90] |
| *Waste cold energy recovery* | | | | | | | | | | | |
| | | 9 | Pentane | PCM | | −130 | 116.43 | 0.173–0.122 | 1.97–2.20 | | [59,60] |

(*continued on next page*)

**Table 12** (*continued*)

| Application | CTES type | TRL | Storage material | Material type | Reason for the material selection | Temperature range* (C°) | Latent heat (kJ/kg) | Thermal conductivity (W/(m·K)) | Specific heat (kJ/(kg·K)) | Role of CTES | Reference |
|---|---|---|---|---|---|---|---|---|---|---|---|
| Boil-off Gas (BOG) re-liquefaction of an LNG terminal | Shell-and-tube | | | | High energy density and fixed temperature | | | | | Use the CTES to capture the excess cold energy of the BOG re-liquefaction process and release the cold during the night; reduce the compression power by 30–60% compared to the conventional method of compressing the BOG for re-liquefaction. | |
| Hydrogen fueling of fuel cell vehicles | Packed-bed and thermocline | 3 | PCM-HS26N | PCM | – | −26 | 205 | – | – | Store the cold energy during hydrogen expansion and pre-cool the incoming hydrogen during the fueling process; reduced the cooling demand of the fueling station. | [214] |

* PCT for PCMs or operation temperature for sensible materials.
** Apparent heat capacity with 20% of ice formation.

#### 5.1.2. Passive refrigeration

In a passive refrigeration system, the cold energy is generated beforehand, and the system focuses more on preserving the cold and control the heat gain, to maintain the cold temperature of the system for a longer time. CTES systems of sub-zero temperature ranges can also be used to provide passive cooling for various applications, especially transportation and warehousing of temperature-sensitive goods, such as food and beverages, medical products, floriculture.

Macroencapsulated CTES is widely used for the transportation of temperature-sensitive goods. CTES units can also be installed in refrigerated trucks. Tassou et al. [229] analyzed the benefits of using eutectic PCMs units for food transportation. The CTES plates or beams can be used alone or combined with the vapor compression system in refrigerated trucks. The CTES units are charged in advance, for example, during the night, and are used to maintain the temperature of the truck during daytime operation. As the refrigeration system accounts for up to 40% of the environmental impacts of a diesel-driven food vehicle, using CTES passive cooling technology can significantly reduce these impacts. The reduction can be larger if renewable energy sources are used during the charging of the CTES units. The authors conclude that this technology is especially suitable for short journeys.

Warehousing facilities using CTES systems of sub-zero temperature ranges are also commercially available. For example, Viking Cold Solutions, Inc. [230] claims that using PCM passive cooling saves over 40% of refrigeration costs of a warehouse maintained at −18 °C.

### 5.2. Electricity storage

Increasing the share of renewable energy sources, especially solar and wind, in the energy mix is crucial to the future of energy transition and climate mitigation. However, these sources are highly intermittent. Electricity storage technologies can decouple the energy supply and demand and support the grid integration of renewable energy sources; these technologies can also help to ensure grid balance and reduce peak-load capacity [231,232]. So far, many concepts of electricity storage systems have been proposed or constructed, and CTES is a crucial part of some promising systems. LAES, PTES, and SFES are the technologies that are taking or can take profit from employing CTES.

#### 5.2.1. Liquid air energy storage (LAES)

LAES refers to the technology that uses liquefied air as the storage medium (−196 °C) to store and release energy in the form of electricity [19,196,233].

The working principle of a conventional LAES is depicted in Fig. 27. A typical LAES system operates in three steps. Step 1 is the charging process whereby excess (off-peak and cheap) electrical energy is used to clean, compress, and liquefy air. Step 2 is the storing process through which the liquefied air in Step 1 is stored in an insulated tank at −196 °C and approximately ambient pressure. Step 3 is the discharging process that recovers the energy through pumping, reheating, and expanding to regenerate electricity during peak hours when electrical energy is in high demand and expensive. Step 2 also includes the storage of heat from the air compression process in Step 1 and high-grade cold energy during the reheating process in Step 3. The stored heat and cold energy can be used, respectively, in Step 3 and Step 1 to increase the power output and reduce the energy consumption of the liquefaction process. In the first pilot plant of a LAES system, a pack-bed type of CTES is used to store the cold energy released during the discharging phase of the LAES. According to Morgan and Dearman [227], the preferred material should have a thermal capacity to conductivity ratio $(c_p \cdot \rho)/k > 180$ s/mm$^2$, and more preferably $(c_p \cdot \rho)/k > 500$ s/mm$^2$, where $c_p$ [kJ/(kg·K)] is the specific heat, $\rho$ [kg/m$^3$] is the density and $k$ [W/(m·K)] is the thermal conductivity. Rock was selected to be the storage material since its $(c_p \cdot \rho)/k = 867$ s/mm$^2$ and the cost is low. As a result, in the analysis conducted by Sciacovelli et al. [19], the amount of cold energy that can

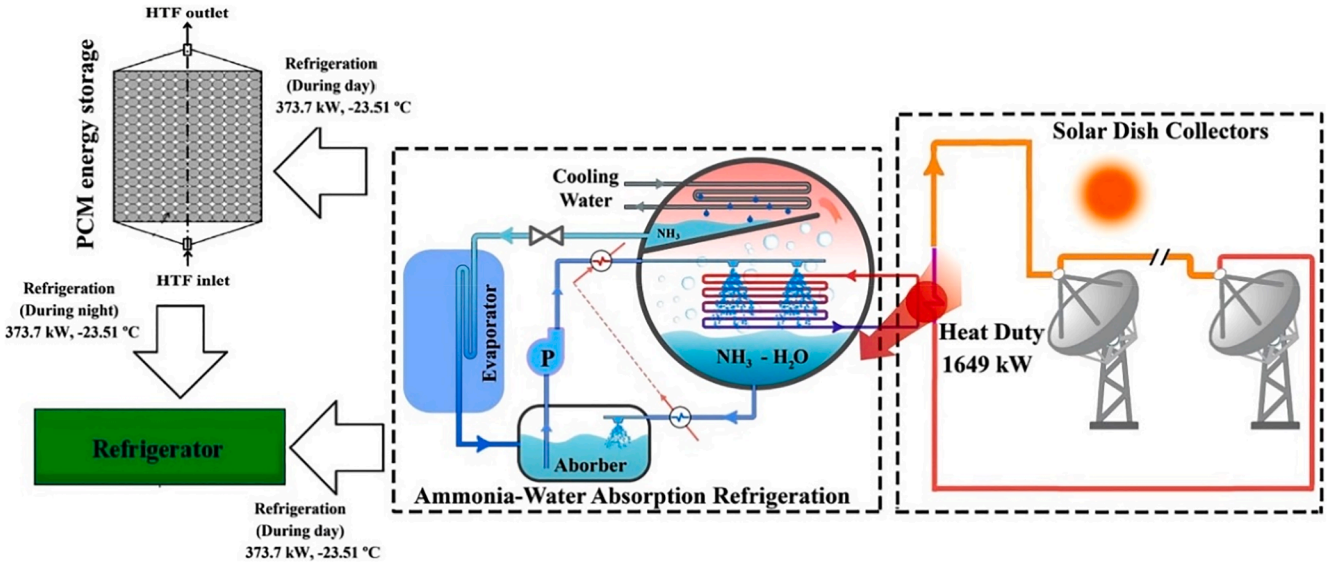


**Fig. 25.** Scheme of the ammonia-water absorption refrigeration system with CTES integration [78].

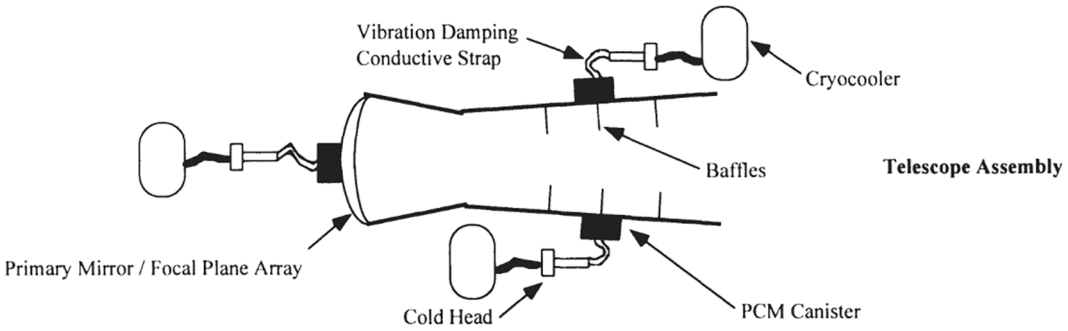


**Fig. 26.** Application of using CTES for cooling and temperature control of a space telescope assembly [56].

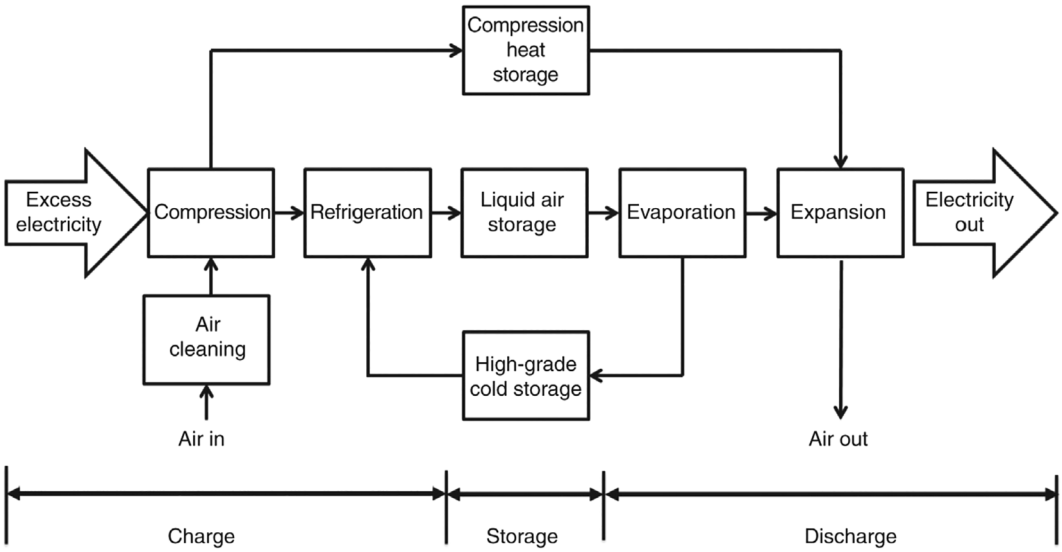


**Fig. 27.** Illustration of the process of a LAES system [233].

be stored is crucial to the overall performance of a LAES system. A 16% increase in the recycled cold energy increases the round trip efficiency by 20% and the liquid yield by 30%.

*5.2.2. Pumped thermal energy storage (PTES)*

Pumped thermal energy storage or pumped thermal electricity storage is another type of promising technology for large scale storage of electricity [234]. CTES is a crucial part of a PTES system. So far,

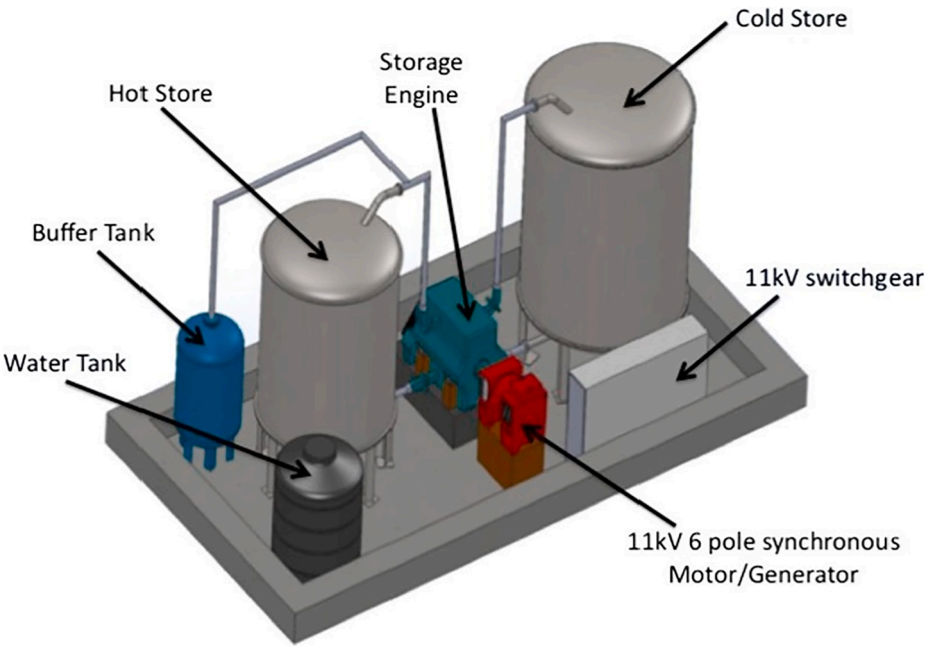


**Fig. 28.** A PTES system developed by Newcastle University [236].

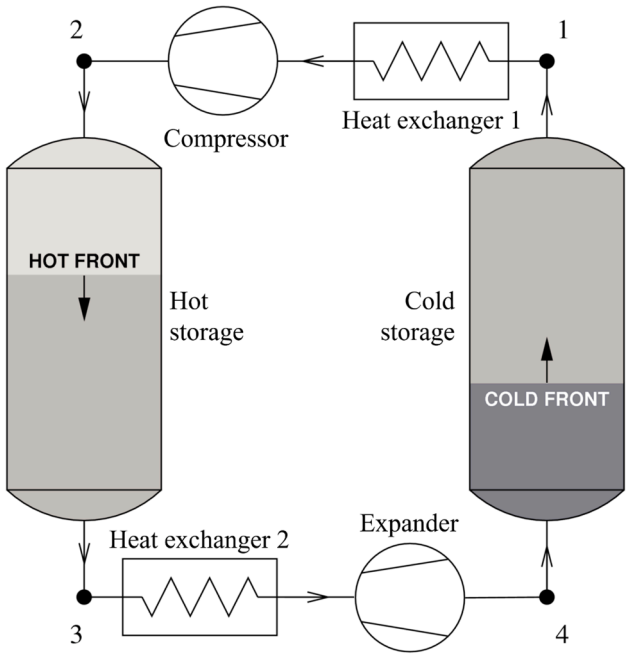


**Fig. 29.** The layout of a PTES system adapted from White et al. [26].

developments of the PTES technology and its CTES system are still in the early stage, mainly focusing on system design and pilot plant construction. A pilot plant has been developed by Isentropic Ltd and Newcastle University with a storage capacity of 600 kWh [215,235] (as illustrated in Fig. 28), but more research efforts may be expected.

A PTES system has two thermal energy storage facilities: one hot TES and one cold TES, with a heat pump/engine cycle in between them. A simple drawing of the working principle of a PTES system [26] is illustrated in Fig. 29. During the charging phase, the system operates like a heat pump, where excess electricity is used to extract heat from the cold storage to the hot storage; during the discharging phase, the system operates as a heat engine, where fluid from the hot store produces electricity via an expander, cools down, and flows back to the cold storage and produces electricity.

Although latent heat CTES using the salt-water solution is also mentioned [234,237], most of the studies propose sensible CTES for the cold storage of the PTES. In the system proposed by White et al. [26], the CTES facility needs to store cold energy as low as around 100 K. Thus, sensible heat CTES materials such as packed-bed of pebbles or gravel, or uniform ceramic matrix are used. The energy density of using gravels can reach 50 kWh/m$^3$, comparing to 1.4 kWh/m$^3$ of pumped hydro energy storage and 10 kWh/m$^3$ of compressed air energy storage. However, Davenne et al. [18] suggested that a liquid thermocline can be significantly more effective than a solid packed-bed (as depicted in Fig. 7) with a much less exergy loss. A sliding divider within the liquid thermocline to separate the cold and warm parts was proposed to further decrease the exergy loss. Laughlin [44] suggested using n-hexane as the liquid sensible cold storage material for PTES. n-hexane is pervasive, biodegradable, and cheap, although it is also highly flammable and neurotoxic.

#### 5.2.3. *Superconducting flywheel energy storage (SFES) system*

Lee et al. [90] proposed and experimented with a concept of CTES integrated superconducting flywheel energy storage system (SFES). Comparing to conventional flywheel energy storage systems, the SFES has a much smaller kinetic energy loss due to the levitation of superconductors. However, superconductors work in cryogenic temperature ranges and require a non-negligible amount of electricity consumed by the refrigeration system. The authors proposed to introduce solid nitrogen CTES into the SFES system. During the charging phase, electricity is not only converted to kinetic energy but also the cold energy of the CTES. During the discharging phase, the stored cold energy is used as the cooling source instead of consuming the kinetic energy to run the cryocooler. Therefore, the energy loss due to cryogenic cooling was greatly reduced, and the energy storage capacity of the SFES was significantly increased. However, the development of applying CTES in superconducting applications is still at an early stage. More superconducting systems using other CTES materials with lower temperatures can be explored.

### 5.3. *Waste cold energy recovery*

Some energy processes that work in sub-zero temperature ranges,

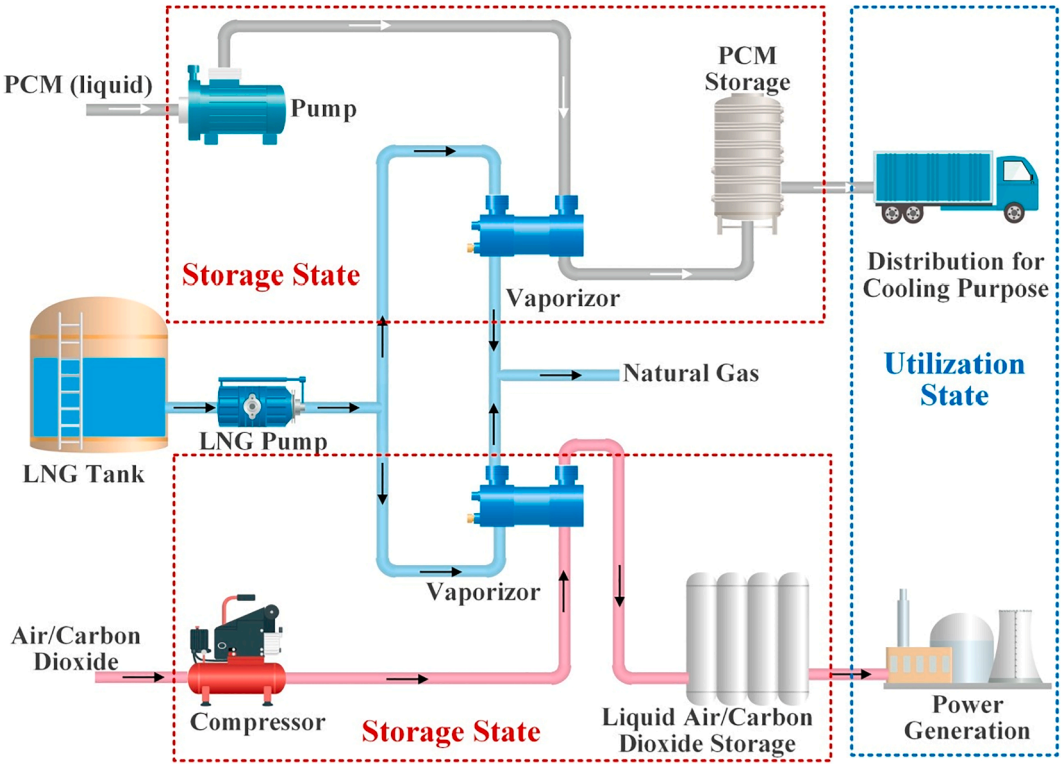


**Fig. 30.** Concepts of CTES for LNG cold energy utilization [5].

such as regasification of liquefied natural gas (LNG) and discharging of high-pressure hydrogen storage tanks, produce waste cold energy that can be captured by CTES for later use. CTES implemented in combination with such energy systems can increase the overall efficiency, reduce energy consumption, and smooth the fluctuation of the energy supply.

*5.3.1. Boil-off Gas (BOG) re-liquefaction of an LNG terminal*

Liquefied natural gas (LNG) plays an essential role in the energy mix

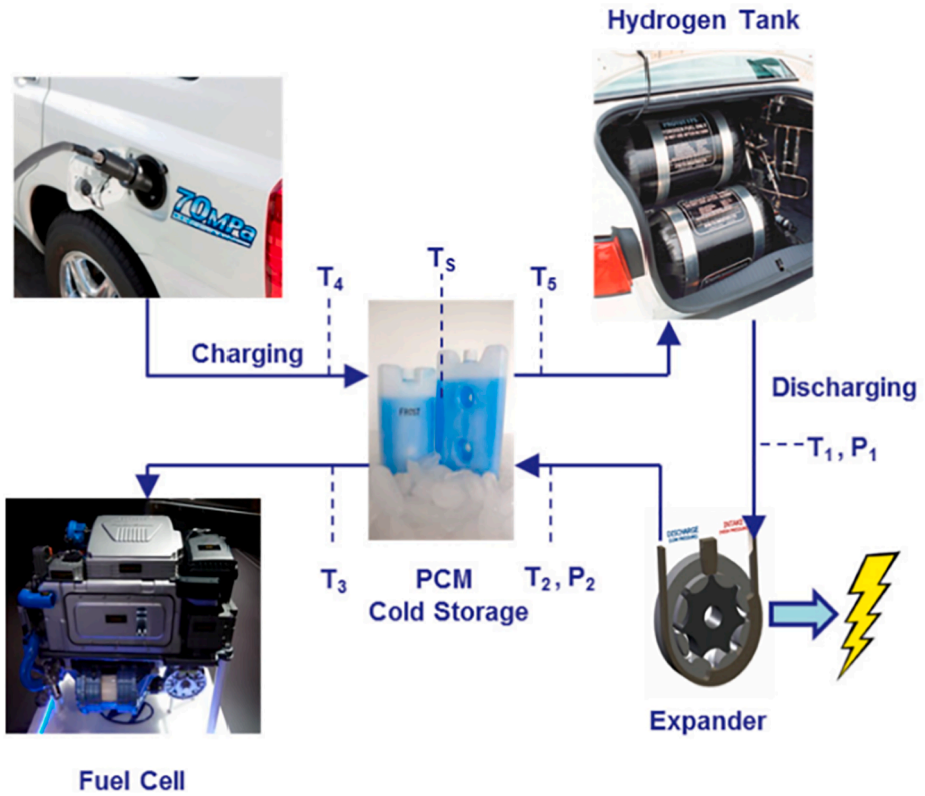


**Fig. 31.** Configuration of the hydrogen pressure energy recovery system using CTES in fuel cell vehicle [214].

of many countries globally, especially in Europe and Asia [238]. Various systems have been proposed to recover the fast-growing liquefied natural gas (LNG) cold energy that is generally wasted during the regasification process [5,239]. However, the daily and seasonal LNG demand of a terminal fluctuates due to the varying electricity and city gas demand, increasing difficulty for utilizing the cold energy directly. CTES can be used to smooth the fluctuation of cold energy supply and effectively make use of the LNG cold energy [59]. Despite the vast potential, using CTES for LNG cold recovery is nonetheless rarely mentioned.

Senboku Terminal II of Osaka Gas installed a BOG re-liquefaction facility with a cold energy storage system [240-244]. Instead of directly compressing the BOG to high pressure, the system pressurizes the BOG to 0.8 MPa and mixes it with the LNG flow. During the daytime operation, where the flow rate of LNG is high, the cold energy of the LNG is enough to re-liquefy the BOG at that pressure. Extra cold energy is stored in the CTES system containing a PCM that freezes at −130 °C. During the night time operation, where the flow rate of LNG is not enough to re-liquefy the BOG in the LNG/BOG two-phase flow, the CTES releases the cold energy for the BOG re-liquefaction. In an analysis conducted by Ito et al. [242], compared to the conventional method of compressing the BOG for re-liquefaction, the use of the CTES system can reduce the compression power by 30–60%.

Besides BOG reliquefication, He et al. [5] described the concept of using PCM to store the LNG cold energy and later use it for other purposes. As shown in Fig. 30, PCM can be used for distribution for cooling purposes, and air or carbon dioxide is suitable for power generation. More CTES systems using CTES to recover LNG's cold energy are worth exploring.

#### 5.3.2. Hydrogen fueling of fuel cell vehicles

As a promising zero-carbon alternative to fossil fuels, hydrogen is gaining increasing attention these days, especially in the transportation sector [245]. Kim et al. [214] proposed a CTES integrated system for high-pressure hydrogen fueling of fuel cell vehicles. The pressure of hydrogen stored in fuel cell vehicles is around 70 MPa. Fast fueling of the high-pressure hydrogen at the fueling stations can significantly increase the temperature inside the hydrogen tanks. Pre-cooling of the hydrogen can help keep the temperature below the maximum allowance tank temperature and increase the amount of hydrogen that can be stored. However, a pre-cooling chiller adds to the investment and operation costs of the fueling station. The authors proposed an on-board system to recover the pressure energy of the hydrogen and reduce the energy consumption of the chiller. During the driving process, high-pressure hydrogen is released to the fuel cell, and the pressure is reduced from 70 MPa to 1 MPa in an expander. The expander provides additional power to the vehicle. Cooled hydrogen is then used to charge the PCM-based CTES. The CTES is filled with a PCM that freezes at −26 °C. During the fueling process, cold energy is released from the CTES to pre-cool the incoming hydrogen. The process of the system is illustrated in Fig. 31. The authors found that the fuel consumption of the vehicle can be reduced by 3–5% due to the additional expander power, and the cooling demand of the fueling station can also be saved. For future studies, more applications of using CTES for the hydrogen industry, not only for pressurized tanks but also other means of storage technologies, especially liquid hydrogen storage, can be investigated.

### 5.4. Summary and outlook of CTES application explorations

As summarized in Table 12, some CTES technologies have already been commercially deployed for refrigeration, electricity storage, and waste cold recovery. However, more applications should be explored with the mechanical design of the CTES facility and performance evaluation of the whole energy system, especially paying more attention to the economic analysis and life cycle assessment (LCA) [25,194].

For refrigeration applications, CTES used for household freezers and food storage chambers, refrigerated transportation, and warehousing, both actively and passively, have been widely studied. Besides, CTES can also be applied to the refrigeration systems used in space exploration devices. In general, CTES enhances the system's performance, reduces energy consumption, improves temperature control, decreases the overall operational cost, and reduces the noise level. However, study about using CTES for large scale refrigeration systems, especially for fast-growing cooling demand of data centers and district cooling systems, and the role of using CTES to help in grid integration of renewable energies has not been fully studied. The use of PCM for catering and medical purposes can also be improved [8].

For electricity storage applications, CTES is an essential part of LAES and PTES systems and has the potential to improve the performance of the SFES significantly. CTES used for LAES has been commercially demonstrated using pack-bed of sensible materials, while the studies of CTES technologies for PTES and SFES are still in the early stages. More CTES units should be designed and tested. Better integration of CTES into these novel electricity storage systems, as well as other electricity storage technologies, can also be further explored.

CTES has been used to recover the waste cold energy from LNG during the re-gasification process and hydrogen fuel from the discharging process to power fuel-cell vehicles. One project has been commercially deployed for using the LNG cold energy for BOG re-liquefaction. Future studies can be carried out to improve the design of the CTES systems, as well as recover the waste cold energy from more cryogenic systems, including liquefied natural gas, liquid hydrogen, liquid ammonia, and air separation.

Table 12 also summarized the materials used for each application, reasons for the selection, and their thermal properties. In general, a suitable temperature range is the foremost criteria for material selection. Other widely considered factors, such as energy density, density, heat capacity, heat conductivity, and corrosion, will be taken into consideration only if the operation temperature is suitable. For commercial applications, cost, environmental influence, and accessibility of the material are also key factors. Regarding different application types, refrigeration, waste cold recovery, and small-scale electricity storage systems prefer PCMs with the desired PCT. In various applications, additives to PCMs are used to enhance the properties. Commercial PCM products are widely used, while some studies used in-house developed formulas with lower cost. If the PCM slurry is used, the viscosity should also be considered. On the other hand, large-scale electricity storage systems still rely on sensible materials due to the cost and temperature range concerns since the cold storage of electricity storage usually operates in cryogenic temperatures, and limited PCMs are available for that temperature range. Table 1, Table 2, and Table 4 show that although numerous materials have been developed or have the potential to be used for CTES systems, only a few have been tested in real applications. Therefore, future studies should be carried out to explore more materials for all of the existing and future applications.

To provide a clear and fast overview of the research stages and potential research directions, Fig. 32 summarizes the key conclusions, including temperature ranges, TRLs, research stages, and potential research opportunities of cold thermal energy storage studies discussed in each section.

## 6. Conclusion

Overall, the current review paper summarizes the up-to-date research and industrial efforts in the development of cold thermal energy storage technology and compiles in a single document various available materials, numerical and experimental works, and existing applications of cold thermal energy storage systems designed for sub-zero temperatures. As the main conclusion, it may be remarked the vast potential of cold thermal energy storage is far from being fully deployed, and more research efforts should be invested to develop cold thermal energy storage technology for sub-zero temperature applications.


**Fig. 32.** Summary of temperature ranges, Technology readiness levels, research stages, and potential research opportunities of CTES studies.

For cold thermal energy storage technology materials, suitable thermal energy storage materials that can be used for cold thermal energy storage, as well as their thermal properties and enhancement methods, are listed and discussed. The amount of available and under-development phase change materials is significantly larger than sensible (both solid and liquid) materials. Fewer phase change materials have been developed for applications below −50 °C, and the energy density reduces remarkably as the melting temperature decreases. Some of the materials present corrosion, safety, and phase separation issues (in the case of phase change materials) to be overcome before being considered as suitable candidates for cold thermal energy storage applications. The future research direction for cold thermal energy storage material development should move towards cryogenic temperature ranges with more favorable thermal properties.

The number of research publications about numerical simulations and experimental studies of cold thermal energy storage at sub-zero temperature ranges is limited but growing fast. The most numerical and experimental analysis focuses on packed-bed and thermocline, shell-and-tube, plate-shaped, and slurry-based cold thermal energy storage systems for different applications. The former two are the most widely studied. Although some cold thermal energy storage systems are commercially available, more numerical and experimental studies should be conducted to develop advanced numerical methods, enhance the heat transfer, improve thermo-mechanical properties, enhance system modularity, and explore more cold thermal energy storage materials for all of the cold thermal energy storage types. Particular attention should be paid to promising slurry-based systems.

Some cold thermal energy storage technologies have already been commercially deployed for sub-zero temperature applications, but the potential of utilizing cold thermal energy storage has not been fully unveiled. Cold thermal energy storage used for refrigeration systems has been widely studied to reduce energy consumption, improve temperature control, and decrease the overall operational cost. For electricity storage systems, cold thermal energy storage is the essential part of the promising liquid air energy storage and pumped thermal energy storage systems and has the potential to significantly improve the performance of the superconducting flywheel energy storage systems. Cold thermal energy storage has been used to recover the waste cold energy from Liquified natural gas during the re-gasification process and hydrogen fuel from the discharging process to power fuel-cell vehicles. Future studies can be carried out to improve the design of the cold thermal energy storage systems for all the applications, as well as explore the usage of cold thermal energy storage in more energy systems and recover the waste cold energy from more sources.

## Declaration of Competing Interest

The authors declare that they have no known competing financial interests or personal relationships that could have appeared to influence the work reported in this paper.

## Acknowledgments

The authors would like to acknowledge the funding support from SJ-NTU Corporate Lab.

This work was partically funded by the Ministerio de Ciencia, Innovación y Universidades de España (RTI2018-093849-B-C31 - MCIU/AEI/FEDER, UE), and the Ministerio de Ciencia, Innovación y Universidades - Agencia Estatal de Investigación (AEI) (RED2018-102431-T). The authors at the University of Lleida would like to thank the Catalan Government for the quality accreditation given to their research group (2017 SGR 1537). GREiA is certified agent TECNIO in the

category of technology developers from the Government of Catalonia. This work is partially supported by ICREA under the ICREA Academia program.

## References


[1] United Nations, Department of Economics and Social Affairs, Population Division. World population prospects 2019: Highlights (ST/ESA/SER.A/423). New York: 2019.
[2] FAO. Food Loss and Food Waste n.d. http://www.fao.org/food-loss-and-food-waste/en/ (accessed June 12, 2020).
[3] United Nations Environment Programme. The importance of energy efficiency in the refrigeration and heat pump sectors; 2018.
[4] Royal Dutch Shell. Shell LNG Outlook 2020; 2020.
[5] He T, Chong ZR, Zheng J, Ju Y, Linga P. LNG cold energy utilization: prospects and challenges. Energy 2019;170:557–68. https://doi.org/10.1016/j.energy.2018.12.170.
[6] Li SF, Liu Z, Wang XJ. A comprehensive review on positive cold energy storage technologies and applications in air conditioning with phase change materials. Appl Energy 2019;255:113667. https://doi.org/10.1016/j.apenergy.2019.113667.
[7] Li G, Hwang Y, Radermacher R, Chun HH. Review of cold storage materials for subzero applications. Energy 2013;51:1–17. https://doi.org/10.1016/j.energy.2012.12.002.
[8] Oró E, de Gracia A, Castell A, Farid MM, Cabeza LF. Review on phase change materials (PCMs) for cold thermal energy storage applications. Appl Energy 2012;99:513–33. https://doi.org/10.1016/j.apenergy.2012.03.058.
[9] Ndanduleni C, Huan Z, Design I, Huan PZ, Ndanduleni C, Huan Z. Review on phase change materials for sub-zero temperature application in transport refrigeration 2019:1–10.
[10] Veerakumar C, Sreekumar A. Phase change material based cold thermal energy storage: materials, techniques and applications - A review. Int J Refrig 2016;67:271–89. https://doi.org/10.1016/j.ijrefrig.2015.12.005.
[11] Agyenim F, Hewitt N, Eames P, Smyth M. A review of materials, heat transfer and phase change problem formulation for latent heat thermal energy storage systems (LHTESS). Renew Sustain Energy Rev 2010;14:615–28. https://doi.org/10.1016/j.rser.2009.10.015.
[12] Xu H, Romagnoli A, Sze JY, Py X. Application of material assessment methodology in latent heat thermal energy storage for waste heat recovery. Appl Energy 2017;187:281–90. https://doi.org/10.1016/j.apenergy.2016.11.070.
[13] IRENA. Innovation Outlook: Thermal Energy Storage. Abu Dhabi: 2020.
[14] Navarro ME, Martínez M, Gil A, Fernández AI, Cabeza LF, Olives R, et al. Selection and characterization of recycled materials for sensible thermal energy storage. Sol Energy Mater Sol Cells 2012;107:131–5. https://doi.org/10.1016/j.solmat.2012.07.032.
[15] Sarbu I, Sebarchievici C. A comprehensive review of thermal energy storage. Sustain 2018;10. https://doi.org/10.3390/su10010191.
[16] Hüttermann L, Span R, Maas P, Scherer V. Investigation of a liquid air energy storage (LAES) system with different cryogenic heat storage devices. Energy Procedia 2019;158:4410–5. https://doi.org/10.1016/j.egypro.2019.01.776.
[17] Hüttermann L, Span R. Influence of the heat capacity of the storage material on the efficiency of thermal regenerators in liquid air energy storage systems. Energy 2019;174:236–45. https://doi.org/10.1016/j.energy.2019.02.149.
[18] Davenne TR, Garvey SD, Cardenas B, Simpson MC. The cold store for a pumped thermal energy storage system. J Energy Storage 2017;14:295–310. https://doi.org/10.1016/j.est.2017.03.009.
[19] Sciacovelli A, Vecchi A, Ding Y. Liquid air energy storage (LAES) with packed bed cold thermal storage – From component to system level performance through dynamic modelling. Appl Energy 2017;190:84–98. https://doi.org/10.1016/j.apenergy.2016.12.118.
[20] Chai L, Liu J, Wang L, Yue L, Yang L, Sheng Y, et al. Cryogenic energy storage characteristics of a packed bed at different pressures. Appl Therm Eng 2014;63:439–46. https://doi.org/10.1016/j.applthermaleng.2013.11.030.
[21] Hüttermann L, Span R. Investigation of storage materials for packed bed cold storages in liquid air energy storage (LAES) systems. Energy Procedia 2017;143:693–8. https://doi.org/10.1016/j.egypro.2017.12.748.
[22] National Institute of Standards and Technology. NIST Chemistry WebBook, NIST Standard Reference Database Number 69. Gaithersburg: 2020. https://doi.org/10.18434/T4D303.
[23] Engineering ToolBox 2001. https://www.engineeringtoolbox.com (accessed February 8, 2021).
[24] Eppelbaum L, Kutasov I, Pilchin A. Applied geothermics. Berlin, Heidelberg: Springer Berlin Heidelberg; 2014. https://doi.org/10.1007/978-3-642-34023-9.
[25] Mohamed SA, Al-Sulaiman FA, Ibrahim NI, Zahir MH, Al-Ahmed A, Saidur R, et al. A review on current status and challenges of inorganic phase change materials for thermal energy storage systems. Renew Sustain Energy Rev 2017;70:1072–89. https://doi.org/10.1016/j.rser.2016.12.012.
[26] White A, Parks G, Markides CN. Thermodynamic analysis of pumped thermal electricity storage. Appl Therm Eng 2013;53:291–8. https://doi.org/10.1016/j.applthermaleng.2012.03.030.
[27] Pan J, Zou R, Jin F. Experimental study on specific heat of concrete at high temperatures and its influence on thermal energy storage. Energies 2016;10:33. https://doi.org/10.3390/en10010033.
[28] Guo Z. Principles of Reinforced Concrete. First. Elsevier; 2014. https://doi.org/10.1016/C2013-0-13698-7.
[29] Choy CL, Greig D. The low temperature thermal conductivity of isotropic and oriented polymers. J Phys C Solid State Phys 1977;10.
[30] Grebowicz J, Lau S-F, Wunderlich B. The thermal properties of polypropylene. J Polym Sci Polym Symp 1984;71:19–37. https://doi.org/10.1002/polc.5070710106.
[31] SpecialChem. The Definitive Guide to Polypropylene (PP); 2020. https://omnexus.specialchem.com/selection-guide/polypropylene-pp-plastic (accessed February 8, 2021).
[32] Springer Nature. Springer Materials; 2020. https://materials.springer.com/ (accessed February 8, 2021).
[33] Thakare KA, Vishwakarma HG, Bhave AG. Experimental investigation of possible use of hdpe as thermal storage material in thermal storage type solar cookers. Int J Res Eng Technol 2015;4:92–9. https://doi.org/10.15623/ijret.2015.0412019.
[34] INEOS. Engineering Properties of High Density Polyethylene. Texas: 2007.
[35] Richet P, Bottinga Y, Denielou L, Petitet JP, Tequi C. Thermodynamic properties of quartz, cristobalite and amorphous SiO2: drop calorimetry measurements between 1000 and 1800 K and a review from 0 to 2000 K. Geochim Cosmochim Acta 1982;46:2639–58. https://doi.org/10.1016/0016-7037(82)90383-0.
[36] Ratcliffe EH. Thermal conductivities of fused and crystalline quartz. Br J Appl Phys 1959;10:22–5. https://doi.org/10.1088/0508-3443/10/1/306.
[37] Sergeev OA, Shashkov AG, Umanskii AS. Thermophysical properties of quartz glass 1982;43:240.
[38] Håkansson B, Andersson P. Thermal conductivity and heat capacity of solid NaCl and NaI under pressure. J Phys Chem Solids 1986;47:355–62. https://doi.org/10.1016/0022-3697(86)90025-9.
[39] Carey EM, Vu T, Choukroun M, Zhong F, Cohen B, Barmatz M, et al. Thermal conductivity and specific heat measurements of hydrated salt mixtures with implications for icy satellites. 49th Lunar Planet Sci Conf 2018;2018(49):6–7.
[40] National Center for Biotechnology Information. Sodium chloride, CID=5234. PubChem Database n.d. https://pubchem.ncbi.nlm.nih.gov/compound/Sodium-chloride (accessed February 8, 2021).
[41] Furukawa GT, Douglas TB, McCoskey RE, Ginnings DC. Thermal properties of aluminum oxide from 0 to 1200 K. J Res Natl Bur Stand 1934;1956(57):67. https://doi.org/10.6028/jres.057.008.
[42] Xie Z, Xue W, Chen H, Huang Y. Mechanical and thermal properties of 99% and 92% alumina at cryogenic temperatures. Ceram Int 2011;37:2165–8. https://doi.org/10.1016/j.ceramint.2011.03.066.
[43] Kim S, Chen J, Cheng T, Gindulyte A, He J, He S, et al. PubChem 2019 update: improved access to chemical data. Nucleic Acids Res 2019;47:D1102–9. https://doi.org/10.1093/nar/gky1033.
[44] Laughlin RB. Pumped thermal grid storage with heat exchange. J Renew Sustain Energy 2017;9:044103. https://doi.org/10.1063/1.4994054.
[45] Rosen MA, Dincer I. Efficiency assessment of glycol cold thermal energy storage and effect of varying environment temperature. Trans Can Soc Mech Eng 2009;33:119–30. https://doi.org/10.1139/tcsme-2009-0011.
[46] Sharma A, Tyagi VV, Chen CR, Buddhi D. Review on thermal energy storage with phase change materials and applications. Renew Sustain Energy Rev 2009;13:318–45. https://doi.org/10.1016/j.rser.2007.10.005.
[47] Salazar A, Sánchez-Lavega A. Low temperature thermal diffusivity measurements of gases by the mirage technique. Rev Sci Instrum 1999;70:98–103. https://doi.org/10.1063/1.1149548.
[48] Engineers Edge LLC. Engineers edge; 2020. https://www.engineersedge.com/ (accessed February 8, 2021).
[49] Nuclear Power for Everybody. Neon – specific heat, latent heat of fusion, latent heat of vaporization; 2020. https://www.nuclear-power.net/neon-specific-heat-latent-heat-vaporization-fusion/ (accessed February 8, 2021).
[50] Wei J. Molecular symmetry, rotational entropy, and elevated melting points. Ind Eng Chem Res 1999;38:5019–27. https://doi.org/10.1021/ie990588m.
[51] Chao J, Hall KR, Yao J. Thermodynamic properties of simple alkenes. Thermochim Acta 1983;64:285–303. https://doi.org/10.1016/0040-6031(83)85005-9.
[52] Yaws CL, Sheth SD, Han M. Handbook of chemical compound data for process safety. Elsevier; 1997.
[53] Yaws CL. Thermal conductivity of liquid – organic compounds. Transp Prop Chem Hydrocarb, Elsevier 2009:299–395. https://doi.org/10.1016/B978-0-8155-2039-9.50012-0.
[54] Air Liquide. Gas Encyclopedia; 2020. https://encyclopedia.airliquide.com/ (accessed February 8, 2021).
[55] Watanabe H. Thermal conductivity and thermal diffusivity of sixteen isomers of alkanes: C n H 2 n +2 (n = 6 to 8). J Chem Eng Data 2003;48:124–36. https://doi.org/10.1021/je020125e.
[56] Glaister DS, Bell KD, Bello M, Stoyanof M. The development and verification of a cryogenic phase change thermal storage unit for spacecraft applications. In: R. G. Ross J, editor. Cryocoolers 8 - Proc. 8th Int. Cryocooler Conf. held June 28–30. 1994, Vaii, Color. New York: Springer Science+Business Media, LLC; 1995.
[57] Messerly JF, Todd SS, Guthrie GB. Chemical thermodynamic properties of the pentadienes. Third law studies. J Chem Eng Data 1970;15:227–32. https://doi.org/10.1021/je60045a036.
[58] Ross RG, editor. Cryocoolers 8. Boston, MA: Springer US; 1995. https://doi.org/10.1007/978-1-4757-9888-3.
[59] Yamashita Y, Hirata Y, Iwata Y, Yamazaki K, Ito Y. Performance and heat transfer characteristics of a latent heat storage unit with finned tubes: experimental study on liquefaction of LNG boil-off gas by melting n-pentane as a phase-change

material. Kagaku Kogaku Ronbunshu 2004;30:399–406. https://doi.org/10.1252/kakoronbunshu.30.399.
[60] Yamashita Y, Hirata Y, Iwata Y, Yamazaki K, Ito Y. Performance and heat transfer characteristics of a latent heat storage unit with finned tubes: experimental study on storage of LNG cold energy by freezing n-pentane as a phase-change material. Kagaku Kogaku Ronbunshu 2005;31:144–50. https://doi.org/10.1252/kakoronbunshu.31.144.
[61] CPR. Cyclopropane Safety Data Sheet; 1999.
[62] Haida O, Suga H, Seki S. Calorimetric study of the glassy state XII. Plural glass-transition phenomena of ethanol. J Chem Thermodyn 1977;9:1133–48. https://doi.org/10.1016/0021-9614(77)90115-X.
[63] Carlson HG, Westrum EF. Methanol: heat capacity, enthalpies of transition and melting, and thermodynamic properties from 5–300°K. J Chem Phys 1971;54:1464–71. https://doi.org/10.1063/1.1675039.
[64] Williams BG, J CB. ICE (Integrated Cooler Experiment) for COOLSAT. In: Cryocoolers 8 - Proc. 8th Int. Cryocooler Conf. held June 28-30. 1994, Vaii, Color. New York: Springer Science+Business Media, LLC; 1995.
[65] Andersson P. Thermal conductivity and heat capacity of cyclopentane in the range 100–300 K and up to 2·1 GPa. Mol Phys 1978;35:587–91. https://doi.org/10.1080/00268977800100411.
[66] Szasz GJ, Morrison JA, Pace EL, Aston JG. Thermal properties of cyclopentane and its use as a standard substance in low temperature thermal measurements. J Chem Phys 1947;15:562–4. https://doi.org/10.1063/1.1746595.
[67] Aston JG, Siller CW, Messerly GH. Heat capacities and entropies of organic compounds. III. Methylamine from 11.5°K. to the Boiling Point. Heat of Vaporization and Vapor Pressure. The entropy from molecular data. J Am Chem Soc 1937;59:1743–51. https://doi.org/10.1021/ja01288a054.
[68] Zhang Y, Baiocco D, Mustapha AN, Zhang X, Yu Q, Wellio G, et al. Hydrocolloids: nova materials assisting encapsulation of volatile phase change materials for cryogenic energy transport and storage. Chem Eng J 2020;382:123028. https://doi.org/10.1016/j.cej.2019.123028.
[69] Donabedian M. Spacecraft thermal control handbook, Volume II: Cryogenics. Washington, DC: American Institute of Aeronautics and Astronautics, Inc.; 2004. https://doi.org/10.2514/4.989148.
[70] Andon RJL, Counsell JF, Martin JF. Thermodynamic properties of organic oxygen compounds. Part XX. The low-temperature heat capacity and entropy of C4 and C5 ketones. J Chem Soc A Inorganic, Phys Theor 1968:1894. https://doi.org/10.1039/j19680001894.
[71] CONCOA. Acetylene properties; 2012. https://www.concoa.com/acetylene_properties.html (accessed February 8, 2021).
[72] Friend M, Stone S. Challenging requirements in resource challenged environment on a time challenged schedule: A technical solution to support the cold chain for the VSV-Zebov (Merck) Ebola vaccine in Sierra Leone Guinea. In: Proc 5th IEEE Glob Humanit Technol Conf GHTC 2015 2015:372–6. https://doi.org/10.1109/GHTC.2015.7343999.
[73] Zhang J, Li Y. Highly accurate prediction method for thermophysical properties of cryogenic phase change materials. Chem Eng Technol 2020:1–10. https://doi.org/10.1002/ceat.201900167.
[74] Andon RJL, Counsell JF, Lees EB, Martin JF. Thermodynamic properties of organic oxygen compounds. Part XXIII. Low-temperature heat capacity and entropy of C6, C7, and C9 ketones. J Chem Soc A Inorganic, Phys Theor 1970:833. https://doi.org/10.1039/j19700000833.
[75] Finke HL, Gross ME, Waddington G, Huffman HM. Low-temperature thermal data for the nine normal paraffin hydrocarbons from octane to hexadecane. J Am Chem Soc 1954;76:333–41. https://doi.org/10.1021/ja01631a005.
[76] Cheng W long, Ding M, Yuan X dong, Han BC. Analysis of energy saving performance for household refrigerator with thermal storage of condenser and evaporator. Energy Convers Manag 2017;132:180–8. https://doi.org/10.1016/j.enconman.2016.11.029.
[77] Xu X, Zhang X, Munyalo JM. Key technologies and research progress on enhanced characteristics of cold thermal energy storage. J Mol Liq 2019;278:428–37. https://doi.org/10.1016/j.molliq.2019.01.040.
[78] Ghorbani B, Mehrpooya M. Concentrated solar energy system and cold thermal energy storage (process development and energy analysis). Sustain Energy Technol Assessments 2020;37:100607. https://doi.org/10.1016/j.seta.2019.100607.
[79] Céondo GmbH. Chemeo; 2016. https://www.chemeo.com/.
[80] Parks GS, Huffman HM, Barmore M. Thermal data on organic compounds. XI. The heat capacities, entropies and free energies of ten compounds containing oxygen or nitrogen. J Am Chem Soc 1933;55:2733–40. https://doi.org/10.1021/ja01334a016.
[81] Stephens MA, Tamplin WS. Saturated liquid specific heats of ethylene glycol homologs. J Chem Eng Data 1979;24:81–2. https://doi.org/10.1021/je60081a027.
[82] Labban AK, Westrum Jr EF. Heat capacity and thermophysical properties of n -heptanoic cid from 5 to 350K. Can J Chem 1991;69:1796–803. https://doi.org/10.1139/v91-903.
[83] Sharma RK, Ganesan P, Tyagi VV, Metselaar HSC, Sandaran SC. Developments in organic solid–liquid phase change materials and their applications in thermal energy storage. Energy Convers Manag 2015;95:193–228. https://doi.org/10.1016/j.enconman.2015.01.084.
[84] Martin JF, Andon RJL. Thermodynamic properties of organic oxygen compounds Part LII. Molar heat capacity of ethanoic, propanoic, and butanoic acids. J Chem Thermodyn 1982;14:679–88. https://doi.org/10.1016/0021-9614(82)90083-0.
[85] Vargaftik NB. Handbook of thermal conductivity of liquids and gases. CRC Press; 1993.
[86] Yaws CL. Thermal conductivity graps for C5 to C7 compounds; 1995, p. 1–367. https://doi.org/10.1016/S1874-8783(06)80004-8.
[87] Aftab W, Huang X, Zou R. The application of carbon materials in latent heat thermal energy storage (LHTES). Therm. Transp. Carbon-Based Nanomater. 1st ed., Elsevier; 2017, p. 243–65. https://doi.org/10.1016/B978-0-32-346240-2.00009-1.
[88] Henchoz S, Favrat D, Marechal F, Girardin L. Novel district heating and cooling energy network using CO 2 as a heat and mass transfer fluid. In: 12th IEA Heat Pump Conf. 2017, Rotterdam: 2017, p. 1–11.
[89] Pellegrini M, Bianchini A. The innovative concept of cold district heating; 2018. https://doi.org/10.3390/en11010236.
[90] Lee J, Jeong S, Han YH, Park BJ. Concept of cold energy storage for superconducting flywheel energy storage system. IEEE Trans Appl Supercond 2011;21:2221–4. https://doi.org/10.1109/TASC.2010.2094177.
[91] National Center for Biotechnology Information. PubChem Compound Summary for CID 222, Ammonia; 2021. https://pubchem.ncbi.nlm.nih.gov/compound/Ammonia#section=Wikipedia (accessed February 8, 2021).
[92] The Editors of Encyclopaedia Britannica. Eutectic. Encycl Br; 2016.
[93] Rasta IM, Suamir IN. Study on thermal properties of bio-PCM candidates in comparison with propylene glycol and salt based PCM for sub-zero energy storage applications. IOP Conf Ser Mater Sci Eng 2019;494. https://doi.org/10.1088/1757-899X/494/1/012024.
[94] Nyoman Suamir I, Made Rasta I, Sudirman, Tsamos KM. Development of corn-oil ester and water mixture phase change materials for food refrigeration applications. Energy Procedia, vol. 161. Elsevier B.V.; 2019, p. 198–206. https://doi.org/10.1016/j.egypro.2019.02.082.
[95] Sze JY, Mu C, Romagnoli A, Li Y. Non-eutectic phase change materials for cold thermal energy storage. Energy Procedia 2017;143:656–61. https://doi.org/10.1016/j.egypro.2017.12.742.
[96] Gunasekara SN, Kumova S, Chiu JN, Martin V. Experimental phase diagram of the dodecane–tridecane system as phase change material in cold storage. Int J Refrig 2017;82:130–40. https://doi.org/10.1016/j.ijrefrig.2017.06.003.
[97] Sidik NAC, Kean TH, Chow HK, Rajaandra A, Rahman S, Kaur J. Performance enhancement of cold thermal energy storage system using nanofluid phase change materials: a review. Int Commun Heat Mass Transf 2018;94:85–95. https://doi.org/10.1016/j.icheatmasstransfer.2018.03.024.
[98] Sidney S, Dhasan M, C. S, Harish S. Experimental investigation of freezing and melting characteristics of graphene-based phase change nanocomposite for cold thermal energy storage applications. Appl Sci 2019;9:1099. https://doi.org/10.3390/app9061099.
[99] Wu T, Xie N, Niu J, Luo J, Gao X, Fang Y, et al. Preparation of a low-temperature nanofluid phase change material: MgCl2–H2O eutectic salt solution system with multi-walled carbon nanotubes (MWCNTs). Int J Refrig 2020;113:136–44. https://doi.org/10.1016/j.ijrefrig.2020.02.008.
[100] Chandrasekaran P, Cheralathan M, Kumaresan V, Velraj R. Enhanced heat transfer characteristics of water based copper oxide nanofluid PCM (phase change material) in a spherical capsule during solidification for energy efficient cool thermal storage system. Energy 2014;72:636–42. https://doi.org/10.1016/j.energy.2014.05.089.
[101] Wu S, Zhu D, Li X, Li H, Lei J. Thermal energy storage behavior of Al2O3–H2O nanofluids. Thermochim Acta 2009;483:73–7. https://doi.org/10.1016/j.tca.2008.11.006.
[102] Sutjahja IM, A U SR, Kurniati N, Pallitine ID, Kurnia D. The role of chemical additives to the phase change process of CaCl 2 .6H 2 O to optimize its performance as latent heat energy storage system. J Phys Conf Ser 2016;739:012064. https://doi.org/10.1088/1742-6596/739/1/012064.
[103] Chieruzzi M, Cerritelli GF, Miliozzi A, Kenny JM. Effect of nanoparticles on heat capacity of nanofluids based on molten salts as PCM for thermal energy storage. Nanoscale Res Lett 2013;8:448. https://doi.org/10.1186/1556-276X-8-448.
[104] Wu X, Wang Y, Sun R, Lai M, Du R, Zhang Z. The anti-supercooling effect of surface-modified nano-scaled SiO 2 in hydrated salts phase transition system. J Phys Conf Ser 2009;188:012046. https://doi.org/10.1088/1742-6596/188/1/012046.
[105] Wang F, Zhang C, Liu J, Fang X, Zhang Z. Highly stable graphite nanoparticle-dispersed phase change emulsions with little supercooling and high thermal conductivity for cold energy storage. Appl Energy 2017;188:97–106. https://doi.org/10.1016/j.apenergy.2016.11.122.
[106] Parameshwaran R, Deepak K, Saravanan R, Kalaiselvam S. Preparation, thermal and rheological properties of hybrid nanocomposite phase change material for thermal energy storage. Appl Energy 2014;115:320–30. https://doi.org/10.1016/j.apenergy.2013.11.029.
[107] Xie N, Huang Z, Luo Z, Gao X, Fang Y, Zhang Z. Inorganic salt hydrate for thermal energy storage. Appl Sci 2017;7:1317. https://doi.org/10.3390/app7121317.
[108] Sathishkumar A, Kumaresan V, Velraj R. Solidification characteristics of water based graphene nanofluid PCM in a spherical capsule for cool thermal energy storage applications. Int J Refrig 2016;66:73–83. https://doi.org/10.1016/j.ijrefrig.2016.01.014.
[109] Liu Y, Liu Y, Hu P, Li X, Gao R, Peng Q, et al. The effects of graphene oxide nanosheets and ultrasonic oscillation on the supercooling and nucleation behavior of nanofluids PCMs. Microfluid Nanofluidics 2015;18:81–9. https://doi.org/10.1007/s10404-014-1411-1.
[110] Sze JY, Mu C, Ayachi F, Yang L, Romagnoli A, Tay BK. Highly efficient nanofiller based on carboxylated graphene oxide in phase change materials for cold thermal energy storage. Energy Procedia 2018;152:198–203. https://doi.org/10.1016/j.egypro.2018.09.080.

[111] He Q, Wang S, Tong M, Liu Y. Experimental study on thermophysical properties of nanofluids as phase-change material (PCM) in low temperature cool storage. Energy Convers Manag 2012;64:199–205. https://doi.org/10.1016/j.enconman.2012.04.010.
[112] Mo S, Zhu K, Yin T, Chen Y, Cheng Z. Phase change characteristics of ethylene glycol solution-based nanofluids for subzero thermal energy storage. Int J Energy Res 2017;41:81–91. https://doi.org/10.1002/er.3599.
[113] Liang L, Chen X. Preparation and thermal properties of eutectic hydrate salt phase change thermal energy storage material. Int J Photoenergy 2018;2018:1–9. https://doi.org/10.1155/2018/6432047.
[114] Py X, Olives R, Mauran S. Paraffin/porous-graphite-matrix composite as a high and constant power thermal storage material. Int J Heat Mass Transf 2001;44:2727–37. https://doi.org/10.1016/S0017-9310(00)00309-4.
[115] Cabeza LF, Mehling H, Hiebler S, Ziegler F. Heat transfer enhancement in water when used as PCM in thermal energy storage. Appl Therm Eng 2002;22:1141–51. https://doi.org/10.1016/S1359-4311(02)00035-2.
[116] Yang X, Bai Q, Zhang Q, Hu W, Jin L, Yan J. Thermal and economic analysis of charging and discharging characteristics of composite phase change materials for cold storage. Appl Energy 2018;225:585–99. https://doi.org/10.1016/j.apenergy.2018.05.063.
[117] Yang X, Feng S, Zhang Q, Chai Y, Jin L, Lu TJ. The role of porous metal foam on the unidirectional solidification of saturating fluid for cold storage. Appl Energy 2017;194:508–21. https://doi.org/10.1016/j.apenergy.2016.09.050.
[118] Chen J, Ling Z, Fang X, Zhang Z. Experimental and numerical investigation of form-stable dodecane/hydrophobic fumed silica composite phase change materials for cold energy storage. Energy Convers Manag 2015;105:817–25. https://doi.org/10.1016/j.enconman.2015.08.038.
[119] Zarajabad OG, Ahmadi R, Ghaffari S. Numerical investigation of cold thermal energy storage using phase change material in freezer. Eur J Eng Res Sci 2017;2:1. https://doi.org/10.24018/ejers.2017.2.9.455.
[120] Cong L, She X, Leng G, Qiao G, Li C, Ding Y. Formulation and characterisation of ternary salt based solutions as phase change materials for cold chain applications. Energy Procedia 2019;158:5103–8. https://doi.org/10.1016/j.egypro.2019.01.690.
[121] Imran Hossen Khan M, Afroz HMM. Effect of phase change material on compressor on-off cycling of a household refrigerator. Sci Technol Built Environ 2015;21:462–8. https://doi.org/10.1080/23744731.2015.1023161.
[122] Du K, Calautit J, Wang Z, Wu Y, Liu H. A review of the applications of phase change materials in cooling, heating and power generation in different temperature ranges. Appl Energy 2018;220:242–73. https://doi.org/10.1016/j.apenergy.2018.03.005.
[123] Liu Z, Zhao D, Wang Q, Chi Y, Zhang L. Performance study on air-cooled household refrigerator with cold storage phase change materials. Int J Refrig 2017;79:130–42. https://doi.org/10.1016/j.ijrefrig.2017.04.009.
[124] Pérez-Masiá R, López-Rubio A, Lagarón JM. Development of zein-based heat-management structures for smart food packaging. Food Hydrocoll 2013;30:182–91. https://doi.org/10.1016/j.foodhyd.2012.05.010.
[125] Khan MIH, Afroz HMM. Effect of phase change material on performance of a household refrigerator. Asian J Appl Sci 2013;6:56–67.
[126] Lu W, Tassou SA. Characterization and experimental investigation of phase change materials for chilled food refrigerated cabinet applications 2013;112:1376–82. https://doi.org/10.1016/j.apenergy.2013.01.071.
[127] PCM Products Ltd. Sub-Zero Eutectic PCM Solutions; n.d. https://www.pcmproducts.net/Eutectic_Refrigeration_PCMs.htm (accessed February 8, 2021).
[128] Rubitherm. PCM SP-LINE 2020. https://www.rubitherm.eu/en/index.php/productcategory/anorganische-pcm-sp (accessed February 8, 2021).
[129] TEAP. PCM phase change material materials manufacturers; 2020. http://teappcm.com/ (accessed February 8, 2021).
[130] Va-Q-Tec. Va-Q-Tec Download Center; 2020. https://va-q-tec.com/en/downloadcenter/ (accessed February 8, 2021).
[131] PURETEMP LLC. Puretemp technical data sheets; 2020. https://www.puretemp.com/stories/puretemp-technical-data-sheets (accessed February 8, 2021).
[132] Cristopia. Cristopia energy systems; 2020. https://www.ciat.uk.com/wp-content/uploads/2017/02/cristopia-brochure.pdf (accessed February 8, 2021).
[133] Microtek Laboratories. Product data sheets; 2020. https://www.microteklabs.com/product-data-sheets (accessed February 8, 2021).
[134] PLUSS. savE PCMs product range; 2020. https://www.pluss.co.in/product-range-PCM.php (accessed February 8, 2021).
[135] Climator. Product data sheets; 2020. https://www.climator.com/en/pcm-climsel/product-data-sheets (accessed February 8, 2021).
[136] Harald Mehling, Cabeza LF. Heat and cold storage with PCM: An up to date introduction into basics and applications. 1st ed. 2008. https://doi.org/10.1007/978-3-540-68557-9.
[137] Aftab W, Huang X, Zou R. The application of carbon materials in latent heat thermal energy storage (LHTES). 1st ed. Elsevier Inc.; 2017. https://doi.org/10.1016/B978-0-32-346240-2.00009-1.
[138] Höhlein S, König-Haagen A, Brüggemann D. Macro-encapsulation of inorganic phase-change materials (PCM) in metal capsules. Materials (Basel) 2018;11. https://doi.org/10.3390/ma11091752.
[139] Materials PC, Transport CC. thermoTab active Materials in Cold Chain Transport; n.d.
[140] Mehling H, Cabeza LF. Heat and cold storage with PCM: An up to date introduction into basics and applications. 1st ed. 2008. https://doi.org/10.1007/978-3-540-68557-9.
[141] Thamaraikannn R, Kanimozhi B, Anish M, Jayaprabakar J, Saravanan P, Nicholas AR. Review of phase change materials based on energy storage system with applications. IOP Conf Ser Mater Sci Eng 2017;197. https://doi.org/10.1088/1757-899X/197/1/012034.
[142] Dhaidan NS, Khodadadi JM. Melting and convection of phase change materials in different shape containers: a review. Renew Sustain Energy Rev 2015;43:449–77. https://doi.org/10.1016/j.rser.2014.11.017.
[143] Oró E, Miró L, Barreneche C, Martorell I, Farid MM, Cabeza LF. Corrosion of metal and polymer containers for use in PCM cold storage. Appl Energy 2013;109:449–53. https://doi.org/10.1016/j.apenergy.2012.10.049.
[144] Abdolmaleki L, Sadrameli SM, Pirvaram A. Application of environmental friendly and eutectic phase change materials for the efficiency enhancement of household freezers. Renew Energy 2020;145:233–41. https://doi.org/10.1016/j.renene.2019.06.035.
[145] Gin B, Farid MM. The use of PCM panels to improve storage condition of frozen food. J Food Eng 2010;100:372–6. https://doi.org/10.1016/j.jfoodeng.2010.04.016.
[146] Selvnes H, Hafner A, Kauko H. Cold thermal energy storage integration in a large industrial refrigeration system. Refrig. Sci. Technol., vol. 2018- June, 2018, p. 1231–8. https://doi.org/10.18462/iir.gl.2018.1383.
[147] Trojanowska A, Nogalska A, Valls RG, Giamberini M, Tylkowski B. Technological solutions for encapsulation. Phys Sci Rev 2017;2:1–20. https://doi.org/10.1515/psr-2017-0020.
[148] Raaijmakers MJT, Benes NE. Current trends in interfacial polymerization chemistry. Prog Polym Sci 2016;63:86–142. https://doi.org/10.1016/j.progpolymsci.2016.06.004.
[149] Zhang P, Ma ZWW. An overview of fundamental studies and applications of phase change material slurries to secondary loop refrigeration and air conditioning systems. Renew Sustain Energy Rev 2012;16:5021–58. https://doi.org/10.1016/j.rser.2012.03.059.
[150] Youssef Z, Delahaye A, Huang L, Trinquet F, Fournaison L, Pollerberg C, et al. State of the art on phase change material slurries. Energy Convers Manag 2013;65:120–32. https://doi.org/10.1016/j.enconman.2012.07.004.
[151] Fan YF, Zhang XX, Wang XC, Li J, Zhu QB. Super-cooling prevention of microencapsulated phase change material. Thermochim Acta 2004;413:1–6. https://doi.org/10.1016/j.tca.2003.11.006.
[152] Jamekhorshid A, Sadrameli SM, Farid M. A review of microencapsulation methods of phase change materials (PCMs) as a thermal energy storage (TES) medium. Renew Sustain Energy Rev 2014;31:531–42. https://doi.org/10.1016/j.rser.2013.12.033.
[153] Schossig P, Gschwander S. PCS-slurries as heat transfer and storage fluids for cooling applications; 2007.
[154] Shi XJ, Zhang P. Cold storage by tetra-n-butyl ammonium bromide clathrate hydrate slurry generated with different storage approaches at 40 wt% initial aqueous solution concentration. Int J Refrig 2014;42:77–89. https://doi.org/10.1016/j.ijrefrig.2014.02.002.
[155] International Institute of Refrigeration. Handbook on Ice Slurries: Fundamentals and Engineering. Paris: 2005.
[156] Dincer I, Ezan MA. Heat Storage: A unique solution for energy systems. Cham: Springer International Publishing; 2018. https://doi.org/10.1007/978-3-319-91893-8.
[157] Meewisse JW. Fluidized Bed Ice Slurry Generator for Enhanced Secondary Cooling Systems. Technische Universiteit Delft; 2004.
[158] Kauffeld M, Wang MJ, Goldstein V, Kasza KE. Ice slurry applications. Int J Refrig 2008;23:1–7. https://doi.org/10.1016/j.ijrefrig.2010.07.018.ICE.
[159] Guilpart J, Stamatiou E, Delahaye A, Fournaison L. Comparison of the performance of different ice slurry types depending on the application temperature. Int J Refrig 2006;29:781–8. https://doi.org/10.1016/j.ijrefrig.2005.11.009.
[160] Melinder Å. Thermophysical properties of aqueous solutions used as secondary working fluids. KTH 2007. https://doi.org/10.1246/nikkashi1898.70.10_1641.
[161] Melinder Å, Granryd E. Using property values of aqueous solutions and ice to estimate ice concentrations and enthalpies of ice slurries. Int J Refrig 2005;28:13–9. https://doi.org/10.1016/j.ijrefrig.2004.07.013.
[162] Klaas Visser, Honorary M.IIR, M Airah MI. Carbon dioxide (CO2) FOR the food processing and cold storage industries. Off J AIRAH 2002:16–23.
[163] Ma ZWW, Zhang P. Pressure drop and heat transfer characteristics of tetra-n-butyl ammonium bromide clathrate hydrate slurry during flow melting and generating in a double-tube heat exchanger. Exp Therm Fluid Sci 2013;44:227–34. https://doi.org/10.1016/j.expthermflusci.2012.06.012.
[164] Hauer A. Sorption Theory for Thermal Energy Storage. In: Paksoy HÖ, editor. Therm. Energy Storage Sustain. Energy Consum. Springer; 2007, p. 393–408. https://doi.org/10.1007/978-1-4020-5290-3_24.
[165] Mugnier D, Goetz V. Energy storage comparison of sorption systems for cooling and refrigeration. Sol Energy 2001;71:47–55. https://doi.org/10.1016/S0038-092X(01)00013-5.
[166] Cot-Gores J, Castell A, Cabeza LF. Thermochemical energy storage and conversion: a-state-of-the-art review of the experimental research under practical conditions. Renew Sustain Energy Rev 2012;16:5207–24. https://doi.org/10.1016/j.rser.2012.04.007.
[167] Li G, Hwang Y, Radermacher R. Review of cold storage materials for air conditioning application. Int J Refrig 2012;35:2053–77. https://doi.org/10.1016/j.ijrefrig.2012.06.003.
[168] Cabeza LF, Mehling H. Review on thermal energy storage with phase change: materials, heat transfer analysis and applications. vol. 23; 2003.
[169] NASA. Technology readiness level definitions 1989:1.

[170] White AJ. Loss analysis of thermal reservoirs for electrical energy storage schemes. Appl Energy 2011;88:4150–9. https://doi.org/10.1016/j.apenergy.2011.04.030.
[171] Azzouz K, Leducq D, Gobin D. Enhancing the performance of household refrigerators with latent heat storage: an experimental investigation. Int J Refrig 2009;32:1634–44. https://doi.org/10.1016/j.ijrefrig.2009.03.012.
[172] Mohammed Ahnkaa, Toma RR. Experimental study on thermal energy storage produced by solar energy for driving domestic freezer. J Eng Sci Technol 2018;13:2829–42.
[173] Oró E, Chiu J, Martin V, Cabeza LF. Comparative study of different numerical models of packed bed thermal energy storage systems. Appl Therm Eng 2013;50:384–92. https://doi.org/10.1016/j.applthermaleng.2012.07.020.
[174] Oró E, Miró L, Farid MM, Cabeza LF. Thermal analysis of a low temperature storage unit using phase change materials without refrigeration system. Int J Refrig 2012;35:1709–14. https://doi.org/10.1016/j.ijrefrig.2012.05.004.
[175] Ortega-Fernández I, Zavattoni SA, Rodríguez-Aseguinolaza J, D'Aguanno B, Barbato MC. Analysis of an integrated packed bed thermal energy storage system for heat recovery in compressed air energy storage technology. Appl Energy 2017;205:280–93. https://doi.org/10.1016/j.apenergy.2017.07.039.
[176] Bejarano G, Vargas M, Ortega MG, Castaño F, Normey-Rico JE. Efficient simulation strategy for PCM-based cold-energy storage systems. Appl Therm Eng 2018;139:419–31. https://doi.org/10.1016/j.applthermaleng.2018.05.008.
[177] Khor JO, Sze JY, Li Y, Romagnoli A. Overcharging of a cascaded packed bed thermal energy storage: effects and solutions. Renew Sustain Energy Rev 2020;117. https://doi.org/10.1016/j.rser.2019.109421.
[178] Subekti M. The effect of turbulence models on coolant temperature and velocity for the pebble-bed typed high temperature reactor. KnE Energy 2016;1:1–10. https://doi.org/10.18502/ken.v1i1.463.
[179] Wu H, Gui N, Yang X, Tu J, Jiang S. Numerical simulation of heat transfer in packed pebble beds: CFD-DEM coupled with particle thermal radiation. Int J Heat Mass Transf 2017;110:393–405. https://doi.org/10.1016/j.ijheatmasstransfer.2017.03.035.
[180] Khor JO, Yang L, Akhmetov B, Romagnoli ABLA. Application of granular materials for void space reduction within packed bed thermal energy storage system filled with macro-encapsulated phase. Change Materials 2020.
[181] Zarajabad OG, Ahmadi R. Numerical investigation of different PCM volume on cold thermal energy storage system. J Energy Storage 2018;17:515–24. https://doi.org/10.1016/j.est.2018.04.013.
[182] Sang WH, Lee YT, Chung JD, Kim ST, Kim T, Oh CH, et al. Efficient numerical approach for simulating a full scale vertical ice-on-coil type latent thermal storage tank. Int Commun Heat Mass Transf 2016;78:29–38. https://doi.org/10.1016/j.icheatmasstransfer.2016.08.011.
[183] Liu M, Saman W, Bruno F. Validation of a mathematical model for encapsulated phase change material flat slabs for cooling applications. Appl Therm Eng 2011;31:2340–7. https://doi.org/10.1016/j.applthermaleng.2011.03.034.
[184] Xiaofeng X, Xuelai Z, Munyalo JM. Simulation study on temperature field and cold plate melting of cold storage refrigerator car. Energy Procedia 2017;142:3394–400. https://doi.org/10.1016/j.egypro.2017.12.476.
[185] Torras S, Castro J, Rigola J, Morales-Ruiz S, Riccius J, Leiner J. Multiphysics modeling and experimental validation of low temperature accumulator for cryogenic space propulsion systems. Aerosp Sci Technol 2019;84:75–89. https://doi.org/10.1016/j.ast.2018.10.010.
[186] Tan H, Li C, Li Y. Simulation research on PCM freezing process to recover and store the cold energy of cryogenic gas. Int J Therm Sci 2011;50:2220–7. https://doi.org/10.1016/j.ijthermalsci.2011.04.017.
[187] Amin NAM, Belusko M, Bruno F, Liu M. Optimising PCM thermal storage systems for maximum energy storage effectiveness. Sol Energy 2012;86:2263–72. https://doi.org/10.1016/j.solener.2012.04.020.
[188] Yu Q, Tchuenbou-Magaia F, Al-Duri B, Zhang Z, Ding Y, Li Y. Thermo-mechanical analysis of microcapsules containing phase change materials for cold storage. Appl Energy 2018;211:1190–202. https://doi.org/10.1016/j.apenergy.2017.12.021.
[189] Wang J, Battaglia F, Wang S, Zhang T, Ma Z. Flow and heat transfer characteristics of ice slurry in typical components of cooling systems: a review. Int J Heat Mass Transf 2019;141:922–39. https://doi.org/10.1016/j.ijheatmasstransfer.2019.07.021.
[190] Kumar A, Yadav SK, Mahato A, Kumar A. On-demand intermittent ice slurry generation for subzero cold thermal energy storage: numerical simulation and performance analysis. Appl Therm Eng 2019;161:114081. https://doi.org/10.1016/j.applthermaleng.2019.114081.
[191] Tiwari VK, Kumar A, Kumar A. Enhancing ice slurry generation by using inclined cavity for subzero cold thermal energy storage: simulation, experiment and performance analysis. Energy 2019;183:398–414. https://doi.org/10.1016/j.energy.2019.06.121.
[192] Ismail KAR, Moraes RIR. A numerical and experimental investigation of different containers and PCM options for cold storage modular units for domestic applications. Int J Heat Mass Transf 2009;52:4195–202. https://doi.org/10.1016/j.ijheatmasstransfer.2009.04.031.
[193] Song Y, Zhang N, Jing Y, Cao X, Yuan Y. Experimental and numerical investigation on dodecane / expanded graphite shape-stabilized phase change material for cold energy storage. Energy 2019;189:116175. https://doi.org/10.1016/j.energy.2019.116175.
[194] Faraj K, Khaled M, Faraj J, Hachem F, Castelain C. Phase change material thermal energy storage systems for cooling applications in buildings: a review. Renew Sustain Energy Rev 2020;119:109579. https://doi.org/10.1016/j.rser.2019.109579.
[195] Peng H, Shan X, Yang Y, Ling X. A study on performance of a liquid air energy storage system with packed bed units. Appl Energy 2018;211:126–35. https://doi.org/10.1016/j.apenergy.2017.11.045.
[196] Morgan R, Nelmes S, Gibson E, Brett G. Liquid air energy storage - Analysis and first results from a pilot scale demonstration plant. Appl Energy 2015;137:845–53. https://doi.org/10.1016/j.apenergy.2014.07.109.
[197] Morgan R, Nelmes S, Gibson E, Brett G. An analysis of a large-scale liquid air energy storage system. Proc Inst Civ Eng - Energy 2015;168:135–44. https://doi.org/10.1680/ener.14.00038.
[198] Li MJ, Jin B, Ma Z, Yuan F. Experimental and numerical study on the performance of a new high-temperature packed-bed thermal energy storage system with macroencapsulation of molten salt phase change material. Appl Energy 2018;221:1–15. https://doi.org/10.1016/j.apenergy.2018.03.156.
[199] Gil A, Medrano M, Martorell I, Lá zaro A, Dolado P, Zalba B, et al. State of the art on high temperature thermal energy storage for power generation. Part 1-Concepts, materials and modellization; n.d. https://doi.org/10.1016/j.rser.2009.07.035.
[200] Castell A, Belusko M, Bruno F, Cabeza LF. Maximisation of heat transfer in a coil in tank PCM cold storage system. Appl Energy 2011;88:4120–7. https://doi.org/10.1016/j.apenergy.2011.03.046.
[201] Tay NHS, Belusko M, Bruno F. Experimental investigation of tubes in a phase change thermal energy storage system. Appl Energy 2012;90:288–97. https://doi.org/10.1016/j.apenergy.2011.05.026.
[202] FIC S.p.A. EUTECTIC PLATES; n.d. https://www.fic.com/en/product/eutectic-plates (accessed February 8, 2021).
[203] Arunachalam S. Latent heat storage: container geometry, enhancement techniques, and applications-A review. J Sol Energy Eng Trans ASME 2019;141:1–14. https://doi.org/10.1115/1.4043126.
[204] Selvnes H, Hafner A, Kauko H. Design of a cold thermal energy storage unit for industrial applications using CO2 as refrigerant. 25th IIR Int. Congr. Refrig., Montréal, Canada 2019:2–5.
[205] Gibb D, Seitz A, Johnson M, Romani J, Gasia J, F. Cabeza L, et al. Applications of thermal energy storage in the energy transition 2018:154.
[206] Liu M, Bruno F, Saman W. Thermal performance analysis of a flat slab phase change thermal storage unit with liquid-based heat transfer fluid for cooling applications. Sol Energy 2011;85:3017–27. https://doi.org/10.1016/j.solener.2011.08.041.
[207] Selvnes H, Allouche Y, Sevault A, Hafner A. CFD modeling of ice formation and melting in horizontally cooled and heated plates CFD modeling of ice formation and melting in horizontally cooled and heated plates. Eurotherm Semin. #112 Adv. Therm. energy storage, Lleida, Spain: 2019.
[208] Selvnes H, Allouche Y, Manescu RI, Hafner A. phase change materials Review on cold thermal energy storage applied to refrigeration systems using phase change materials. Therm Sci Eng Prog 2020:100807. https://doi.org/10.1016/j.tsep.2020.100807.
[209] Tassou SA, Chaer I, Bellas I. Studies into the thermal and transport properties of ice slurries for low energy cooling applications in buildings. Uxbridge, Middlesex, UK: 2002.
[210] Meewisse JW, Ferreira CAI. Fluidised bed ice slurry generator : operating range. In: 5th Work. Ice Slurries IIR, Stockholm (Sweden): 2002.
[211] Liu X, Li Y, Zhuang K, Fu R, Lin S, Li X. Performance study and efficiency improvement of ice slurry production by scraped-surface method. Appl Sci 2018;9. https://doi.org/10.3390/app9010074.
[212] Tiwari VK, Kumar A, Kumar A. Enhancing ice slurry generation by using inclined cavity for subzero cold thermal energy storage: simulation, experiment and performance analysis. Energy 2019;183:398–414. https://doi.org/10.1016/j.energy.2019.06.121.
[213] Viking Cold Solutions I. Thermal energy storage in an ammonia refrigerated low-temperature warehouse. vol. 28. 1990.
[214] Kim YM, Shin DG, Kim CG. On-board cold thermal energy storage system for hydrogen fueling process. Energies 2019;12. https://doi.org/10.3390/en12030561.
[215] Davenne TR, Peters BM. An analysis of pumped thermal energy storage with decoupled thermal stores. Front Energy Res 2020;8:1–22. https://doi.org/10.3389/fenrg.2020.00160.
[216] Liu M, Saman W, Bruno F. Development of a novel refrigeration system for refrigerated trucks incorporating phase change material. Appl Energy 2012;92:336–42. https://doi.org/10.1016/j.apenergy.2011.10.015.
[217] Chirino H, Xu B, Xu X, Guo P. Generalized diagrams of energy storage efficiency for latent heat thermal storage system in concentrated solar power plant. Appl Therm Eng 2018;129:1595–603. https://doi.org/10.1016/j.applthermaleng.2017.10.153.
[218] Palomba V, Brancato V, Frazzica A. Thermal performance of a latent thermal energy storage for exploitation of renewables and waste heat: an experimental investigation based on an asymmetric plate heat exchanger. Energy Convers Manag 2019;200:112121. https://doi.org/10.1016/j.enconman.2019.112121.
[219] Saeed RM, Schlegel JP, Sawafta R, Kalra V. Plate type heat exchanger for thermal energy storage and load shifting using phase change material. Energy Convers Manag 2019;181:120–32. https://doi.org/10.1016/j.enconman.2018.12.013.
[220] Dufour T, Hoang HM, Oignet J, Osswald V, Clain P, Fournaison L, et al. Impact of pressure on the dynamic behavior of CO2 hydrate slurry in a stirred tank reactor applied to cold thermal energy storage. Appl Energy 2017;204:641–52. https://doi.org/10.1016/j.apenergy.2017.07.098.
[221] Oró E, Miró L, Farid MM, Martin V, Cabeza LF. Energy management and CO2 mitigation using phase change materials (PCM) for thermal energy storage (TES)

in cold storage and transport. Int J Refrig 2014;42:26–35. https://doi.org/10.1016/j.ijrefrig.2014.03.002.
[222] Mastani Joybari M, Haghighat F, Moffat J, Sra P. Heat and cold storage using phase change materials in domestic refrigeration systems: the state-of-the-art review. Energy Build 2015;106:111–24. https://doi.org/10.1016/j.enbuild.2015.06.016.
[223] Kumar V, Shrivastava R, Nandan G. Energy saving using phase change material in refrigerating system; 2016.
[224] Bista S, Hosseini SE, Owens E, Phillips G. Performance improvement and energy consumption reduction in refrigeration systems using phase change material (PCM). Appl Therm Eng 2018;142:723–35. https://doi.org/10.1016/j.applthermaleng.2018.07.068.
[225] Oró E, Miró L, Farid MM, Cabeza LF. Improving thermal performance of freezers using phase change materials. Int J Refrig 2012;35:984–91. https://doi.org/10.1016/j.ijrefrig.2012.01.004.
[226] Viking Cold Solutions I, Viking Cold Solutions. Case study: butterfield and vallis uses PCM thermal storage to cut refrigeration costs 40%; 2016. https://www.vikingcold.com/case-study-butterfield-and-vallis-uses-pcm-thermal-storage-to-cut-refrigeration-costs-40/ (accessed April 14, 2020).
[227] Morgan R, Dearman M. Method and apparatus for storing thermal energy; 2016.
[228] Thienel L. Heat pipe (CRYOFD) flight experiment; 1998.
[229] Tassou SA, De-Lille G, Ge YT. Food transport refrigeration - Approaches to reduce energy consumption and environmental impacts of road transport. Appl Therm Eng 2009;29:1467–77. https://doi.org/10.1016/j.applthermaleng.2008.06.027.
[230] Viking Cold Solutions. Case Study: Butterfield and Vallis uses PCM thermal storage to cut refrigeration costs 40%; 2016. https://www.vikingcold.com/case-study-butterfield-and-vallis-uses-pcm-thermal-storage-to-cut-refrigeration-costs-40/ (accessed February 8, 2021).
[231] International Energy Agency (IEA). Technology roadmap - energy storage. Paris: 2014.
[232] IRENA, IEA-ETSAP. Technology brief - electricity storage; 2012.
[233] Ding Y, Tong L, Zhang P, Li Y, Radcliffe J, Wang L. Chapter 9 – Liquid Air Energy Storage. Elsevier Inc.; 2016. https://doi.org/10.1016/B978-0-12-803440-8.00009-9.
[234] Benato A, Stoppato A. Pumped thermal electricity storage: a technology overview. Therm Sci Eng Prog 2018;6:301–15. https://doi.org/10.1016/j.tsep.2018.01.017.
[235] Newcastle University connects first grid-scale pumped heat energy storage system; 2019. https://www.theengineer.co.uk/grid-scale-pumped-heat-energy-storage/.
[236] Smallbone A, Jülch V, Wardle R, Roskilly AP. Levelised cost of storage for pumped heat energy storage in comparison with other energy storage technologies. Energy Convers Manag 2017;152:221–8. https://doi.org/10.1016/j.enconman.2017.09.047.
[237] Morandin M, Maréchal F, Mercangöz M, Buchter F. Conceptual design of a thermo-electrical energy storage system based on heat integration of thermodynamic cycles - Part A: Methodology and base case. Energy 2012;45:375–85. https://doi.org/10.1016/j.energy.2012.03.031.
[238] International Energy Agency (IEA). World Energy Outlook 2019. Paris: 2019.
[239] Kanbur BB, Xiang L, Dubey S, Choo FH, Duan F. Cold utilization systems of LNG: a review. Renew Sustain Energy Rev 2017;79:1171–88. https://doi.org/10.1016/j.rser.2017.05.161.
[240] Yamamoto T, Fujiwara Y. The accomplishment of 100 % utilisation of LNG cold energy. 25th World Gas Conf 2012:1–19.
[241] Yamamoto T, Fujiwara Y, Kitagaki S. Challenges of advanced utilization of LNG cold in osaka gas senboku LNG terminals. Des Innov Value Towar a Sustain Soc 2012:148–53. https://doi.org/10.1007/978-94-007-3010-6_30.
[242] Ito Y, Oshio A, Okamoto H, Nii T, Yamane M, Abuyama T. Dynamic simulation of cold energy storage and process control for BOG re-liquefied Systems. KOBE STEEL Eng REPORTS 1998;48:363–363. https://doi.org/10.2307/j.ctv16wn4.32.
[243] KANAGAWA T. Japan ' s LNG Utilization and Enviromental Efforts; n.d.
[244] Otsuka T. Evolution of an LNG terminal: Senboku Terminal of Osaka gas. In: Int. Gas Union World Gas Conf. Pap., vol. 5; 2006, p. 2617–30.
[245] Bloomberg New Energy Finance. Hydrogen economy outlook 2020:12.